The Study on Performance of Transition Metal Loaded H-ZSM-5 Catalysts for Conversion of Ethanol to Liquid Fuels

Setthawat Sitthithai

A THESIS SUBMITTED IN PARTIAL FULFILLMENT OF THE REQUIREMENT FOR THE DEGREE OF MASTER OF SCIENCE IN PETROCHEMICALS AND HYDROCARBON CHEMISTRY

DEPARTMENT OF CHEMISTRY

FACULTY OF SCIENCE

KING MONGKUT'S INSTITUTE OF TECHNOLOGY LADKRABANG

2018

KMITL-2017-SC-M-015-001

Thesis Title	The Study on Performance of Transition Metal loaded H-ZSM-5 catalysts for Conversion of Ethanol to Liquid Fuels
Student Name	Setthawat Sitthithai
Student ID	58605036
Degree	Master of Science (Petrochemicals and hydrocarbon chemistry)
Department	Chemistry
Year	2018
Thesis Advisor	Assoc. Prof. Dr. Tawan Sooknoi

Abstract

In this project, the catalytic conversion of ethanol to higher hydrocarbons over the double bed system of metal/SiO_2 and H-ZSM-5 will be investigated. In order to generate C-C bond, the ethanol is dehydrogenated to acetaldehyde over the first bed of metal catalyst. While the aldol condensation/deoxygenation can be promoted over the secondary bed of acid function e.g. H-ZSM-5. In the single bed system of H-ZSM-5 (28), ethanol can be converted to higher hydrocarbons by dehydration and oligomerization at higher contact time (25-42 g.h/mol.). However, the formation of hydrocarbons is not feasible because the oligomerization of ethylene proceeds via the formation of unstable primary carbocation. For the double bed system of Ag/SiO_2 and H-ZSM-5 (28), this catalytic system shows higher hydrocarbons, as compared to the single bed. Nonetheless, the Ag catalyst can promote decarbonylation of ethanol to methane in parallel. For dehydrogenation of ethanol, the Cu/SiO_2 gives higher selectivity to acetaldehyde. However, the Cu/SiO_2 shows a rapid deactivation due to strongly adsorption of η^2(C, O)-carbonyl species on Cu metal surface. When the secondary metal is added to Cu based catalyst, the Cu-Zn/SiO_2 shows high activity and selectivity for dehydrogenation of ethanol to acetaldehyde, as compared to the Cu-Fe, Cu-Ni, Cu-Ag over SiO_2.

For the second bed, the H-ZSM-5 with Si/Al~28 provides higher hydrocarbons than the catalysts with Si/Al~40, 140, 250, and 500. However, a severe deactivation is still observed. Incorporation of metal (Ni, Cu, Zn) on H-ZSM-5 (28) provides higher stability, as compared to the parent H-ZSM-5 (28). The Zn/H-ZSM-5 (28) exhibits higher performance for ethanol conversion to hydrocarbons, as compared to Ni and Cu/H-ZSM-5 (28). The conversion of ethanol over the double bed system (Cu-Zn/SiO_2 and Zn/H-ZSM-5 (28)) proceeds via the ethanol dehydrogenation to acetaldehyde in the first bed. Acetaldehyde undergoes further condensation over the second bed to form higher aldehyde intermediate that subsequently dehydrates and cyclizes into higher hydrocarbons.

Keywords: Double bed system, aldol condensation/deoxygenation, hydrocarbons

Acknowledgement

The author desires to appreciatively thank my advisors, Assoc. Prof. Dr. Tawan Sooknoi for suggestions, inspiration, carefulness, reassurance, experimental instrument, and knowledge in catalysis throughout this research

I would like to gratefully acknowledge chairperson and committee, Dr. Natthida Numwong, Dr. Amnat Permsubscul, and Assist. Prof. Dr sabaithip Tungkamani for judgment and valuable comments.

Moreover, I would like to acknowledge the financial support from the Faculty of Science, King Mongkut's Institute of Technology Ladkrabang for the equipment, chemicals, and facilities.

Sincerely thanks to Suranaree University of Technology, Scientific and Technological Research Equipment Centre, Department of Chemistry, Chulalongkorn University for the characterization of catalyst in this research.

Unforgettable, I would like to grateful to my friends, my brothers in Catalytic Chemistry Research Unit (CCR group) for their help, advice, support, and encouragement.

Finally, I deeply appreciate and thank our parents and family for their love and support.

Mr. Setthawat Sitthithai.

LIST OF CONTENTS

LIST OF CONTENTS (Continued)

LIST OF CONTENTS (Continued)

LIST OF TABLES

LIST OF FIGURES

LIST OF SCHEMES

LIST OF SCHEMES (Continuted)

Chapter 1

Introduction

1.1 Motivation

Although fossil fuels have become dominant energy resource for the modern world and it is essential in daily life, the fossil energy is decreasing and causes pollution problem. Renewable feedstock becomes increasingly interesting for the production of fuels. Nowadays, one of the most abundant renewable feedstock is ethanol, that is obtained from agricultural products such as sugar cane and cassava [1].

Ethanol is commonly used to power other vehicles such as farm tractor and car by mixing in gasoline, so called gasohol. This blending of ethanol into gasoline for cleaner combustion, decreased carbon monoxide and hydrocarbon exhaust emission. In addition, ethanol used as additive in fuel to increase octane number for engine to replace methyl tertiary butyl ether (MTBE), because MTBE is more toxic chemicals that has been found to contaminate groundwater. [2]. However, higher mixture ratio of ethanol per gasoline leads to corrosion of engine parts [3].

Alternatively, the direct production of gasoline from ethanol was studied for several years. This can be achieved from acid-catalyzed dehydration and oligomerization over H-ZSM-5 catalyst [4]. The modification of Si/Al ratio on H-ZSM-5 framework is the common way to significantly enhance the acidic property and hence the activity [5]. However, ethanol dehydration over acid site favored at high temperature while the oligomerization of ethylene to gasoline proceeds via the formation of primary carbocation that is thermodynamically unfavorable [6,7].

Accordingly, this work will investigate ethanol conversion to hydrocarbons via dehydrogenation of ethanol to acetaldehyde followed by aldol condensation to higher aldehyde and higher alcohol. The higher alcohol produced can be readily dehydrated into hydrocarbon over acid catalysts [8]. It is proposed that rate of the C-C coupling will be increased because the acetaldehyde can be protonated over acid function to form enol or an enolate intermediate. This intermediate is more stable than the primary carbocation intermediate formed by protonation of ethylene. In this concept, the dehydrogenation can be promoted over the first bed of transition metals catalysts for example; Ag, Cu, Cu-Fe, and Cu-Zn alloy etc. whiles the aldol condensation,

dehydration, and oligomerization can be performed over the second bed of acid function such as H-ZSM-5 catalyst. As the aldol condensation of aldehyde is readily promoted, the metal phase indicates a key role in controlling ethanol conversion to acetaldehyde. Among acid catalyst, H-ZSM-5 possesses high surface area and thermal stability [9]. It has been considered as the most selective catalysts for the ethanol to hydrocarbons process due to its unique structural properties that selectively produce hydrocarbon mixtures [10]. In this work, the optimization of these two reaction conditions will be required. In addition, types of metal and effect of contact time on both dehydrogenation and aldol condensation will be studied. Moreover, acidity of H-ZSM-5 that effects aldol condensation will be investigated.

1.2 Objectives

1). To produce liquid fuels from ethanol via the dehydrogenation and aldol condensation approach.

2). To understand the reaction pathway for dehydrogenation and condensation reaction over double bed system of metal/SiO_2 and H-ZSM-5.

3). To understand the effect of temperature, contact time, acidic property and type of metals on the conversion of ethanol to liquid fuels.

1.3 Scope of the study

1). Catalyst preparation by wetness impregnation for metal (Ag, Cu, Cu-Fe, Cu-Ni, Cu-Ag, and Cu-Zn) supported silica and ion exchange method for the incorporated metal (Ni, Cu, and Zn) on H-ZM-5.

2). Characterization of catalyst by X-Ray diffraction spectroscopy (XRD), X-ray fluorescence (XRF), temperature-programmed reduction (TPR), temperature programmed desorption (TPD), gas adsorption analysis (BET), thermogravimetric analysis (TGA), inductively coupled plasma-mass spectroscopy (ICP-MS), and transmission Electron Microscopy (TEM)

3). Testing efficiency of the reaction over the double bed system in a continuous fixed- bed reactor.

4). Study effect of carrier gas, temperature (400-500 °C), contact time (15-42 g.h/mol), acidity of H-ZSM-5 (Si/Al ratio :28, 40 140, 250, 500) and types of metals.

5). Analysis and quantification of liquid products from the reactions by online gas chromatograph equipped with a flame ionization detector (GC-FID).

1.4 Expected results

The new approach for production of gasoline from ethanol can be obtained. This technology can benefit from raw materials available in the country.

Chapter 2

Theory and literature

2.1 Ethanol

Ethanol (ethyl alcohol, grain alcohol) is an alcohol, a group of chemical compounds whose molecules contain a hydroxyl group, –OH, bonded to a carbon atom. It is a clear, colorless liquid with a characteristic agreeable odor. Ethanol melts at –114.1°C, boils at 78.5°C, and has a density of 0.789 g/mL at 20°C. Its low freezing point has made it useful as the fluid in thermometers for temperatures below –40°C, the freezing point of mercury, and for other low-temperature purposes, such as for antifreeze in automobile radiators [11].

2.1.1 Ethanol production

Alternative and renewable energy resources have attracted increased interest in recent research due to with increased demands for energy, environmental problem, and continued decreasing of fossil feedstock. Biomass has been recognized as one of the most viable resources to produce biofuels, such as ethanol due to its renewable nature with low CO_2 emission and reduce carbon monoxide (CO) 20 to 30% [12,13]. The production of ethanol can be produced from two different ways, as shown in Figure 2.1, from the petroleum route becoming less attractive because oil prices continue to rise and fossil feedstock is decreasing. Conversely, the production of ethanol from biomass has become increasing efficient for several years because less expensive. Nowadays, 90% of the ethanol on the market is biomass-derived [14].

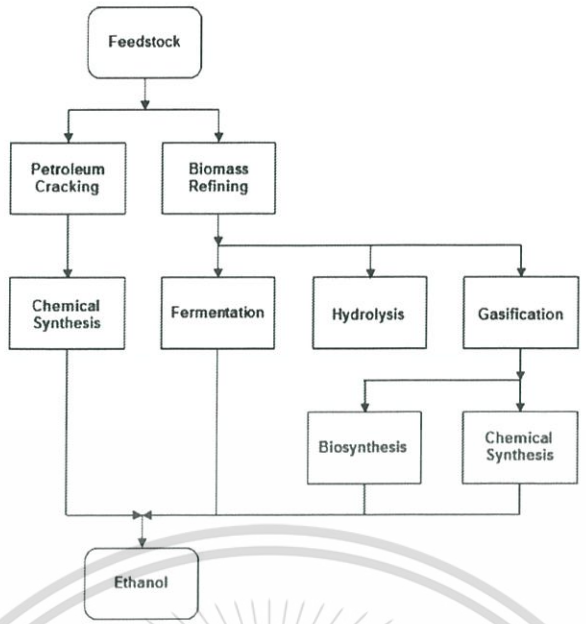

Figure 2.1 Overview of the ethanol production pathways.

Ethanol can be produced from agricultural feedstock by fermentation in anoxic environment. In the most of the fermentation, ethanol is made from corn. However, it can be produced other agricultural raw materials such as sugarcane, potato, cassava, and cellulose. In addition, fermentation of garbage to ethanol was studied [15,16]. The fermentation of sugarcane and corn employed yeast for production of ethanol directly. Starches (from potato, cassava) must first be hydrolyzed by enzymes amylase to fermentable sugar. While, cellulose (from wood, paper) similar to starches must hydrolyzed by acids before fermentation. Generally, the fermentation of three types can produce ethanol with 10% concentration, then the mixture is separated and purified, usually by distillation and dehydration.

2.2 Ethanol to chemical

2.2.1 Ethanol to ethylene

Ethylene is the most produced organic compound on earth. It is mostly used in the production of polymers (e.g., polyethylene, polyvinylchloride), ethylene oxide, and ethylene glycol, etc. Ethylene is typically obtained from petroleum through thermal cracking process. Recently, ethanol dehydration has gained increasing importance as an alternative route for producing ethylene. The most catalysts of ethanol dehydration are a H-ZSM-5 and γ-alumina. However, it is important to note

that it is not possible to produce all the required ethylene from renewable sources because the demand for ethylene worldwide is approximately three times the amount of ethanol that is currently produced [14, 17].

2.2.2 Ethanol to acetaldehyde

Acetaldehyde is a naturally occurring intermediate in the enzymatic degradation of ethanol to acetic acid and, finally, CO_2 (Scheme 1) [18]. Acetaldehyde is also an important intermediate in the synthesis of many bulk chemicals, such as acetic acid, acetic anhydride, ethyl acetate, etc. Currently, most acetaldehyde is produced by the so-called Wacker process through the direct oxidation of ethylene to acetaldehyde with a $PdCl_2/CuCl_2$ catalyst in water in the presence of air or other oxidants.

Scheme 1 The complete oxidation of ethanol to form CO_2.

Alternatively, the bioethanol industry has made the direct synthesis of acetaldehyde through ethanol dehydrogenation, with or without the presence of oxygen
(Scheme 2). The catalytic oxidation of ethanol over silver oxide as the catalyst has been reported [19]. While the dehydrogenation route is copper catalysts supported on rice husk ash [14, 20].

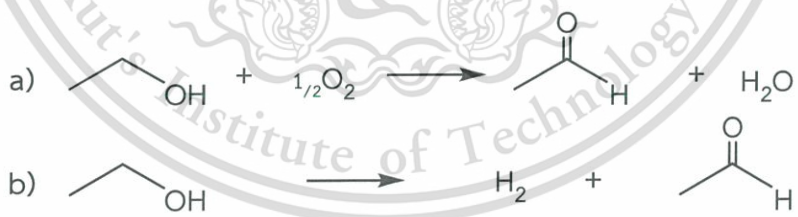

Scheme 2 Acetaldehyde production from ethanol via a) an oxidation or b) a dehydrogenation pathway.

2.2.3 Ethanol to ethyl acetate

Ethyl acetate is commonly used as a solvent in chromatography, for extraction processes, and in glues and cigarettes because of its characteristic sweet smell. Industrially, it is mainly produced by the esterification of acetic acid with ethanol. Another possible method to synthesize ethyl acetate is the so-called Tishchenko reaction, which involves the disproportionation of aldehydes, a process that is catalyzed by a strong base such as an alkoxide (Scheme 3a). Alternatively, a direct one-step conversion of two molecules of ethanol is also feasible (Scheme 3b). Both routes can be based on bioethanol if the ethanol is first oxidized to obtain the aldehyde, which can be employed in ethyl acetate production [14].

Scheme 3 Ethyl acetate production from a) acetaldehyde and b) ethanol.

2.2.4 Ethanol to butanol

Butanol is a commodity chemical used as a solvent and for the production various esters and ethers, some of which are important monomers for the polymer industry. It is also well known that butanol can be used as a fuel, lower corrosiveness [21]. Butanol is mainly produced by using the so-called oxo process (Scheme 4), which consists of propylene hydroformylation followed by butyraldehyde hydrogenation to yield n-butanol.

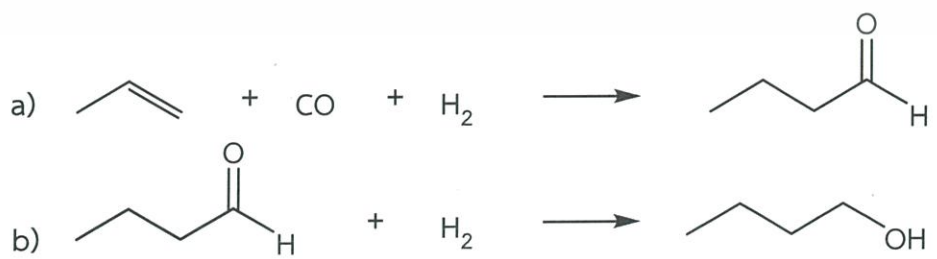

Scheme 4 The oxo process to produce n-butanol.

Nevertheless, it is based on a homogeneous catalyst, the process suffers from drawbacks such as difficult separation of the desired compound, costly catalyst preparation, and environmental issues. Therefore, the development of a heterogeneous catalyst for direct butanol synthesis is more worth. The solid base-catalyzed, one step conversion of ethanol to n-butanol could be an attractive alternative [22, 23]. Two possible mechanisms, that is a bimolecular condensation or Guerbet reaction (Scheme 5) were considered. The observation of acetaldehyde as the main byproduct and the condensation occurs between one ethanol and one acetaldehyde molecule forming butyraldehyde, which is finally reduced to butanol [14].

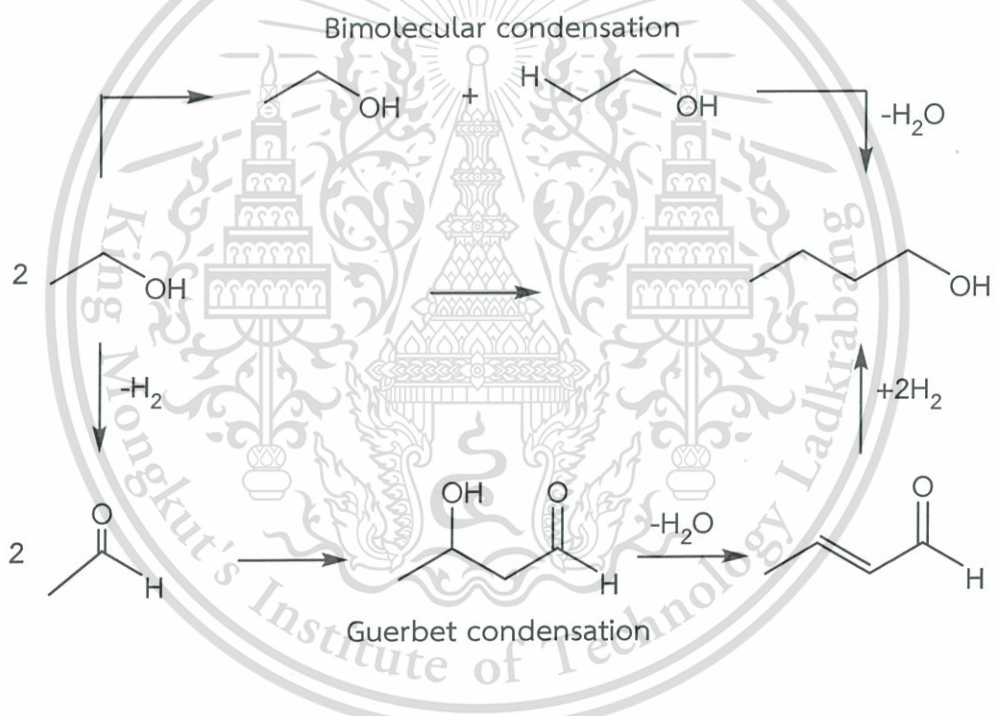

Scheme 5 Two proposed mechanisms for the one-step synthesis of n-butanol from ethanol.

2.2.5 Ethanol to 1,3-butadiene

Butadiene is one of the most important bulk chemicals produced in the petrochemical industry. It is widely used in the production of polymers and polymer intermediates such as styrene–butadiene rubber (used in the production of car tires), polybutadiene and acrylonitrile–butadiene–styrene (ABS) copolymer [24]. There are two processes for its industrial synthesis: isolation from naphtha steam cracker fractions of paraffinic hydrocarbons for the manufacture of ethylene and other olefins, or the catalytic and oxidative dehydrogenation of n-butane and n-butene [25].

The process to produce butadiene from ethanol was purposed by Toussaint and co-workers [26]. The mechanism based on the aldol condensation between two acetaldehyde molecules formed upon ethanol dehydrogenation to 3-hydroxybutanal then dehydrated to crotonaldehyde and finally dehydrated to yield butadiene (Scheme 6).

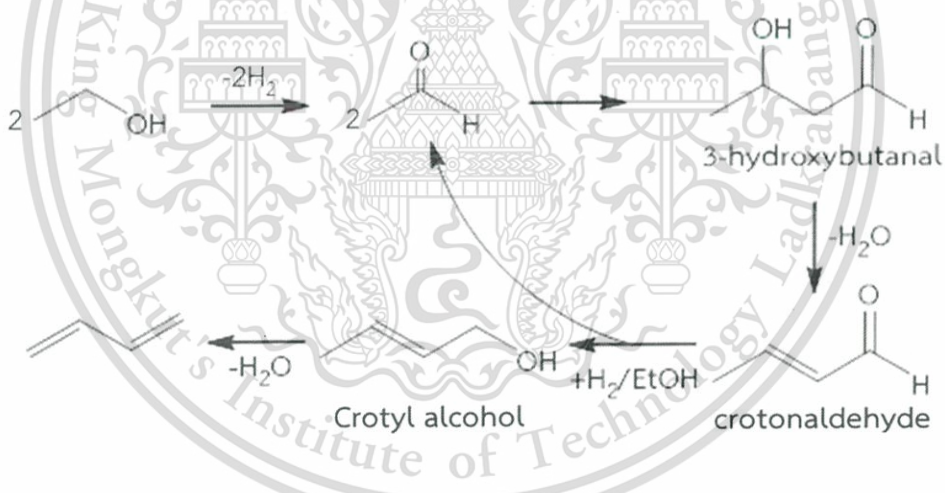

Scheme 6 The aldol condensation mechanism, as proposed by Toussaint et al.

2.3 Catalyst

2.3.1 ZSM5 zeolite [27-34]

Zeolite ZSM-5, Zeolite Socony Mobil-5, is one type of family zenolite, it has shape selective catalysts with unique channel structures. The secondary building unit of framework of ZSM-5 including mor 8T, case 12T, mel 14T, and mfi 14T shown in **Figure 2.2** These secondary building units can be connected to form sheet and the

linking of the sheet lead to a three-dimensional framework structure by the chains extend along the *z*-axis. The sheets parallel to [010] and [100] are shown in **Figure 2.3** and **2.4**

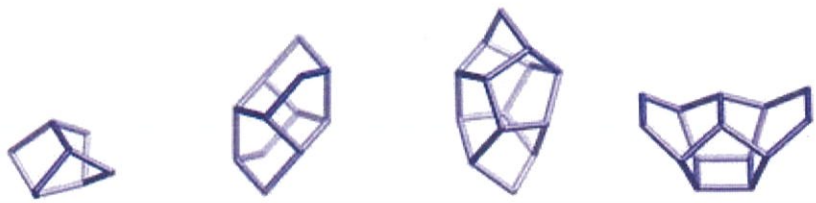

Figure 2.2 the secondary building unit of framework of ZSM-5

Figure 2.3 shows that the *x*-axis is horizontal and the *z*-axis vertical and the 10-membered ring apertures shown are the entrances to the straight channels which run parallel to [010] plane. While, **Figure 2.4** shows that the *y*-axis is horizontal and the *z*-axis vertical and the circular 10-membered ring apertures shown are the entrances to channels which run parallel to [100] plane.

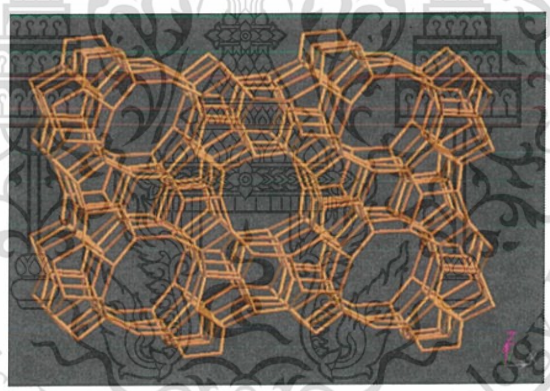

Figure 2.3 Skeletal diagram of the [010]-plane of the ZSM-5-unit cell.

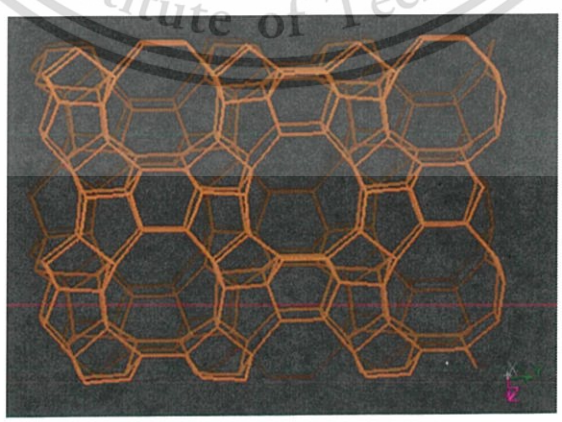

Figure 2.4 Skeletal diagram of the [100]-plane of the ZSM-5-unit cell.

ZSM-5 has chemical formula is Na^{+}_{n} $(H_2O)_{16}$| $[Al_nSi_{96-n}$ $O_{192}]$-MFI, n < 27. It is widely used in used in many catalytic reactions of industrial interest such as xylene isomerization, benzene ethylation, and ethanol, methanol-to-gasoline conversion. Their individual catalytic properties are mainly due to their regular framework with a pore size which is intermediate to the large pore sized zeolites (for instance, zeolites X and Y) and the small pore sized zeolite (for instance the A zeolite). The shape selectivity of the pentasil zeolite is catalytically expressed by many features, such as;

1. The sieving effect, i.e. the capability of zeolite to admit in to its pores or to reject reactive molecules having a critical diameter falling within a well-defined range;
2. The (reverse) sieving effect, i.e. the capability of the zeolite to allow product molecules having a certain critical diameter to diffuse out of its pores. Thus, in the case of a product molecule having a diameter exceeding the pore size of the zeolite, this molecule will have to undergo cracking or rearrangement into a smaller molecule before diffusing out of the zeolite
3. The effect on the reaction intermediates, i.e. the capability of certain active site to determine the length and structure of reaction intermediate species.

The unique catalytic properties of zeolite ZSM5 are attributed to both the three-dimensional system of intersecting channels and its strong acid sites. ZSM5 zeolite has pore system which is believed to be significant for their low coke formation.

While most industrial applications of zeolite catalyst make use of these in acid form, zeolite is also excellent support for metal species. Zeolite supported metal species called a bifunctional catalyst is an acid zeolite on which a metal species phase is deposited. The function of the metal is to catalyze dehydrogenation and hydrogenation reaction while H-ZSM-5 possesses excellent dehyadration and oligomerization properties which bifunctional catalyst can further undergo a variety of metal species and acidity reactions to form desirable product.

2.4 Related chemical reactions

2.4.1 Dehydrogenation of alcohol

Dehydrogenation is a chemical reaction that involves the removal of hydrogen from a molecule. It is the reverse process of hydrogenation. The first step in this process is ethanol adsorption on the catalyst surface by O atom of hydroxyl group attached on the metal surface (such as Ag, Cu) to produce η^1 (O)-carbonyl species (a). After that, dissociation of O-H bond is generated alkoxide intermediate. Finally, the dehydrogenation of ethanol can occur via an alkoxide intermediate to produce acetaldehyde with a metal hydride (di-hydride). In addition, η^2 (C, O)-carbonyl species (b) can occur with alkoxide intermediate by α-C and O atom attached on metal surface (such as Ni) to form acyl intermediate (η^1 (C)-acyl)) that may well desorb as acetaldehyde. However, yield of acetaldehyde obtained from η^2 (C, O)-carbonyl species is less than that from η^1 (O)-carbonyl species because formation of the acyl intermediate can lead to decarbonylation to CH_4 and CO (**Scheme 7**) [35, 36].

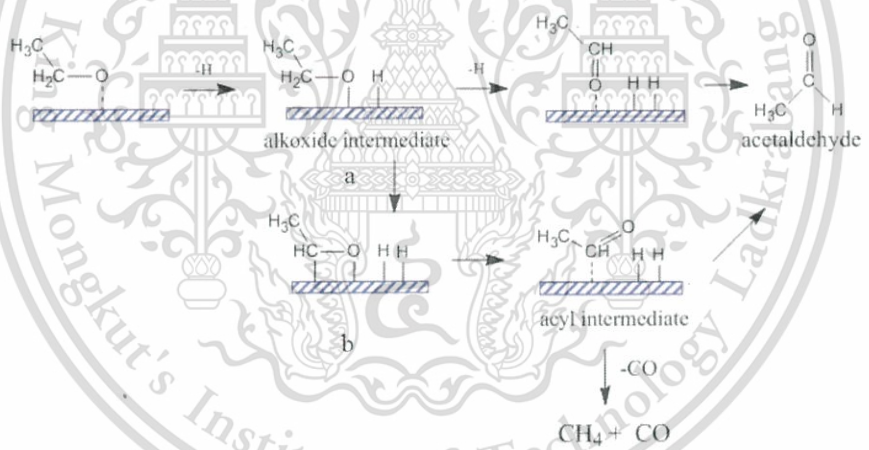

Scheme 7 Dehydrogenation of ethanol (a) η^1 (O)-alcohol species. (b) η^2 (C, O)-alcohol species.

2.4.2 Aldol condensation of aldehyde

Aldol reactions can occur under acid catalysis, in which the reaction generally leads to the α, β-unsaturated product by direct dehydration of the β-hydroxyl aldehyde intermediate. When an acid catalyst is used, the first step in the reaction mechanism involves acid-catalyzed tautomerization of the carbonyl compound to the

enol. The acid also serves to activate the carbonyl group of another molecule by protonation, rendering it highly electrophilic. The enol is nucleophilic at the α-carbon, allowing it to attack the protonated carbonyl compound, leading to the β-hydroxyl aldehyde intermediate after deprotonation. This usually dehydrates to give the unsaturated carbonyl compound. The scheme shows a typical acid-catalyzed self-condensation of an aldehyde [37, 38].

Acid-catalyzed aldol mechanism

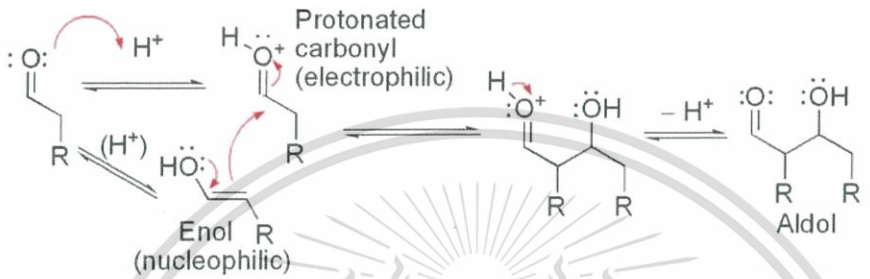

Acid-catalyzed dehydration

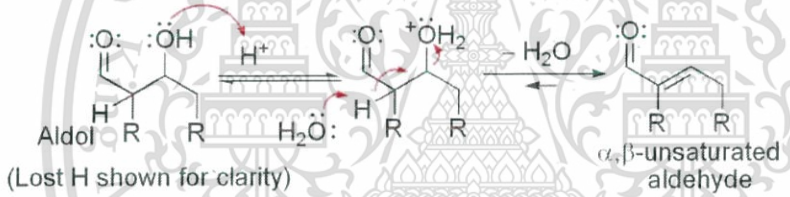

Scheme 8 Aldol condensation.

2.4.3 Hydrogenation of olefin and aldehyde

Hydrogenation is a chemical reaction between molecular hydrogen (H_2) and another compound, usually in the presence of a catalyst such as nickel, cobalt, palladium or platinum. The process is commonly employed to reduce or saturated organic compounds. The hydrogenation typically constitutes the addition of pairs of hydrogen atoms to a molecule, generally an alkene. The first step of alkene, C=C double bond, adsorbed on the catalyst surface and H_2 dissociates follow by an H atom bonds to one C atom. While another C atom is still attached to the surface. Finally, a second C atom bonds to an H atom and then the molecule leaves the surface to alkane. Additionally, the formyl group can be readily reduced to a primary alcohol (-CH_2OH) [38, 39].

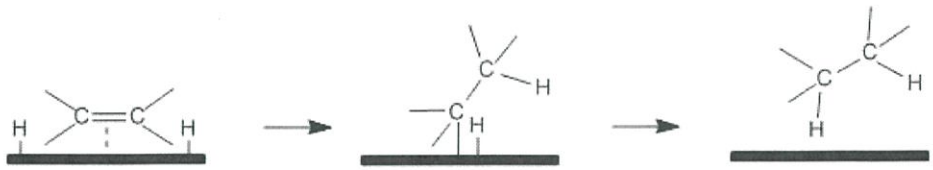

Scheme 9 Hydrogenation of Alkane.

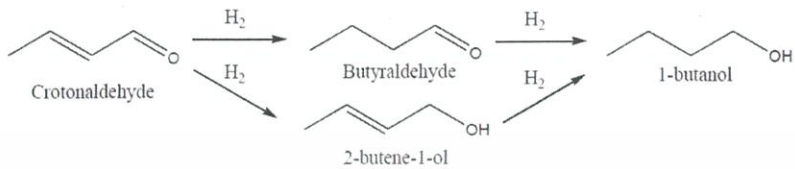

Scheme 10 Hydrogenation of formyl group.

2.4.4 MPV reaction

MPV reaction is Meerwein–Ponndorf–Verley reaction, it was discovered by Meerwein and Schmidt, and separately by Verley in 1925 [40]. Heterogeneous catalysts for the MPV reactions include zeolites, grafted alkoxides, metal oxides such as magnesium oxide, zirconia, silica, alumina. The reaction mechanism for MPV reaction is believed to go through a catalytic cycle involving a six-member ring transition state as shown in scheme 11 and 12. The ketone/aldehyde (oxidant) and the alcohol (reductant) are coordinated to the metal center of a metal alkoxide catalyst. The alcohol is coordinated as an alkoxide while the carbonyl group binds to the metal center via the oxygen. Activation of the carbonyl by coordination to metal center initiates the hydride transfer from the bound alcoholate to the carbonyl. The resulting alkoxide leaves the catalyst via an alcoholysis reaction with the bulk alcohol [41].

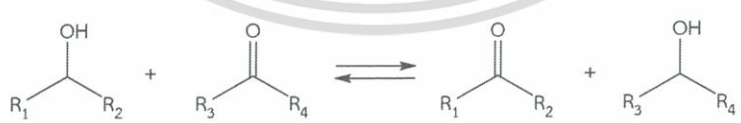

Scheme 11 The MPV reaction.

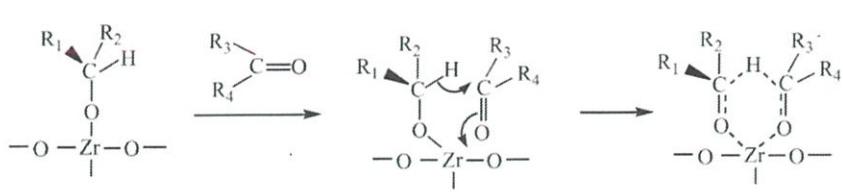

Scheme 12 Mechanism of MPV reaction over zirconia.

2.4.5 Dehydration of alcohol

Dehydration reaction is a chemical reaction that involves the loss of a water molecule from the reacting molecule. The reverse of a dehydration reaction is a hydration reaction. The dehydration may go by either the E1 or E2 mechanism, with primary alcohols favoring the E2 mechanism, and secondary and tertiary alcohol generally reacting by the E1 mechanism. The first step of either mechanism involves protonation of the hydroxyl oxygen atom by the acid, in order to convert the -OH group into a better leaving group, $-OH_2^+$ [38].

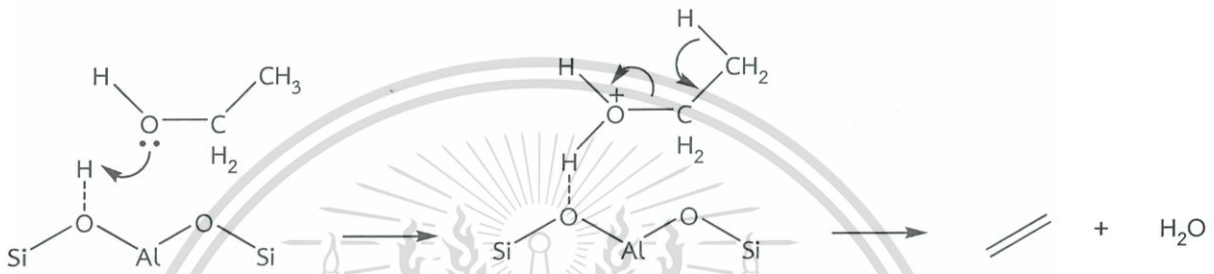

Scheme 13 Acid catalyzed dehydration of ethanol to produce ethylene.

2.4.6 Oligomerization of olefin

Oligomerization is chemical process that converts light olefins, usually propylene, butylene or their mixtures, contained in mixtures with light paraffins to higher hydrocarbon over catalysis or heat. In this process (ETG), olefins which obtained from dehydration reaction will be reacts with other olefins to forms heavier olefinic compounds follow by hydrogenation to higher hydrocarbon. For example, in previous research, the oligomerization is promoted by H-ZSM-5 as catalyst in important step of the Mobil olefin-to-distillate-and-gasoline process. When operated at relatively low temperature and high pressure (200-300 °C, 20-105 atm.), the products are higher molecular weight iso-olefins. Under these conditions light olefins are first converted to high oligomers. Subsequently, isomerization and cracking give intermediate C4-C7 olefins. Finally, the latter participate in copolymerization to yield the product [42,43].

2.5 Literature review

Nagabhatla Viswanadham, *et al* [9] tested conversion of ethanol to higher aromatics for production of gasoline. The catalyst includes H-ZSM-5 with micro-crystallite size (micro H-ZSM-5 Si/Al ratio~30, 100), and nano-crystallite size (nano H-ZSM-5 size Si/Al ratio~30). The acidity, porosity and catalytic performance were compared at 450 and 500°C. It was found that nano H-ZSM-5 catalyst having high acidity and mesoporosity showed higher production of aromatic yields, as compared to the micro H-ZSM-5 with Si/Al ratio~30 and micro H-ZSM-5 with Si/Al ratio~100. The aromatic yield is increased from 38.6 wt% to 50.6 wt% when temperature is increased from 450°C to 500°C over nano H-ZSM5 catalyst.

Xianlong Zhang, *et al* [44] studied hydrothermal synthesis of 1-butanol from ethanol over different metals (Fe, Co, Ni, Raney Cu, copper chromite, $CoCO_3$, and Co_2O_3) as catalyst in $NaHCO_3$ solution. Effect of ethanol concentration (0.10-0.25 mol), $NaHCO_3$ concentration (0.005-0.025 mol), and catalyst content (0.005-0.015 mol) were compared at 200°C for 3 days. It was found that the optimized hydrothermal reaction conditions were 0.15 mol of ethanol, 0.01 mol of $NaHCO_3$, and 0.005 mol of Co powder. The effects of the reaction time (1-30 days) and reaction temperature (140-240 °C) were also investigated. It was found that the 1-butanol was increased with reaction time and then remained constant at 9.8 mol% after 20 days. However, the selectivity to 1-butanol was decreased from 74% to 62% from 1 to 30 days. In addition, the variation of reaction temperature showed that yield of 1-butanol (1.2 to 5.5 mol%) was increased with temperature (140 to 240°C). The selectivity to 1-butanol was increased from 50% to 74% when the reaction temperature was increased from 140 to 180°C and remained constant.

T. Tsuchida, *et al* [45] investigated the effect of Ca/P ratio of hydroxyapatite on the conversion of ethanol. The catalysts were prepared by precipitation method using calcium nitrate ($Ca(NO_3)_2$) and diammoniumhydrogenphosphate ($(NH_4)_2HPO_4$) solutions as reactants. The Ca/P ratio was controlled by controlling the pH of the mixture (7, 9, 10 and 10.5). The results showed that hydroxyapatite gave low catalytic activity (20% conversion at 300°C). However, hydroxyapatite with higher Ca/P ratio provided higher

selectivity to C4-C8 alcohols, as compared to those with lower Ca/P ratio at the same level of conversion. It was also reported that the basicity came from the presence of Ca^{2+} ions. Hydroxyapatite with the Ca/P ratio of 1.67 presented the highest selectivity to higher alcohols (~70%).

S. Totong, *et al* [46] studied the hydrogen production from catalytic dehydrogenation of ethanol at relatively low temperature (<500°C). Copper (Cu) silver (Ag) and bimetallic catalysts (Ag-Cu) supported on silica (SiO_2) were compared at 300-375°C. The hydrogen production from ethanol dehydrogenation using bimetallic catalyst (Ag-Cu/SiO_2) was found to be higher than that over monometallic catalyst (Cu/SiO_2 and Ag/SiO_2). However, the hydrogen yield is decreased due to decomposition of ethanol to light gases.

The effect of zinc addition on copper catalysts for dehydrogenation of isoamyl alcohol was studied by Ching-Yeh Shiau, *et al* [47]. The reaction was carried out at atmospheric pressure in a fixed bed reactor at the temperature range of 230–290°C. The catalysts were prepared by sequential impregnation of Cu and then Zn on SiO_2 with a Cu loading of 10 wt.%. The Zn loading on Cu was varied from 0 to 5 wt.%. It was found that the addition of zinc (5%) into copper catalyst can increase both activity and stability.

E. V. Makshina, *et al* [48] studied the conversion of ethanol to 1,3-butadiene over MgO-SiO_2 catalysts. The catalysts were doped with various metal oxides e.g. CuO ZnO and metallic Ag. The experiments were performed at temperature range of 350–400°C. The results showed that at 350°C, undoped MgO-SiO_2 did not provide satisfying 1,3-butadiene yields of 14.5 mol% with ethylene yields of 11.8 mol% at the 37.0% conversion. The metal and metal oxide doped MgO-SiO_2 catalysts showed a significantly improved 1,3-butadiene yields (60%) and the conversion was significantly boosted to almost 100%. The butadiene selectivity was increased from 39% to 53-60%. The ethylene yields and selectivity was decreased from 11.8 mol% to 5.5-6.2 mol% and from 32% to 6%, respectively. This was due to the enhanced dehydrogenation rate by the incorporated metal oxide and metal on MgO-SiO_2.

In addition, Vitaly L. Sushkevich, *et al* [49] studied the effect of metal (Ag, Cu, Ni), (0.3-2 wt.%). metal oxide (Al_2O_3, ZrO_2, TiO_2), (1-18 wt.%) supported on SiO_2 on the conversion of ethanol to 1,3-butadiene. Kinetic study suggested that the key reaction steps of butadiene synthesis include five consecutive reaction steps: (i) ethanol dehydrogenation into acetaldehyde; (ii) aldol condensation of acetaldehyde; (iii) dehydration of 3-hydroxybutanal; (iv) MPV of crotonaldehyde with ethanol; and (v), dehydration of crotyl alcohol to butadiene. The optimized catalyst contained 1 wt.% silver and 10 wt.% zirconia on silica providing butadiene selectivity to 74 mol% with 88% ethanol conversion at 593 K.

Chapter 3

Experimental

3.1 Chemicals and substrates

Chemical	Grade of purity	Manufacturers
1. Silver nitrate ($AgNO_3$)	99.6%	BAKER ANALYZED (A.C.S. REAGENT)
2. Nickel nitrate hexahydrate ($Ni(NO_3)_2 \cdot 6H_2O$)	99%	CARLO ERBA
4. Copper nitrate trihydrate ($Cu(NO_3)_2 \cdot 3H_2O$)	99.5%	CARLO ERBA
5. Zinc nitrate hexahydrate ($Zn(NO_3)_2.6H_2O$)	98%	TECHNICAL
6. Iron nitrate nonahydrate ($Fe(NO_3)_3.9H_2O$)	98.5%	QRëC
7. Absolute ethanol (CH_3CH_2OH)		CARLO ERBA
8. Sillicon dioxide (SiO_2)		CARLO ERBA
9. NH_4^+-ZSM-5 (Si/Al = 28, 40, 140, 250, 500)		ZEOLYST INTERNATIONAL
10. Deionized water		
11. Air zero gas, high purity	99.99%	PRAXAIR
12. Hydrogen gas, high purity	99.99%	PRAXAIR
13. Nitrogen gas, high purity	99.99%	PRAXAIR

3.2 Apparatus and instruments.

1. Catalytic testing rig
2. Mass flow controller (AALBORG)
3. Hot air oven
4. Tube furnace with a programmed temperature controller (CARBOLITE)
5. Heating tape with a programmed temperature controller
6. Clamp

7. Gas chromatograph (Model 910, BUCK SCIENTIFIC)
8. Laboratory glassware
9. Laboratory plasticware
10. Trap condenser
11. Syringe (10 ml)
12. Syringe pump
13. Vial
14. Sieve (U.S.A standard sieve, AASHO N-92)
15. X-ray powder diffractometer (D8 Advance, Bruker AG)
16. X-ray fluorescence spectrometer (Wavelength Dispersive, Philips, PW2400, Scientific and Technological Research Equipment Centre 2-3 Building, Chulalongkorn University) and (Energy Dispersive, Oxford, ED-2000, Scientific and Technological Research Equipment Centre 2-3 Building, Chulalongkorn University)
17. Gas adsorption analysis (Autosorb-1C, Quantachrome)
18. Temperature programmed reduction (TPR, Model TCD2-NIFED)
19. Temperature programmed desorption (TPD, Model TCD2-NIFED)
20. Transmission electron microscopy (TEM, Model JEM-2100)
21. Thermogravimetric analyzer (Perkin-Elmer, Scientific Instrument Service Center, KMITL)
22. Inductively coupled plasma mass spectrometry (ICP-MS, Model iCAP Qc)

3.3 Catalyst preparation

3.3.1 Metal supported on silica catalysts (M/SiO_2)

The metal supported silica (SiO_2) catalysts (10 grams) with different type of loaded metals (Ag, Cu and Cu alloy) were prepared by wet impregnation method.

In the first step, 10 %wt. silver supported on silica (Ag/SiO_2) was impregnated using silver nitrate ($AgNO_3$) solution as a metal precursor. Detail of precursor preparation are shown in Table 3.1. In a similar procedure, 10%wt. copper on silica was prepared by impregnation using $Cu(NO_3)_2{\cdot}3H_2O$ solution.

For the 12%wt copper metal alloys, Cu-Ni, Cu-Fe, Cu-Ag, Cu-Zn alloys on SiO_2 were prepared by co-impregnating using $Cu(NO_3)_2{\bullet}3H_2O$, $Ni(NO_3)_2{\bullet}6H_2O$, $Fe(NO_3)_3.9H_2O$, $AgNO_3$ and $Zn(NO_3)_2.6H_2O$ solution, respectively. The solid was dried in an oven at 80°C for 24 h. The prepared catalyst was calcined in a horizontal tube furnace under a flow

of air zero (60 mL/min) at 450°C, with a heating rate of 10°C/min and hold at that temperature for 5 h. Finally, the catalyst was pressed, crushed, and sieved into 600-850 μm pallet.

Table 3.1 Preparation of metal supported on silica catalysts.

Catalyst	Metal precursor	Weight of metal procure (g)	Deionization Water (mL)	Weight of SiO_2 (g)
10%wt. Ag/SiO_2	$AgNO_3$	1.5975	9.2	9.08
10%wt. Cu/SiO_2	$Cu(NO_3)_2 \cdot 3H_2O$	3.8420	16	9.01
10%wt. Cu-2%wt. Zn/SiO_2	$Cu(NO_3)_2 \cdot 3H_2O$ $Zn(NO_3)_2.6H_2O$	3.8487 0.9306	19	8.97

3.3.2 The incorporated metal on H-ZSM-5 (Ni, Cu, and Zn/H-ZSM-5)

The incorporated metal on H-ZSM-5 catalyst was prepared by aqueous phase ion-exchange method. In the first step, nickel, copper or zinc precursors were dissolved in deionized water, then the NH_4^+-ZSM-5 (4g) was stirred in 0.5 M $Ni(NO_3)_2 \cdot 6H_2O$ solution (100mL) at 70 °C for 12 h for example. After that, the ion-exchanged sample was washed with excess deionized water. The catalyst was dried in an oven at 80°C for 24 h. Then, the dried catalyst was calcined in a horizontal tube furnace under a flow of air zero (60 mL/min) at 550°C for 5 h with a heating rate at 2°C /min.

3.4 Characterization of catalysts

3.4.1 X-Ray powder diffraction

The structure of catalyst was determined by X-ray diffractometer (XRD). The sample was prepared by packing the catalyst into the sample holder. CuKα X-ray beam was used for analysis at 40 kV and 30 mA. The sample was scanned over the angle ranged from 2θ: 5° to 90° with 2 deg./min. and 0.02 2θ/step increments. X-ray diffraction pattern of the sample was compared with the X-ray diffraction pattern of standard catalyst for structure determination.

3.4.2 X-ray fluorescence

The chemical composition of a catalyst was analyzed by a wavelength-dispersive X-ray fluorescence spectrophotometer (WD-XRF), Bruker, Tiger. Approximately 0.5 g of a catalyst was mixed with 4.5 g of boric acid. The mixture was then manually grinded, and compressed into a pellet. The data was recorded by X-ray source and quantitative calculated by theoretical formulas.

3.4.3 Surface area analysis

Surface area of the catalyst was determined by surface area analyzer. The sample was prepared by weighing approximately 40-50 mg of sample and loaded into a cleaned and dried sample cell. After that, the sample was degassed at the out-gas station at 350°C for 24 hours. The sample cell was then removed from the out-gassing station after nitrogen was filled and was attached to the analysis station. The adsorption isotherm was measured in a pressure range of 0.05-0.30 P/P_0 at -196°C.

3.4.4 Temperature programmed reduction

Temperature-programmed reduction (TPR) provides information on the active site species of the catalysts by monitoring their reducibility. Temperature programmed reduction was measured using thermal conductivity detector (TCD). The sample weighed 2.5 mg was placed into a quartz tube reactor, which was located inside a temperature-regulated furnace. Prior to the H_2-TPR, each sample was heated to its activations temperature in air zero (30 ml/min) for 1 h with 10°C /min (2°C/min for H-ZSM-5) and was cooled down to below 40°C. The heating rate of 10°C/min, 30 ml/min of 10% H_2 in Ar was applied for TPR analysis. Water production during the reduction process was removed in a U-shape glass trap at -196°C (liquid nitrogen) before entering the TCD.

3.4.5 Temperature programmed desorption

Acid sites of the catalysts were evaluated on the basis of temperature-programmed desorption of ammonia (NH_3-TPD). Samples were pretreated by activations at 450°C under a flow of Air-Zero (30 ml/min) with 2 °C/min for an hour and reduction at 400°C under a flow of H_2 (30 ml/min) for 3 hours in order to reduce metal cation to metal, then NH_3 was introduced at a flow rate of 50 ml/min at 30°C for 1 h.

The physisorbed NH_3 was removed at 30°C by He for 1 h. After that, the NH_3-TPD profiles were obtained by heating sample at a rate of 10°C /min in a flow of He (30 ml/min).

3.4.6 Transmission Electron Microscopy (TEM)

Transmission electron microscope (TEM) is the commonly applied for studying supported catalysts. It is used to investigate the morphology, structure, and dispersion of metal in the catalysts. TEM uses a beam of highly energetic electron (voltage 80-120 kV) and signals from TEM depending on the sample density and thickness. Electrons that passes through the sample without energy loss it shows bright filed image and electrons are diffracted (scattered) by particles obtain dark-field images at magnification of 100,000 – 120,000x.

3.4.7 Thermogravimetric Analysis (TGA)

The coke deposit of samples was measured by thermogravimetric analyzer (Pyris). Approximately 15 mg of samples was loaded to the platinum plan, after which the exact mass was recorded by the instrument. The sample was then heated from temperature 50 °C to 900 °C at the heating rate of 10 °C/min under the flow of Air Zero atmosphere (20 mL/min). The mass of the sample as the function of temperature was recorded.

3.4.8 Inductively Coupled Plasma Mass Spectrometry (ICP-MS)

Inductively coupled plasma mass spectrometry (ICP-MS) was used to determine the metal loading amount. ICP-MS was performed on a Thermo Scientific iCAP Qc ICP-MS. An accurate 100 mg of sample was weighed and then digested with aqua regia solution [36]. Then, sample solvents were evaporated, and the organic components were removed by heating at 625 °C for several hours and analyzed by ICP-MS. The flow rate on the instrument was 1 mL/min and dual detector mode was employed. A blank was subtracted after internal standard correction and the value reported are an average of three reading.

3.5 Catalytic testing

Gas phase catalytic conversion of ethanol was investigated at atmospheric pressure in a continuous fixed-bed reactor made with glass tube (8.0 mm O.D.). Schematic of the catalytic testing rig is shown in Figure 3.1. The single bed system (H-ZSM-5 or M/SiO_2) was packed in the middle of the reactor and sandwiched with glass wool and glass beads. While the double bed system (M/SiO_2 and H-ZSM-5), the M/SiO_2 was packed on top of the H-ZSM-5 bed, both catalysts were packed in the middle of the reactor and again sandwiched with glass wool and glass beads, likewise with the single bed system. The reactor was then installed inside a temperature-controlled electrical furnace. The gas flows were controlled by the mass flow controllers and checked by bubble flow meter. Before the catalytic testing, the catalyst was activated by heating at 10°C/min (2°C/min for H-ZSM-5) to 450°C and hold at that temperature for 1 h under the stream of air (100 mL/min). Then N_2 was flowed to eliminate the remaining air in the line. Finally, the gas stream was switched to a flow of H_2 gas for reduction with a heating of 5°C/min to 400°C and hold for 3 h. After that the reaction was run at 400°C for 6 h.

In each run, ethanol was passed through the catalyst bed under a 166 ml/min flow of H_2. The catalytic testing was continued for at least 6 h on stream. The reacted gaseous mixture was flowed out of the reactor and passed through a gas sampling loop. In order to prevent condensation of products, the line after reactor was heated by heating tape. Description of the reactor set up and the reaction conditions are summarized in Table 3.2

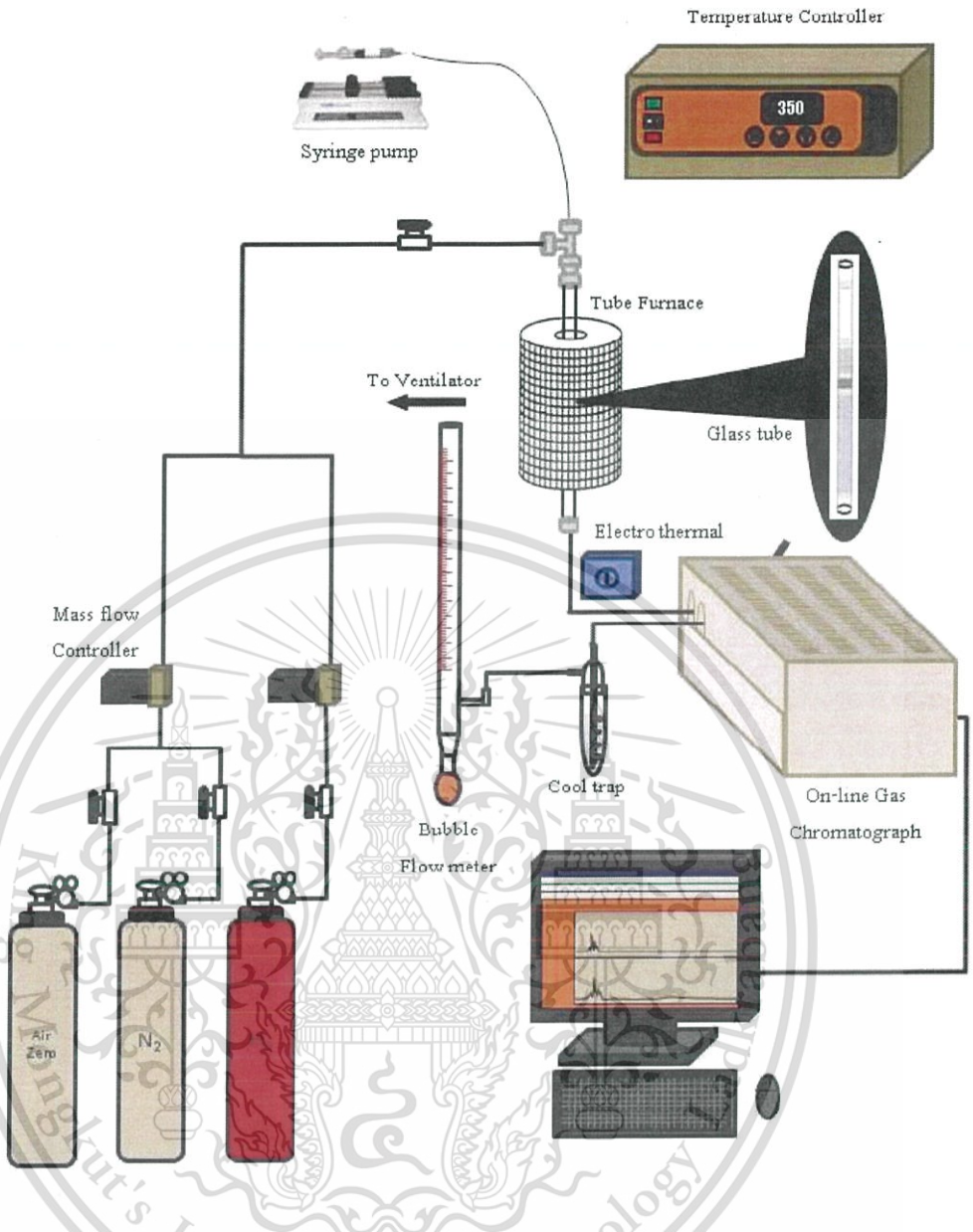

Figure 3.1 Schematic of the catalytic testing rig.

Table 3.2 Description of the reactor set up and the reaction condition.

Parameters	Value
Reactor outside diameter (mm)	8
Bed length (mm)	10-30
Total flow (ml/min)	166
Catalyst weight (g)	0.18-0.35
Contact time: W/F (g.h/mol)	15-42
Catalyst pallet size (μm)	600-850
Catalyst activation (before reaction)	Heating rate: 10°C/min (2°C/min for H-ZSM-5) Calcination temperature: 450 °C Gas: air zero (100 ml/min)
Catalyst reduction (before reaction)	Heating rate: 5 °C/min Reduction temperature: 400 °C and 500 °C Gas: Hydrogen (100 ml/min)
Reaction temperature (°C)	400-500 °C
Total reaction pressure	Atmospheric pressure (1 atm)

3.6 Products analysis

The product analysis was generally performed using an online gas chromatograph. The gas sample was collected in gas sampling loop, then periodically injected into GC column (Equity-1, 30 m length, 0.53 mm internal diameter, 5 μm film thickness) connected to flame ionized detectors (FID). The following temperature program was used for the analysis: holding at 33°C for 5 min, followed by the ramping to 85°C at the rate of 15°C/min. holding for 2 min., then ramping to 220°C at rate of 10°C/min., before a final holding at that temperature for 3 min. N_2 was used as a carrier gas (linear velocity~40cm/sec). Each component was separated as passed though the column with an inert carrier N_2 gas and their presence in the effluent were recorded as a chromatogram. Each peak area from the chromatogram was measured and calculated. Then each peak was identified by comparing with standard and the composition of each product was determined by normalization.

Chapter 4

Results and discussion

4.1 Characterization

4.1.1 X-ray Diffraction (XRD)

X-ray powder diffraction pattern of all catalysts, including Cu, Cu-Ag, Cu-Ni, Cu-Fe and Cu-Zn loaded on SiO_2, after calcined and reduced were determined by XRD technique. The X-ray powder diffraction patterns of the metal supported on silica catalysts are shown in **Figure 4.1**.

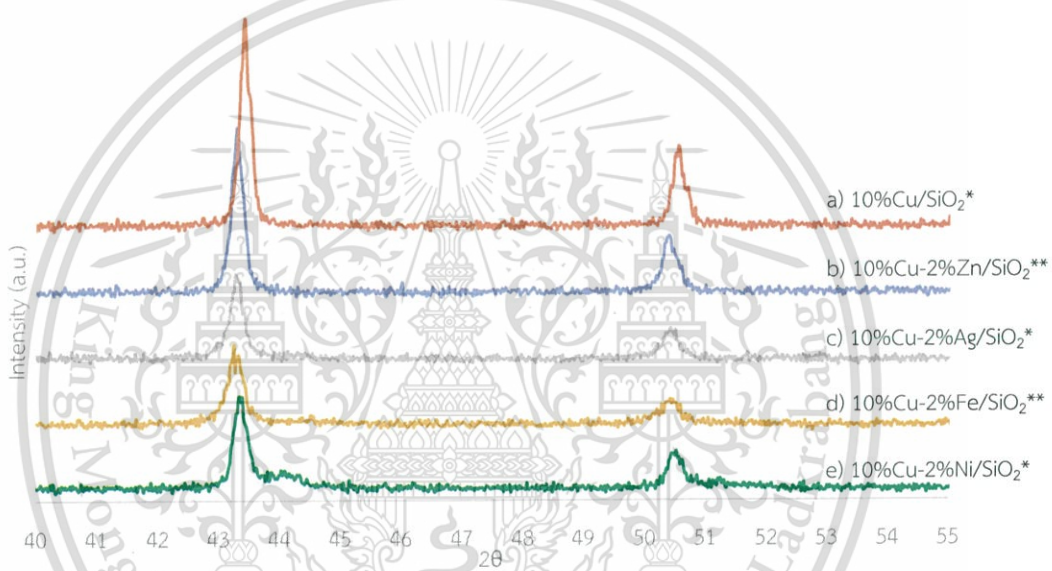

Figure 4.1 XRD pattern of a) 10%Cu/SiO_2, b) 10%Cu-2%Zn/SiO_2, c) 10%Cu-2%Ag/SiO_2, d) 10%Cu-2%Fe/SiO_2, e) 10%Cu-2%Ni/SiO_2.

(*calcined 450°C reduced 400°C, **calcined 450°C and reduced 500°C)

All catalysts show a broad peak at 2θ around 22° attributed to amorphous silica as shown in Appendix A1. **Figure 4.1a**, Cu/SiO_2 showed the diffraction peak at 43.4° and 50.6°, which are attributed to Cu metal phase dispersed on silica [47, 50, 51]. For XRD pattern of bimetallic, Cu-Zn (**Figure 4.1b**) revealed diffraction peaks at 43.3° and 50.4° that slightly shift to lower 2θ. No reflection assigned to ZnO or metallic Zn was observed in this catalyst. The shift of metal phase and lack of separated Zn phase indicates that Cu and Zn were successfully alloyed to bimetallic Cu-Zn phase, likewise with Cu-Ag as shown in **Figure 4.1c** [52, 53]. For bimetallic Cu-Fe, the catalyst showed diffraction peaks at 43.2°, 43.3°, and 50.4° (**Figure 4.1d**). The first peak indicated to

diffraction peak of Fe_2O_3 [54]. While the peaks at 43.3° and 50.4° slightly shift to lower 2θ, in a manner similar to the bimetallic Cu-Zn and Cu-Ag. It suggests that some Fe can be alloyed with Cu. While the diffraction peaks of Cu-Ni are not changed significantly when compared with Cu/SiO_2. However, the phase diagram of Cu-Ni alloy shows that 83 wt%. Cu and 17 wt%. Ni composition can be completely formed to Cu-Ni alloy phase (Appendix A8).

4.1.2 Elemental Analysis and Gas Adsorption

The elemental composition of the catalysts was determined by X-ray fluorescence spectroscopy (XRF). The specific surface area of the catalysts was determined by N_2 gas adsorption using BET method. The results are shown in **Table 4.1**.

Table 4.1 Elemental analysis and gas adsorption characteristics of catalysts.

Catalysts	$^aS_{BET}$ (m^2/g)	Metal loading (wt%.)					Hydrogon consumption (mmol/g)
		Cu.	Zn	Ag	Fe	Ni	
SiO_2	319	-	-	-	-	-	-
Cu/SiO_2	229	7.8[b]	-	-	-	-	1.8
Ag/SiO_2	206	-	-	12.0[b]	-	-	0.05
$Cu\text{-}Zn/SiO_2$	244	7.8[b]	1.9[b]	-	-	-	1.83
$Cu\text{-}Ag/SiO_2$	213	7.4[b]	-	0.9[b]	-	-	1.53
$Cu\text{-}Fe/SiO_2$	243	9.8[b]	-	-	2.0[b]	-	1.22
$Cu\text{-}Ni/SiO_2$	233	7.3[b]	-	-	-	1.8[b]	1.31
H-ZSM-5(28)	479	-	-	-	-	-	-
Cu/H-ZSM-5 (28)	350	0.8[c]	-	-	-	-	0.1
Ni/H-ZSM-5 (28)	408	-	-		-	0.5[c]	0.09
Zn/H-ZSM-5 (28)	429	-	1.4[c]	-	-		-

[a] Determined by BET

[b] Determined by XRF

[c] Determined by ICP-MS

It can be seen that monometallic content (Cu and Ag) in the catalysts is similar to the expected loading; that is 10 wt%. In the case of bimetallic catalysts, Cu content was fixed to 10 wt%. and the secondary metal (Ag, Zn, Fe and Ni) was imposed at 2

wt%. However, a variation of the loading obtained may be accounted for the deviated concentration of the metal precursor during preparation.

Silica support shows relatively high surface area of 319 m^2/g. The surface area of all 10 wt%. monometallic and 12 wt%. bimetallic supported catalysts are obviously decreased upon metal loading. Again, metal supported H-ZSM-5 shown lower surface area (350-429 m^2/g), as compared with H-ZSM-5 (479 m^2/g). However, all catalysts exhibit comparatively high surface area.

4.1.3 Temperature program reduction (TPR)

Reducibility of Cu/SiO_2, $Cu\text{-}Fe/SiO_2$, $Cu\text{-}Ag/SiO_2$, $Cu\text{-}Zn/SiO_2$ and $Cu\text{-}Ni/SiO_2$ catalysts were investigated by H_2-temperature programmed reduction (H_2-TPR). The H_2-TPR profiles of those catalysts prepared by impregnated and co-impregnation method are shown in **Figure 4.2.**

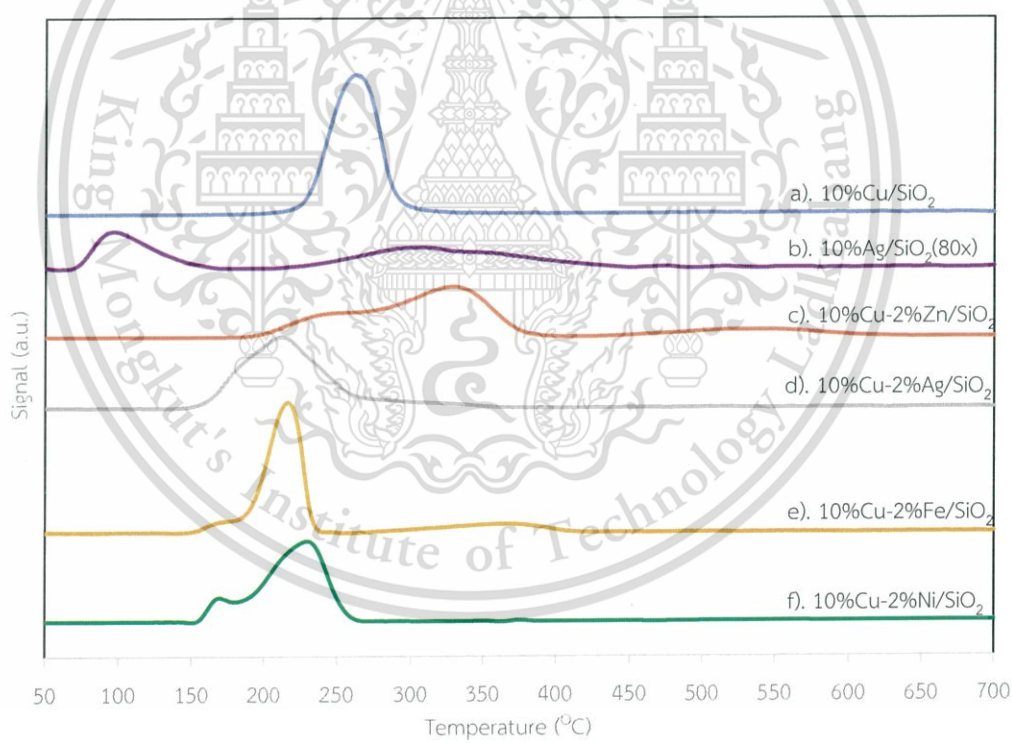

Figure 4.2 TPR profile of a) $10\%Cu/SiO_2$, b) $10\%Ag/SiO_2$, c) $10\%Cu\text{-}2\%Zn/SiO_2$, d) $10\%Cu\text{-}2\%Ag/SiO_2$, e) $10\%Cu\text{-}2\%Fe/SiO_2$. f). $10\%Cu\text{-}2\%Ni/SiO_2$.

As seen from **Figure 4.2a** the reduction of Cu^{2+} to metallic Cu take places as a single peak at 270 °C. For Ag/SiO_2 catalyst (**Figure 4.2b**), the TPR shows reduction peak at 100 °C and a broad peak at 300 °C represents the reduction of Ag^+ to Ag cationic cluster and such cationic cluster to metallic Ag, respectively [55].

For $Cu-Zn/SiO_2$ bimetallic catalyst (**Figure 4.2c**), two reduction peaks also reveal at 254 °C, 336 °C. The first peak is attributed to the reduction of a small particle of CuO [47], and the second peak is suggested that the reduction of CuO-ZnO to Cu-Zn alloy. This is consistent with XRD result discussed previously. While the broad peak around 450-600 °C is consistent with the reduction of Cu^+ to metallic Cu that requires high reduction temperature [56].

For $Cu-Ag/SiO_2$ catalyst (**Figure 4.2d**), the H_2 consumption shows a broad peak around 219 °C that is referred to the reduction of $CuO-Ag_2O$ to bimetallic Cu-Ag [46]. This indicated interaction between Cu and Ag in this catalyst in consistent with XRD result.

For $Cu-Fe/SiO_2$ catalyst demonstrate two reduction peaks at 176 °C and 221 °C, corresponding to the reduction of high dispersed of CuO and bulk CuO, respectively [57, 58]. In addition, these peaks shift to low temperature, as compared with Cu/SiO_2 catalyst (**Figure 4.2e**). This is because, when the Fe is added to Cu/SiO_2 catalyst, a small particle of CuO is generated. Moreover, the broad peak at 250-400°C is assigned to the reduction of Fe_2O_3 to metallic Fe [56, 57]. In line with XRD (**Figure 4.1d.**), this suggests that Fe_2O_3 is retained in the catalyst and the actual amount of Fe alloying with Cu could be lower than the expected concentration.

In the case of Cu-Ni catalyst, two reduction peaks at 174 °C and 235 °C are observed (**Figure 4.2f**). The first peak is assigned to the reduction of a small particle of CuO, in a manner similar to the case of $Cu-Fe/SiO_2$. While the second peak suggests the reduction of CuO-NiO to Cu-Ni alloy as also evidenced by XRD. From **Table 4.1**, the monometallic (Cu and Ag) showed H_2 consumption at 1.8 and 0.05 mmol/g, respectively. While the bimetallic metal showed hydrogen consumption varies from 1.22-1.83 mmol/g.0

In the case of metal loaded H-ZSM-5 (M/H-ZSM-5, M=Ni, Cu, Zn), the catalysts were prepared by ion exchange method. The reducibility of these catalysts is shown in **Figure 4.3**.

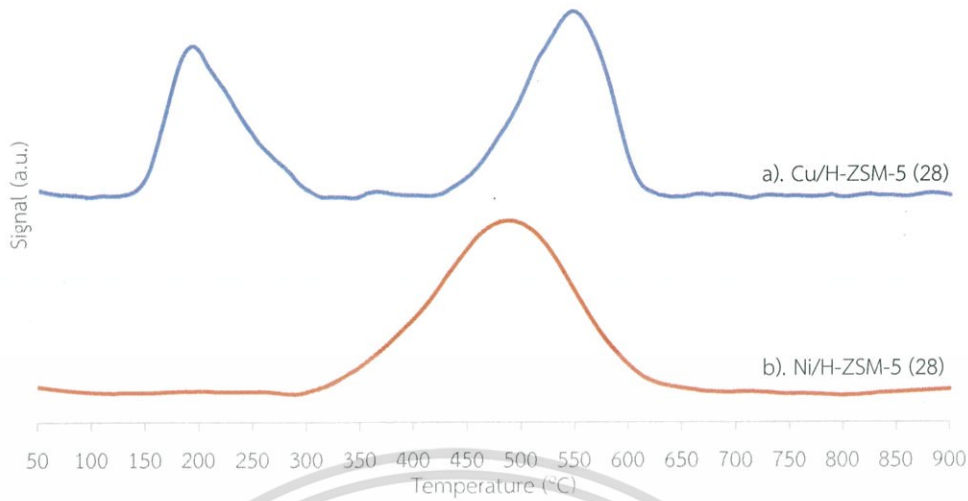

Figure 4.3 TPR profile of metal ion exchange a) Cu/H-ZSM-5, b) Ni/H-ZSM-5.

The H_2-TPR profile of Cu/H-ZSM-5 show a reduction peak of CuO aggregates at 200 °C and another peak at 550 °C indicating the reduction of charge balancing Cu ion in H-ZSM-5 [59, 60, 61]. While NiO over H-ZSM-5 shows single broad reduction peak at 500 °C. The reducibility of exchangeable Ni cation was lower, as compared to typical of NiO (~400 °C). This is because the Ni ion strongly interacts with the negative framework charge and thus highly dispersed as small nanoparticles as shown by TEM image (**Figure 4.4**).

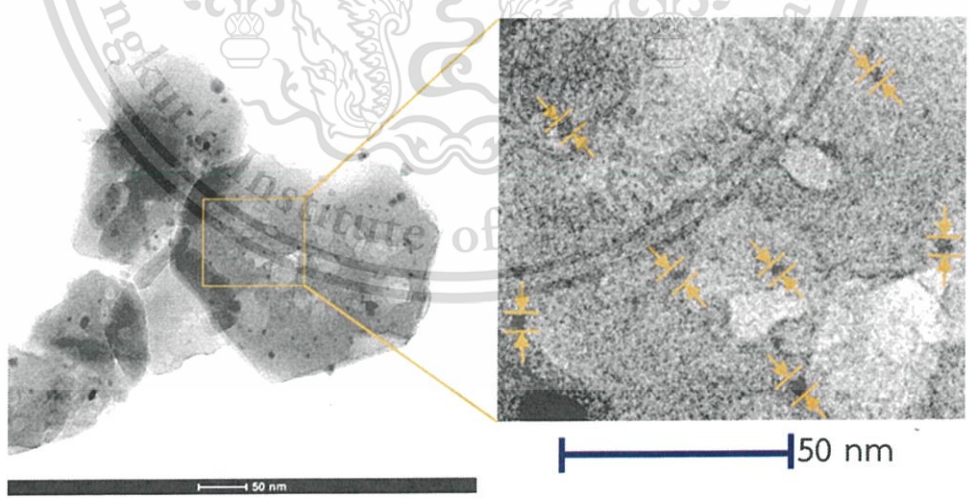

Figure 4.4 TEM image of Ni/H-ZSM-5.

It can be seen from TEM that, the Ni/H-ZSM-5 shows a high dispersion of Ni particle size of approximately 5 nanometers diameter (right image). Some of Ni particles are well aligned in the pore of H-ZSM-5 (as also shown in Appendix A6). The Cu and/or Ni loaded H-ZSM-5 revealed the same H_2 consumption of at 0.1 mmol/g. While Zn over H-ZSM-5 cannot be completely reduced at 900 °C [72].

4.2 Understanding the production of hydrocarbons from ethanol

The production of hydrocarbons from ethanol over acid catalyst (H-ZSM-5) was tested at contact time of 10-42 g.h/mol, 400°C as shown in **Figure 4.5.**

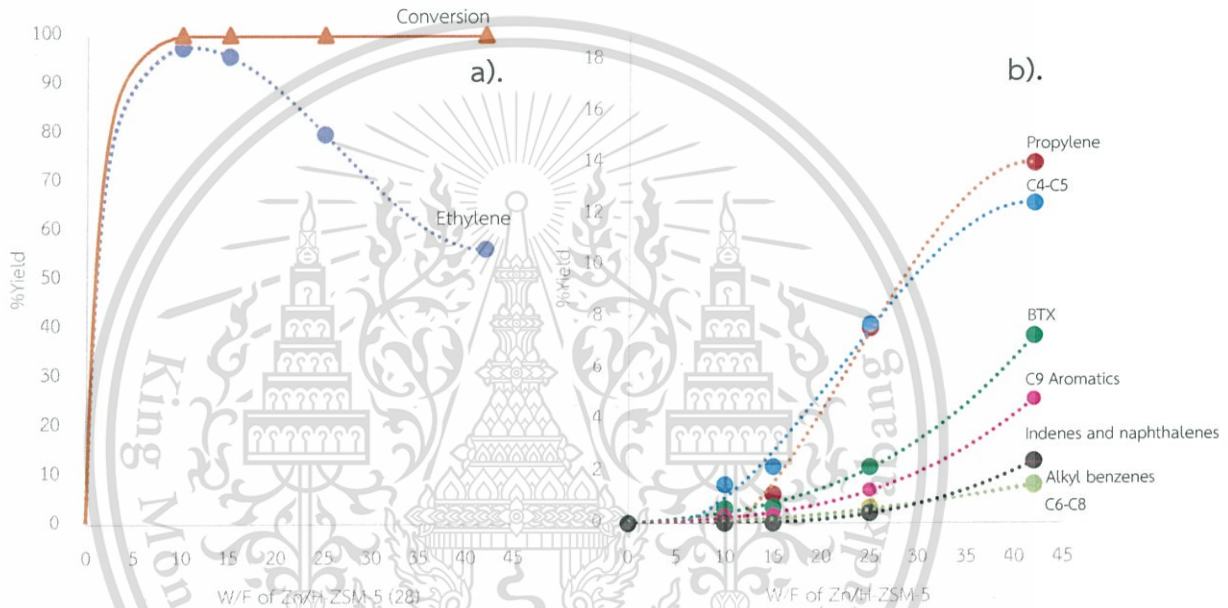

Figure 4.5 Product distribution from ethanol conversion over H-ZSM-5 (28).
a). Conversion and ethylene yield, b). Minor products yield
(Reaction temperature; 400°C, Feed rate; 0.0085 mol/h of absolute ethanol,
Contact time; 10-42 g.h/mol.)

It can be seen that the 100% conversion of ethanol is observed over H-ZSM-5 (28). Only ethylene was produced via dehydration of ethanol at low contact time. Ethylene cannot be converted to higher hydrocarbons at low contact time because the rate of ethylene oligomerization is relatively slow, as compared to the rate of dehydration. This is presumably because the direct ethylene protonation leads to formation of unstable primary carbocation. As the contact time is increased, ethylene is notably decreased, while the higher hydrocarbons including light hydrocarbons (C3-C5), BTX aromatics, C6-C8, C9 aromatics, alkylbenzenes, indenes, and naphthalenes are

observed. The light hydrocarbons (C3-C5) is significantly increased at higher contact time (~25 g.h/mol). While the higher hydrocarbon (BTX aromatics, C6-C8, C9 aromatics, alkylbenzenes, indenes, and naphthalenes) are pronounced at contact time of 42 g.h/mol. This suggests that the ethylene initially oligomerizes to C4-C6 hydrocarbons at low contact time (10-15 g.h/mol). The C4-C6 hydrocarbons successively crack to propylene at higher contact time. The higher hydrocarbons are produced from propylene that undergoes alkylation, isomerization, cyclization, and aromatization at high contact time (25-42 g.h/mol), as typically observed for acid zeolite (hydrocarbon pool mechanism) [9, 62, 63, 64] as shown in **scheme 14**.

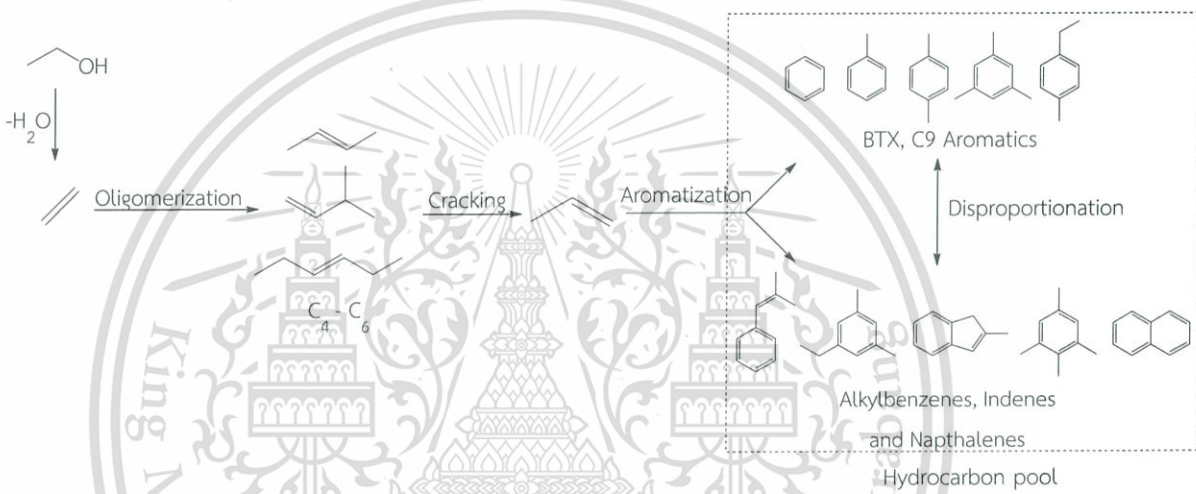

Scheme 14. Conversion of ethanol to hydrocarbons over H-ZSM-5 (28).

As ethylene oligomerization initially proceeds via the formation of primary carbocation that is thermodynamically unfavorable, the direct conversion of ethylene to hydrocarbons only acid site is not feasible. Hence, to improve ethanol conversion to higher hydrocarbons, the metal bed was added on top of the acid bed, in order to virtually convert ethanol to acetaldehyde prior to entering the acid bed. The product distribution from the reaction over a double bed system of Ag/SiO_2 and H-ZSM-5 (28) were compared with a single bed of H-ZSM-5 (28) as shown in **Table 4.2.**

Table 4.2 Product distribution of conversion of ethanol over single bed of H-ZSM-5 (28) catalyst compared with double bed of Ag/SiO_2(top) and H-ZSM-5(bottom) catalysts.

Catalysts	%Conversion	%Yield									
		Methane	Ethylene	Propylene	Acetaldehyde	C4-C5	BTX	C6-C8	C9 Aromatics	Alkylbenzees	Indenes & naphthalenes
H-ZSM-5 (28)	100	-	92.8	1.4	-	2.6	1.7	0.2	1.3	-	-
Ag/SiO_2 and H-ZSM-5 (28)	100	1.5	-	1.7	6.2	0.1	7.6	0.2	12.4	5.0	65.3

(Reaction temperature; 400°C, feed rate; 0.0085 mol/h of absolute ethanol, single bed of H-ZSM-5 ; contact time; 15 g.h/mol. double bed of Ag/SiO_2+H-ZSM-5; contact time of Ag/SiO_2; 60 g.h/mol and contact time of H-ZSM-5; 15 g.h/mol)

The result shows that the double bed system gives higher selectivity to BTX, C9 aromatics, alkylbenzenes, indenes, and naphthalenes. While the only ethylene and small amounts of hydrocarbons (C3-C9) were observed over a single bed of H-ZSM-5 (28) at the same contact time. It is suggested that the reaction pathway for ethanol to hydrocarbons over the double bed system is not similar to that over the single bed of H-ZSM-5 (28). In the single bed of H-ZSM-5 (28), the hydrocarbons are produced from protonation of ethylene and then oligomerization (hydrocarbons pool) as discussed earlier. While over the double bed system, the ethanol is dehydrogenated to acetaldehyde over the first bed. The acetaldehyde then undergoes aldol condensation/deoxygenation in the second bed. It is suggested that the rate of aldol condensation (of acetaldehyde) is faster than the rate of oligomerization (of ethylene). This is because the acetaldehyde can be protonated over H-ZSM-5 to form enol or an enolate intermediate. Such intermediate is much more stable than the primary carbocation intermediate formed by protonation of ethylene.

However, the methane is observed over Ag catalyst, presumably produced from decarbonylation of ethanol over Ag/SiO_2. From previous research [65], Cu/SiO_2 gives high activity for dehydrogenation of ethanol to acetaldehyde while decarbonylation of ethanol is suppressed, as compared to Ag/SiO_2. Hence, the Cu based catalyst is chosen for the top bed in further study (**Figure 4.6**).

4.3 Dehydrogenation of ethanol to acetaldehyde over Cu supported SiO_2

In order to enhance the hydrocarbons yield via the aldol condensation /deoxygenation of acetaldehyde, The Cu based catalyst (top bed) should provide high activity in ethanol dehydrogenation and high selectivity to acetaldehyde. Hence, the dehydrogenation of ethanol was primarily investigated over the single bed of Cu catalyst for the effect of carrier gas, temperature, type of metal alloyed, and contact time.

4.3.1 Effect of carrier gas

The effect of carrier gas on ethanol conversion over Cu/SiO_2 catalyst was investigated as shown in **Figure 4.6.**

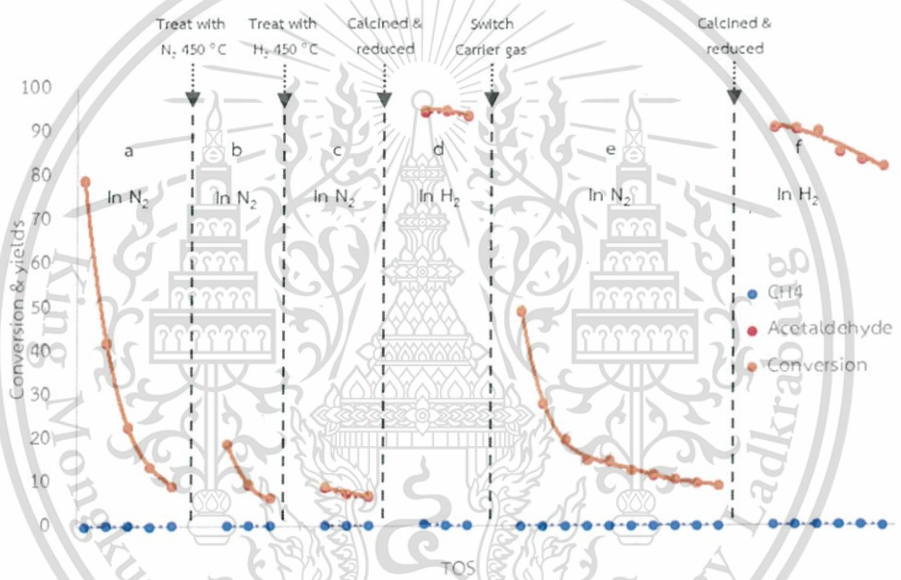

Figure 4.6. Dehydrogenation of ethanol over Cu/SiO_2 a) calcined in N_2 at 450 °C with N_2 as a carrier gas; b) treated under N_2 at 450 °C, carrier gas N_2; c). treated under H_2 at 450 °C, carrier gas N_2; d) regenerated catalyst, carrier gas H_2, e) carrier gas N_2, f) regenerated catalyst, carrier gas H_2.

(Reaction temperature; 400°C, Feed rate; 0.012 mol/h of absolute ethanol, Contact time; 30 g.h/mol.)

It can be seen that (**Figure 4.6 section a**) ~80% conversion of ethanol is initially observed with higher than 99.6% selectivity to acetaldehyde over Cu/SiO_2 catalyst under N_2 flow. However, a severe deactivation is observed over this catalyst. This deactivation is not derived from the sintering according to transmission electron micrographs (**Figure 4.7**).

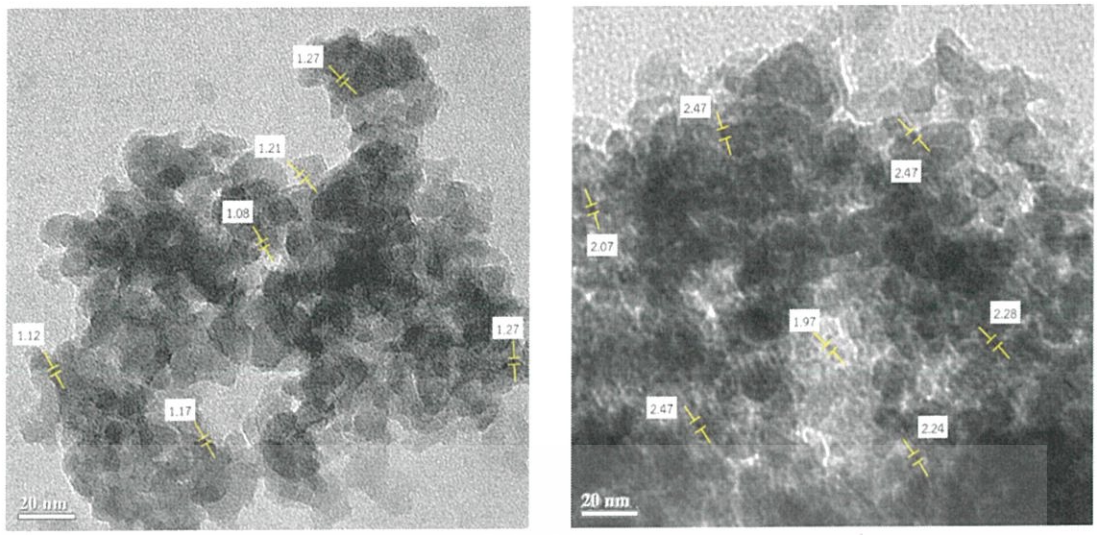

Figure 4.7 TEM images of Cu/SiO_2: (a) fresh catalyst, (b) spent catalyst.

It can be seen that the Cu particle size of the spent catalyst remains intact, as compared to the fresh one. Alternatively, cause of deactivation may well resulted from coke formation. However, the TGA of the spent catalyst shows no weight loss. In turn, the catalyst weight is increased at temperature range 200-400 °C as shown in **Figure 4.8.**

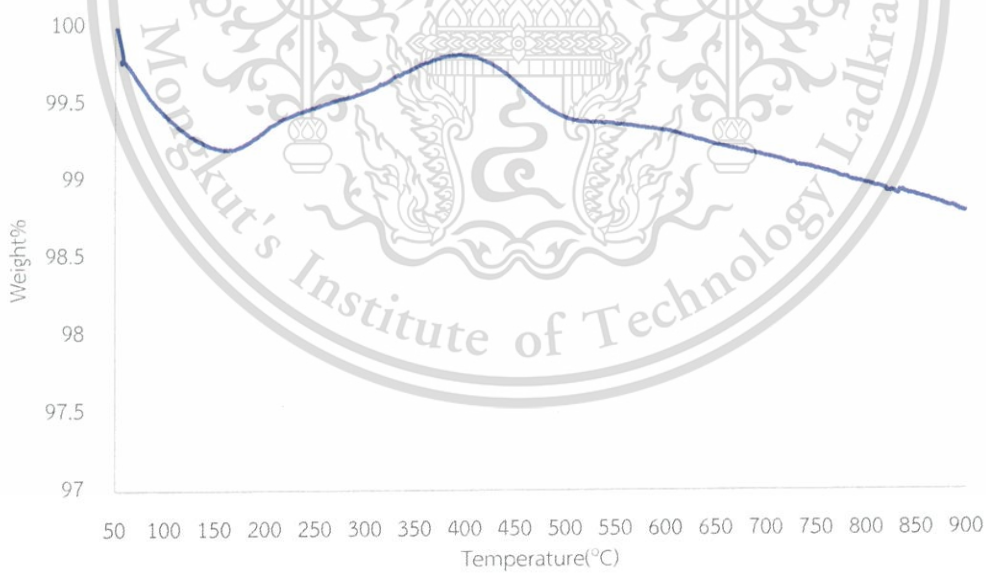

Figure 4.8 TGA profile of Cu/SiO_2

The observed weight gain is presumably due to the formation of CuO when Cu metal is oxidized by air zero (carrier gas). This does not only suggest that no coke formation is present after reaction, but also that Cu remains as a metallic phase in the spent catalyst.

Another possibility for the observed deactivation is that the adsorption of intermediate species over Cu metal surface. To verify this hypothesis, the catalyst is then treated under N_2 gas at 450 °C for an hour and re-operated at the same condition (**Figure 4.6 section b**). It can be seen that the catalytic activity is not completely recovered. This implies that the feed may strongly adsorb on Cu metal surface.

The adsorption of alcohol on the Cu surface was reported in the literature [66] that η^1(O)-alkoxide intermediate species (a) is initially formed via dissociation of O-H bond. At higher temperature, this species can eliminate an α-hydrogen to produce two possible aldehyde intermediates including (i) η^1(O)-carbonyl species and/or (ii) η^2(C, O)-carbonyl species on Cu metal surface as shown below.

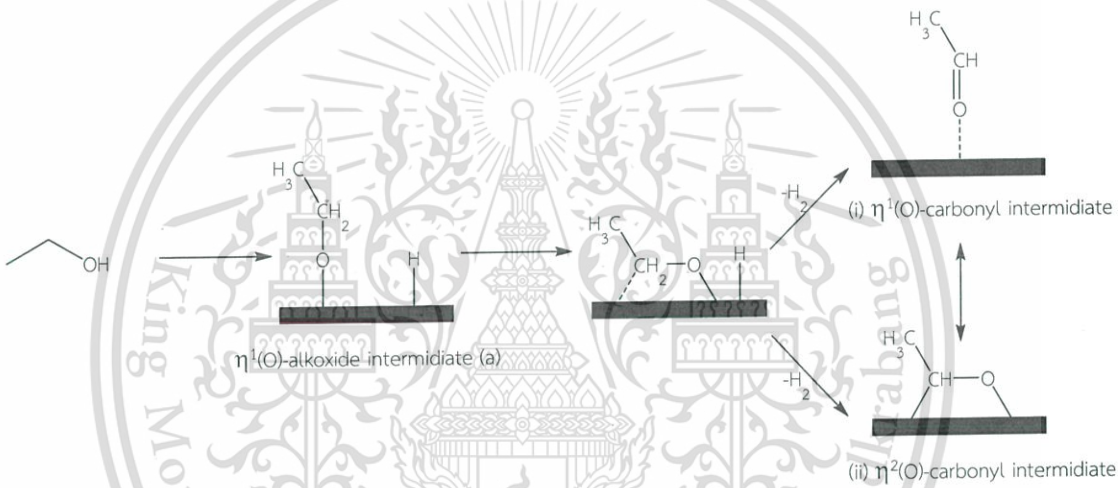

. It is likely that only η^1(O)-carbonyl species can be removed at 450 °C under N_2 gas because η^1(O)-carbonyl species is relatively less stable and tend to desorb more readily, as compared to η^2(C, O)-carbonyl species [65]. However, the deactivation is still observed suggesting that the η^2(C, O)-carbonyl species is strongly adsorbed and remain on the Cu metal surface after treatment at 450°C under N_2 gas as shown below.

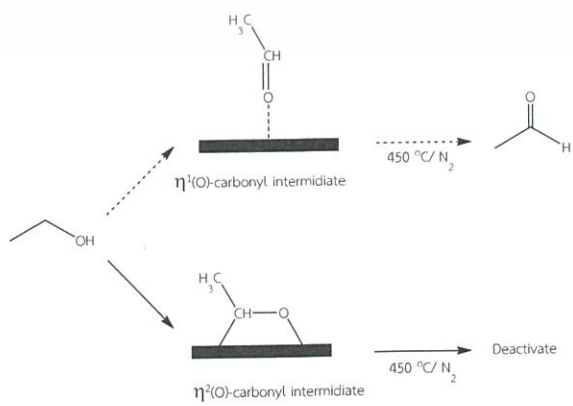

Although the catalyst is further treated under H_2 gas at 450°C for an hour (**Figure 4.6 section c**), the catalytic activity cannot be recovered. This suggests that the η^2(C, O)-carbonyl species is not possible desorbed by hydrotreating process because the surface is fully covered with η^2(C, O)-carbonyl species. Hence, H_2 gas cannot co-adsorption with ethanol on Cu metal surface.

In order to completely regenerate the catalyst surface, the catalyst is calcined in air at 450 °C and reduced at 400 °C then tested under H_2 as a carrier gas. It is clearly seen that the catalyst shows a high activity and stability (**Figure 4.6 section d**). This suggests that H_2 gas can be co-adsorbed with the ethanol and may well be dissociated, which leads to an increased electron density of the Cu surface. The increased surface electron density is known to weaken the adsorption of η^2(C, O)-carbonyl species, but stabilize η^1(O)-carbonyl species on Cu surface. This result indicates that the desorption of η^2(C, O)-carbonyl species can be facilitated in the presence of H_2 gas leading to a cleaner Cu surface and hence higher stability.

To validate this assumption, the carrier gas is switched to N_2 as shown in **Figure 4.6 section e**. The catalytic activity is suddenly decreased. After regeneration and repeating the test under H_2 gas (**Figure 4.6 section f**), the catalytic activity can be recovered with a conversion similar to that in **section d**. This again confirms that when co-feed with H_2, η^1(O)-carbonyl species is preferred on Cu surface and then readily desorbed to produce acetaldehyde as shown below.

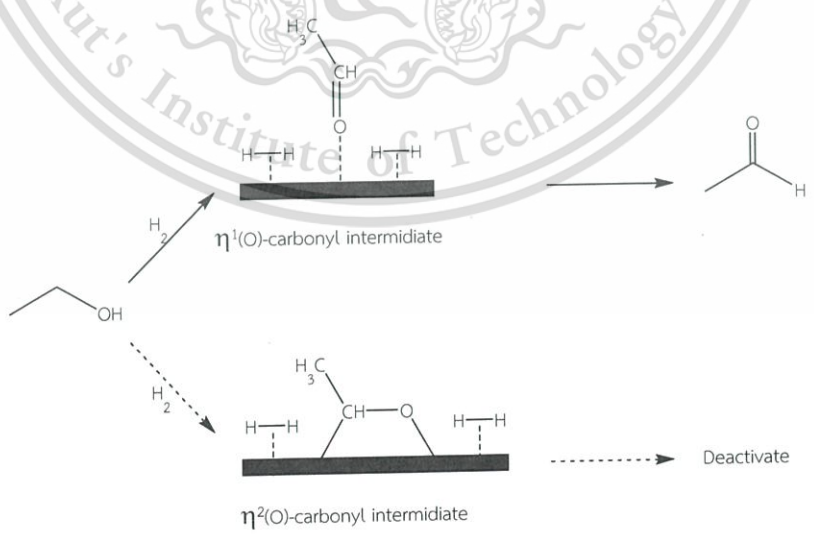

However, a small fraction of strongly adsorbed of η^2(C, O)-carbonyl species may well be presented and that lead to the slight deactivation even in H_2 gas.

4.3.2 Effect temperature

The effect of temperature on the selectivity of acetaldehyde was investigated as shown in **Table 4.3.**

Table 4.3 Product distributions from ethanol dehydrogenation over Cu/SiO_2 catalyst.

Contact time (g.h/mol)	Temperature (°C)	% Conversion	% Yield		% Selectivity	
			CH_4	Acetaldehyde	CH_4	Acetaldehyde
30	400	89.7	0.5	89.2	0.6	99.4
15	400	70.8	0.1	70.7	0.1	99.9
15	500	85	1.0	84.0	1.3	98.7

(Reaction temperature; 400-500°C, Feed rate; 0.012 mol/h of absolute ethanol)

It is found that when the contact time is increased from 15 to 30 g.h/mol), the conversion of ethanol is increased while a small amount of methane is observed. However, when the temperature is increased (400 to 500 °C) the selectivity of methane is significantly increased as shown in **Table 4.3.** In addition, at temperature of 500 °C the catalyst shows an improved stability, as compared to the reaction temperature at 400 °C (**Figure 4.9**) suggesting that the η^2(C, O)-carbonyl species can be decarbonylated to methane and carbon monoxide, leaving a cleaner Cu surface.

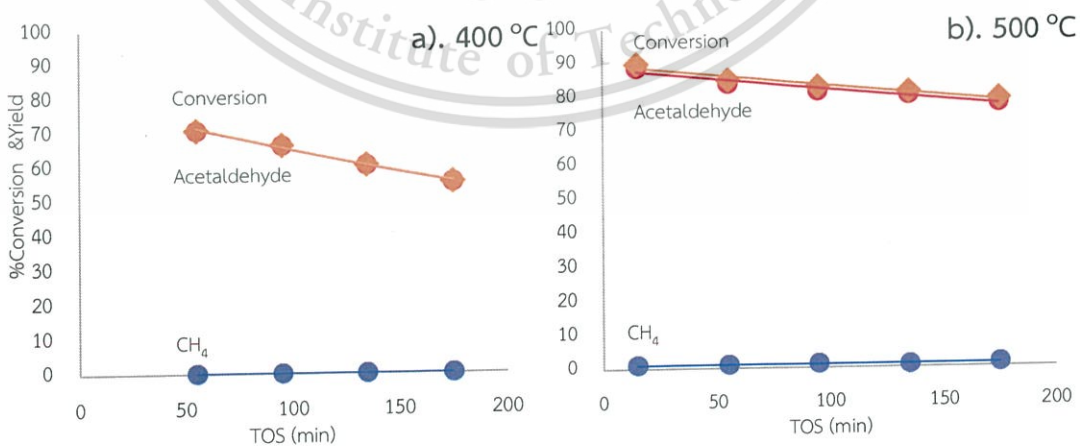

Figure 4.9 Dehydrogenation of ethanol at a) 400 °C and b) 500 °C.

This is because the decarbonylation requires relatively higher activation energy, as compared to that of dehydrogenation. For the decarbonylation, ethanol could be initially dissociated on Cu surface to form η^1(O)-alkoxide intermediate that can partially dissociate an α-hydrogen forming η^2(C, O)-carbonyl species as discussed previously. However, some of the η^2(C, O)-carbonyl species can further dissociate the carbonyl hydrogen to form η^1(C)-acyl intermediated as shown **Scheme 15**.

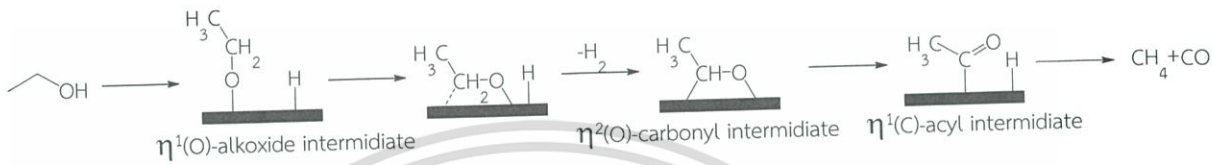

Scheme 15 Decarbonylation of ethanol to methane.

Therefore, the reaction at temperature 500°C gives some selectivity of methane. To diminish methane formation, the temperature at 400°C are chosen for further study.

4.3.3 Effect of alloyed metal with Cu

The effect of the secondary metal was investigated to improve the stability of Cu catalysts for the dehydrogenation of ethanol to acetaldehyde as shown in **Figure 4.10**.

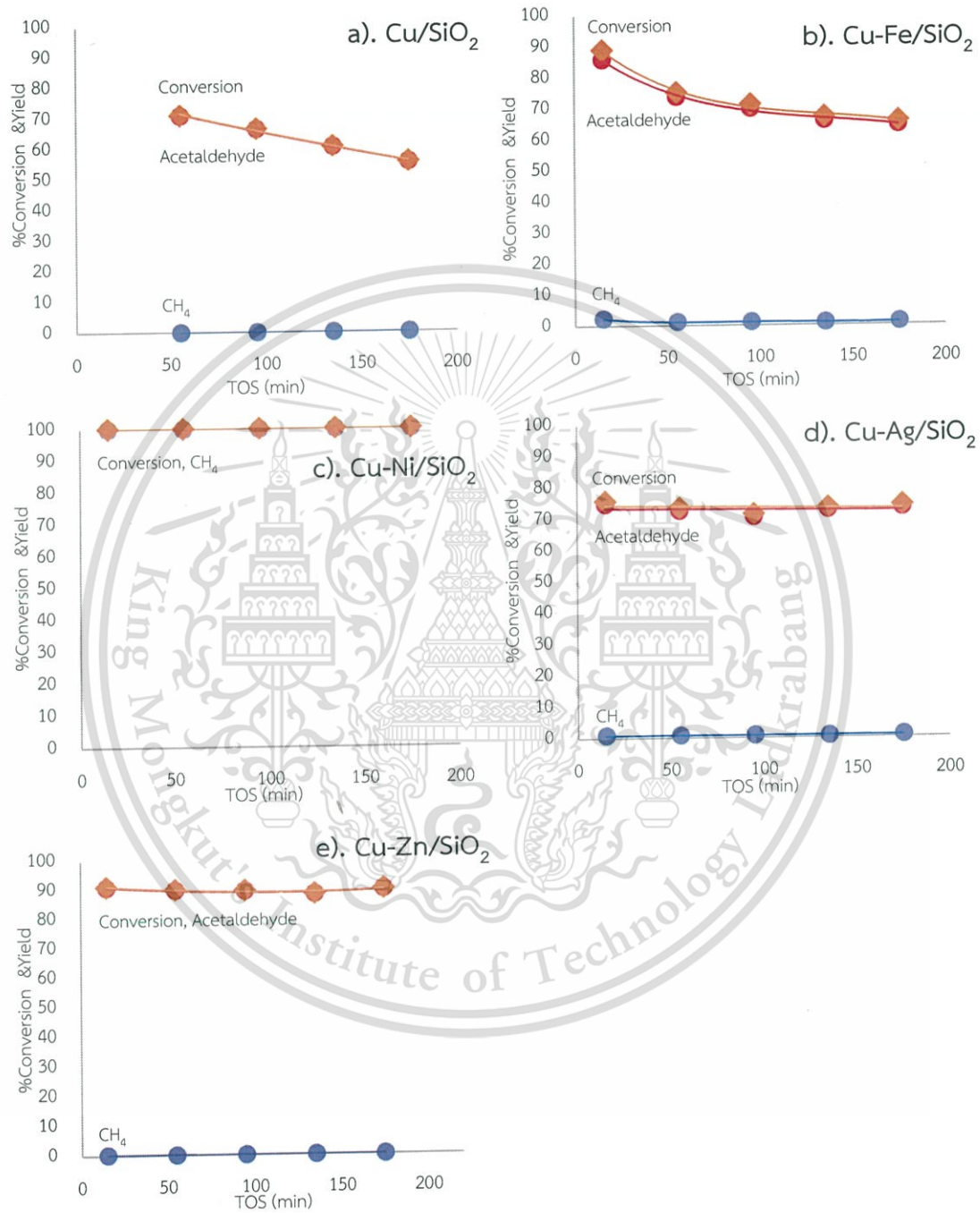

Figure 4.10 Product distribution of ethanol dehydrogenation over a). Cu/SiO_2, b) 10%Cu-2%Fe/SiO_2, c) 10%Cu-2%Ni/SiO_2, d) 10%Cu-2%Ag/SiO_2, and e). 10%Cu-2%Zn/SiO_2.

(Reaction temperature; 400°C, Feed rate; 0.012 mol/h of absolute ethanol, Contac time; 15 g.h/mol.)

The result shows that an improved stability can be observed over Ni, Zn, Ag alloyed with Cu catalysts. For Cu-Fe/SiO_2 (**Figure 4.10b**), the deactivation is still observed. However, the catalyst gives higher initial conversion for ethanol dehydrogenation as compared to Cu/SiO_2. It is suggested that the dispersion of Cu over Cu-Fe/SiO_2 is enhanced because the addition of Fe leads to higher dispersion of Cu loaded, as evidenced by lower reduction temperature in TPR (**Figure 4.2**). In addition, some of Fe cannot alloy with Cu, forming disaggregated Fe particles as shown by XRD (**Figure 4.1**) and TPR (**Figure 4.2**). It is suggested that such Fe particles may be oxidized to iron oxide by the feed, resulting in the formation of Lewis acid sites over this catalyst. Accordingly, the small amount of propylene is observed (**Table 4.4**) presumably from the secondary reactions of acetaldehyde over such Lewis acid sites (iron oxide) [49, 67, 68, 69].

Table 4.4 Product distributions from ethanol dehydrogenation over Cu alloy catalyst.

Catalysts	% Conversion	% Yield			% Selectivity		
		CH_4	Acetaldehyde	Propylene	CH_4	Acetaldehyde	Propylene
Cu/SiO_2	70.8	0.1	70.7	-	0.1	99.9	-
Cu-Fe/SiO_2	88.7	2.5	85.7	0.5	2.7	96.6	0.6
Cu-Ni/SiO_2	100	100	-	-	100	-	-
Cu-Ag/SiO_2	73.5	0.9	72.7	-	1.2	98.8	-
Cu-Zn/SiO_2	90.8	0.2	90.6	-	0.2	99.8	-

(Reaction temperature; 400°C, Feed rate; 0.012 mol/h of absolute ethanol, Contac time; 15 g.h/mol.)

It is suggested that over Lewis acid site, the ethyl acetate can be preliminarily produced from Tishchenko reaction of acetaldehydes (**Scheme 16a**). The ethyl acetate can be hydrolyzed to acetic acid, that undergoes ketonization to acetone (**Scheme 16b**). Then the acetone can be further hydrodeoxygenated to propylene as observed (**Table 4.4**).

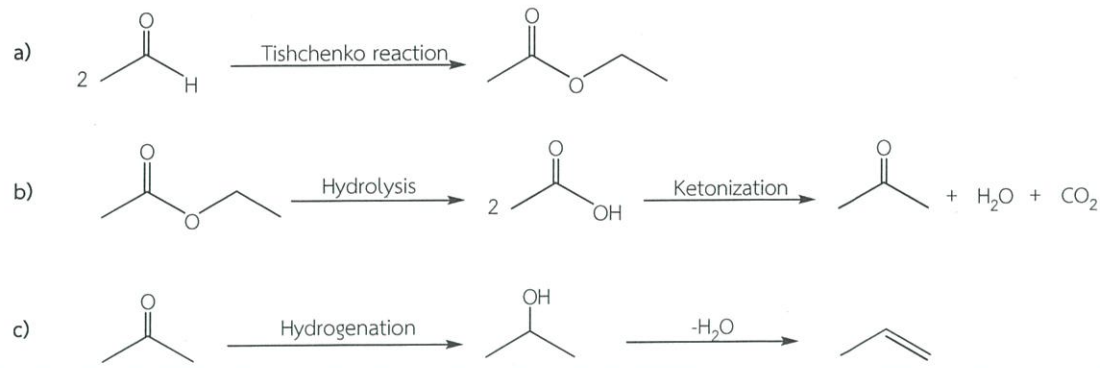

Scheme 16. The reaction of acetaldehyde to propylene.

In the case of Cu-Ni/SiO_2, the catalyst gives 100% conversion of ethanol. Unfortunately, 100% selectivity of methane is observed (**Table 4.4**). It is suggested that ethanol is successively decarbonylated to methane over Ni catalyst presumably because the η^2(C, O)-carbonyl intermediate species is preferred over Cu-Ni [70]. Accordingly, the decarbonylation to methane and carbon monoxide is promoted as discussed earlier (**Scheme 15**). Hence, the Cu-Ni alloy is not desired for production of acetaldehyde.

For Cu-Ag/SiO_2, the catalyst shows greater stability, as compared to Cu/SiO_2. This suggests that the addition of Ag does not improve dispersion of Cu but only improve surface coverage over Cu-Ag/SiO_2. Likewise, Cu catalyst, both η^1 and η^2(C, O)-carbonyl species can be observed over Cu-Ag alloy as reviewed in literature [71]. However, the η^2(C, O)-carbonyl species over the Cu-Ag catalyst can be readily decarbonylated to methane bearing vacant site on the surface. Hence, the deactivation over Cu-Ag/SiO_2 is inhibited by eliminating of η^2(C, O)-carbonyl species via decarbonylation. In line with this view, small amount of methane can be observed over Cu-Ag catalyst (**Table 4.4**).

In the case of Cu-Zn/SiO_2, the catalyst show a high catalytic activity and stability as compared to Cu/SiO_2. The higher conversion is suggested to derive from the higher dispersion of Cu with the addition of Zn [47]. This is because when Zn is added, a small Cu particle is obtained as discussed in TPR (**Figure 4.2**). Moreover, the observed high stability suggests that the incorporation of Zn reduced η^2(C, O)-carbonyl species on the surface. This behavior is ascribed to the electropositive nature of Zn, that result in a higher electron density of Cu and hence lower stability of the η^2(C, O)-carbonyl species as compared to the pure Cu surface. The Cu-Zn alloyed surface also hinders the formation of η^1(C)-acyl species and stabilizes η^1(O)-carbonyl species on the surface

(**Scheme 17**). Therefore, high selectivity of acetaldehyde is observed for Cu-Zn alloyed catalyst.

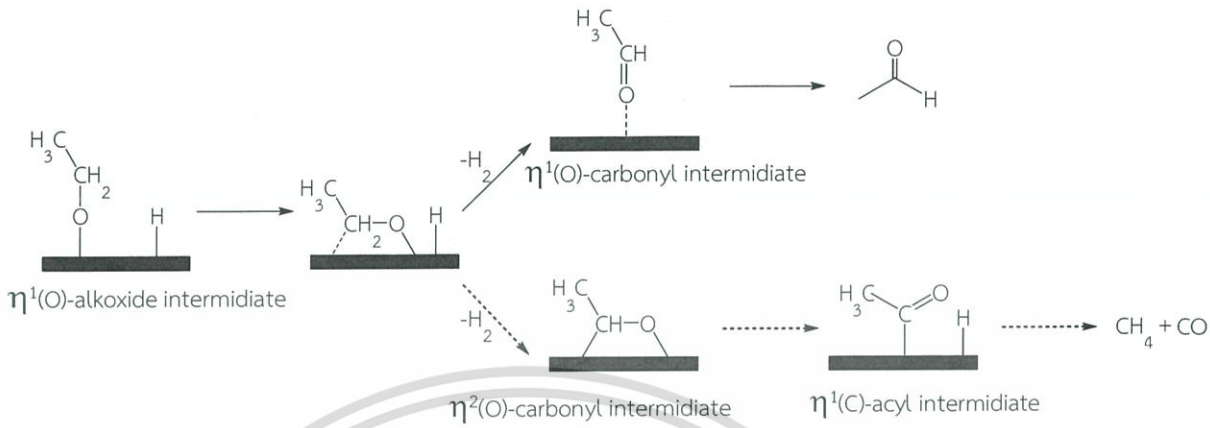

Scheme 17 Dehydrogenation of ethanol over Cu-Zn catalyst.

4.3.4 Effect of contact time

The conversion of ethanol and yield of products over Cu-Zn/SiO_2 catalyst at various contact time are shown in **Figure 4.11** and **Table 4.5.**

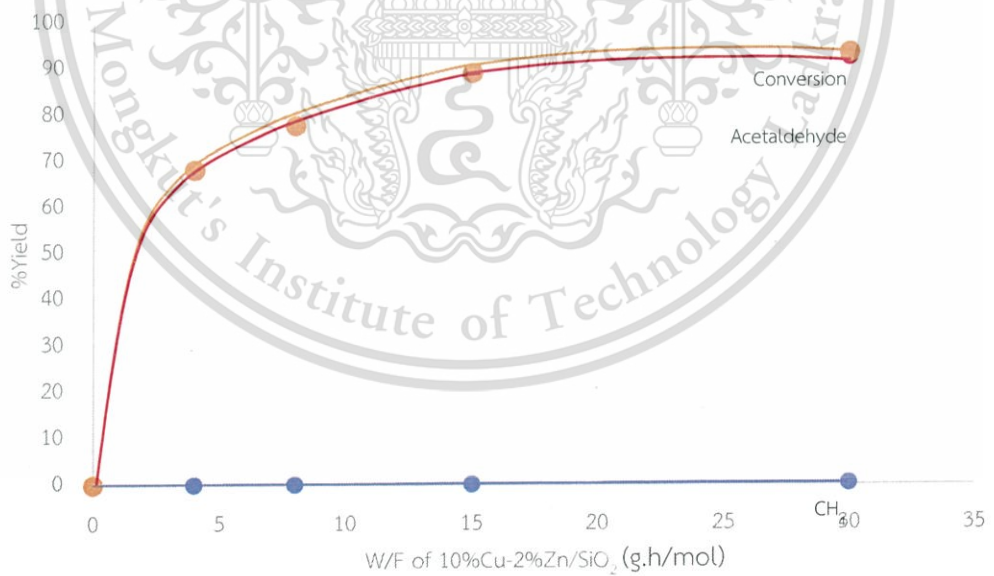

Figure 4.11 Conversion of ethanol and yield of products over Cu-Zn/SiO_2 catalyst. (Reaction temperature; 400°C, Feed rate; 0.012 mol/h of absolute ethanol, Contac time; 4-30 g.h/mol.)

The result shows that the conversion is readily increased with contact time as generally expected since the increase in contact time allows a better chance for the ethanol to interact with the active sites. For the products yield, it can be seen that ethanol is selectively converted to acetaldehyde with very small amount of methane. As discussed earlier, acetaldehyde can be produced by dehydrogenation of the η^1(O)-carbonyl species while methane is produced by decarbonylation of the η^1(C)-acyl species derived from the η^2(C, O)-carbonyl species. It is suggested again that Cu-Zn surface prefer the η^1(O)-carbonyl species adsorption rather than the η^2(C, O)-carbonyl species. However, at high contact time (30 g.h/mol) small amount of butanal and butanol are observed (**Table 4.5**).

Table 4.5. The product distributions from ethanol dehydrogenation over Cu-Zn/SiO_2 catalyst.

Contact time (g.h/mol)	% Conversion	% Yield			
		CH_4	Acetaldehyde	Butanal	Butanol
4	68.2	0.1	68.1	-	-
8	77.8	0.2	77.7	-	-
15	89.2	0.1	89.0	-	-
30	93.7	0.3	92.7	0.6	0.1

(Reaction temperature; 400°C, Feed rate; 0.012 mol/h of absolute ethanol, Contac time; 4-30 g.h/mol.)

The butanol and butanal might be produced by aldol condensation of the acetaldehyde produced over the trace of ZnO present in the catalyst (**Scheme 18**).

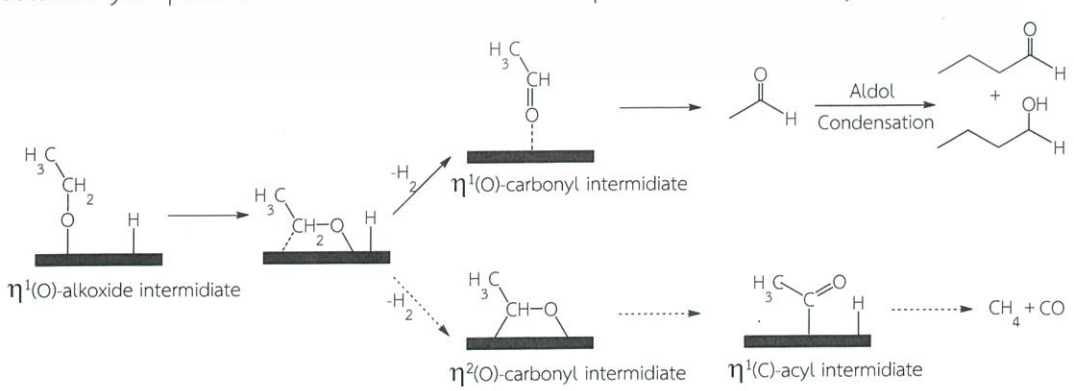

Scheme 18. Overall reaction over Cu-Zn catalyst.

4.4 Production of hydrocarbons from ethanol over double bed system of Cu-Zn/SiO_2 and H-ZSM-5 catalysts

4.4.1 Effect of acidity

As Cu-Zn/SiO_2 shows high stability and selective for production of acetaldehyde as compared to the other metal alloyed with Cu, this catalyst is used for double bed system on top of the H-ZSM-5 bed. The effect of acidity in the secondary bed is tested for production of hydrocarbons. The product distribution from ethanol conversion over double bed system of Cu-Zn/SiO_2 and H-ZSM-5 catalyst are shown in **Table 4.6.**

Table 4.6 Product distribution from ethanol conversion over various Si/Al of H-ZSM-5.

Catalysts	Strong acid site (mmol/g)	%Conversion	%Yield								
			Ethylene	Propylene	Acetaldehyde	C4-C5	BTX	C6-C8	C9 Aromatics	Alkylbezenes	Indenes & naphthalenes
H-ZSM-5 (500)	0.03	100	6.0	1.1	68.4	2.3	4.5	0.3	3.2	6.5	7.7
H-ZSM-5 (250)	0.03	100	6.3	1.4	63.3	2.5	5.6	0.3	3.7	8.0	8.8
H-ZSM-5 (140)	0.09	100	2.1	1.3	18.8	0.7	13.8	0.6	16.4	19.6	26.8
H-ZSM-5 (40)	0.44	100	5.9	3.2	1.5	0.3	20.7	0.5	25.6	15.0	27.1
H-ZSM-5 (28)	0.48	100	5.2	3.5	2.1	1.1	26.0	0.5	20.2	9.2	32.3

(Reaction temperature; 400°C, Feed rate; 0.012 mol/h of absolute ethanol, contact time of Cu-Zn/SiO_2; 15 g.h/mol and contact time of H-ZSM-5; 15 g.h/mol)

The result shows that all double bed systems give 100% conversion of ethanol. As the Cu-Zn/SiO_2 catalyst in the first bed provides up to 90% conversion of ethanol to acetaldehyde (**Figure 4.11**), about 10% of ethanol retained can be additionally dehydrated to ethylene over the secondary bed (H-ZSM-5). Nevertheless, only 6% of ethylene is observed from the double bed system. This suggests that some of ethylene can undergo oligomerization to hydrocarbons over H-ZSM-5. However, the most of hydrocarbons are produced from acetaldehyde. This is because the rate of aldol condensation of acetaldehyde is faster than that rate of oligomerization of ethylene.

As discussed earlier (**Table 4.2**), the enol-enolate intermediate in the aldol condensation is more stable than the primary carbocation formed by protonation of ethylene.

From **Table 4.6**, a small amount of hydrocarbons are obtained over H-ZSM-5 (500) and H-ZSM-5 (250), is due to the lower number of the strong acid sites in these catalysts. With low acid density (0.03 mmol/g), the acetaldehyde produced from the first bed cannot be converted to hydrocarbons. This is because aldol condensation is a bimolecular reaction that requires two close proximate sites. When the strong acid site is increased (0.09-0.48 mmol/g. as in H-ZSM-5 140, 40, 28), the acetaldehyde is markedly decreased, while the hydrocarbons including BTX, C9 aromatics, alkylbenzenes, indenes, and naphthalenes are significantly increased. This indicates that the increased in a number of the strong acid site provides appropriate site proximity to promote aldol condensation/deoxygenation of acetaldehyde to higher molecular weight intermediate. Such intermediate can undergo dehydration, cyclization, aromatization, disproportionation, and crack to hydrocarbons [72]. Furthermore, the alkylbenzenes are decreased over the catalyst with higher strong acid site (0.09-0.48 mmol/g), while BTX and C9 aromatics are increased. This suggests that alkylbenzenes can be disproportionated to C9 aromatics, indenes, and naphthalenes. While BTX and light hydrocarbons (ethylene and propylene) are produced by cracking of some high molecular weight hydrocarbons (**Scheme 19**). Accordingly, the H-ZSM-5 (28) with high acidity (0.48 mmol/g) provides a higher yield of BTX hydrocarbons as compared to the H-ZSM-5 other Si/Al ratio.

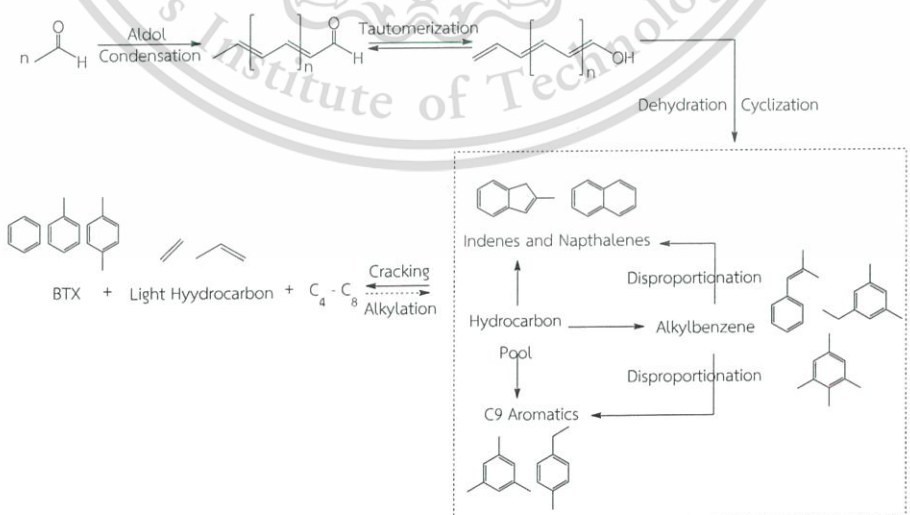

Scheme 19. The reaction pathway of ethanol over double bed system of Cu-Zn/SiO_2 and H-ZSM-5 (28).

4.4.2 Effect of metal incorporated on H-ZSM-5

Although incorporation of H-ZSM-5 (28) in the double bed system provides high yield of aromatic hydrocarbons, a severe deactivation is still observed over this catalyst as shown in **Figure 4.12a**.

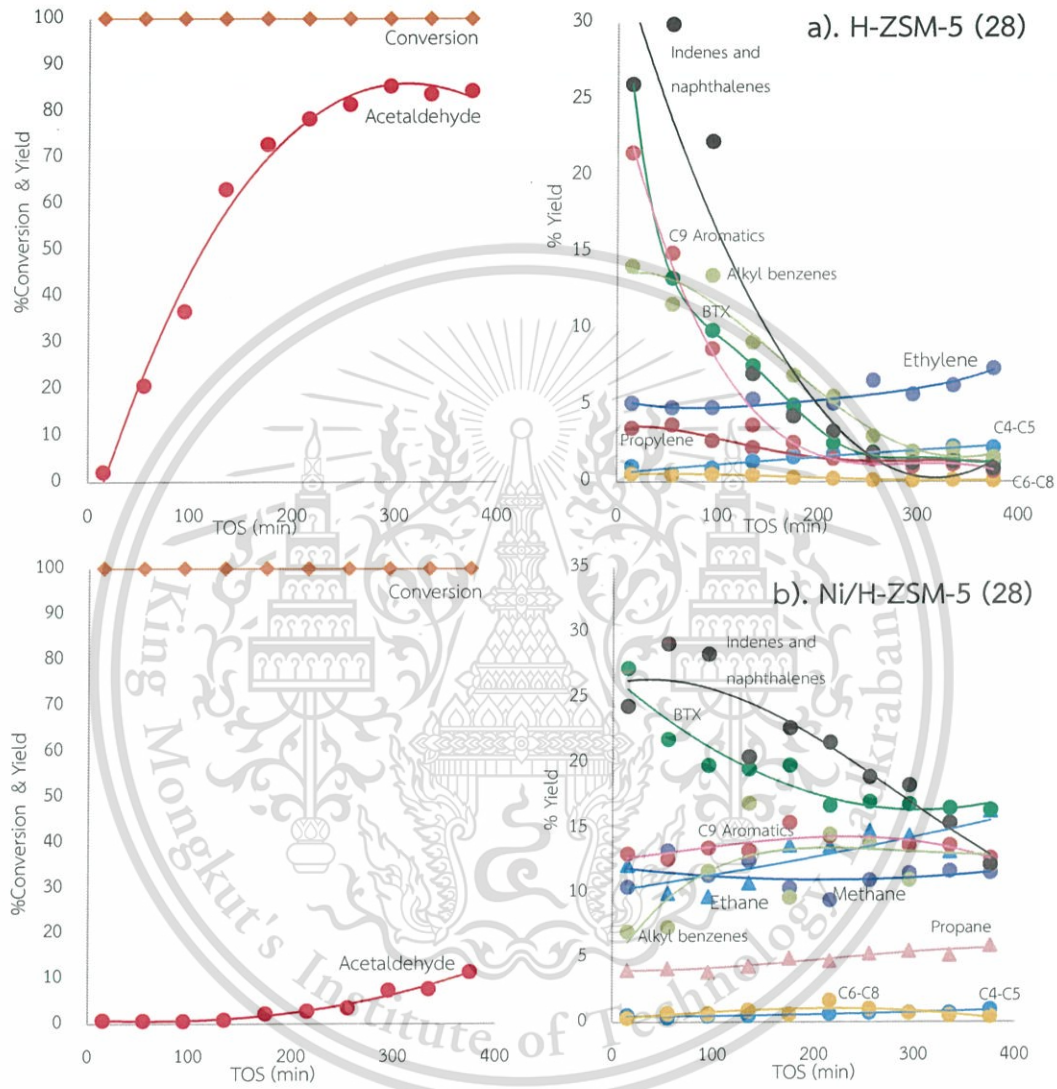

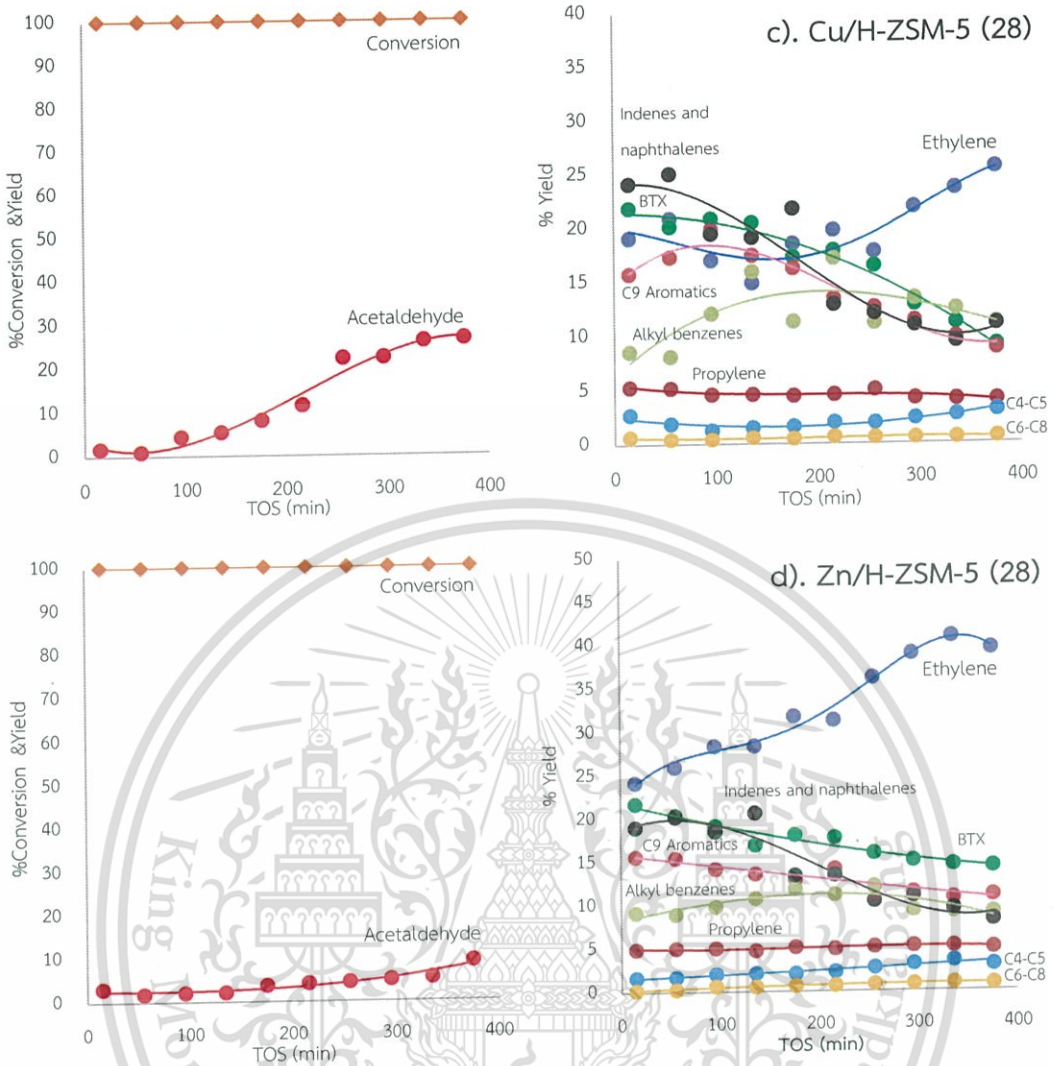

Figure 4.12 Effect of metal ion exchange over double bed system of a). H-ZSM-5 (28), b). Ni/H-ZSM-5 (28), c). Cu/H-ZSM-5 (28), d). Zn/H-ZSM-5 (28) (Reaction temperature; 400°C, Feed rate; 0.012 mol/h of absolute ethanol, Contac time of Cu-Zn/SiO_2; 15 g.h/mol, and contact time of a-d 15 g.h/mol.)

In line with this observation, BTX, C9 aromatics, indenes, and naphthalenes hydrocarbons are significantly decreased with time on stream while the ethylene, propylene, C4-C8 hydrocarbons remain similar. It is suggested that C9 aromatics, alkylbenzenes, indenes, and naphthalenes are precursors for the formation of higher molecular weight products deposit in the zeolite cavities, blocking access of the feed to the strong acid sites.

To overcome the deactivation of catalyst, the metal (Ni, Cu, Zn) is added to H-ZSM-5. It is expected that the incorporated metal can assist the dissociative adsorption of hydrogen and hence hydrogenation of the coke precursor formed over the acid sites. The result shows that the metal/H-ZSM-5 (28) demonstrate a stability greater than that

of H-ZSM-5 (28) (**Figure 4.12b, c, and d**). The coke formation is significantly decreased over all metal incorporated H-ZSM-5 (28) as compared with H-ZSM-5 (28). According to TGA profile (**Table 4.7**), the H-ZSM-5 (28) shows 9wt% loss of coke while the Zn/H-ZSM-5 (28) shows only 5wt% loss for example. It indicates that the incorporated metal possesses cleaning effect on the coke precursor formed over the strong acid site.

Table 4.7 TGA data of catalysts

Catalysts	Coke	
	Temperature (°C)	Weight loss %
H-ZSM-5 (28)	400-650	9
Zn/H-ZSM-5 (28)	400-650	5

From **Table 4.8**, the metal/H-ZSM-5 (28) provide lower heavy hydrocarbons product (BTX, C9 aromatics, alkylbenzene, indenes and naphthalenes) as compared with those over H-ZSM-5 (28).

Table 4.8 Product distribution from ethanol conversion over various Metal/H-ZSM-5.

Catalysts	%Conversion	%Yield											
		Methane	Ethane	Propane	Ethylene	Propylene	Acetaldehyde	C4-C5	BTX	C6-C8	C9 Aromatics	Alkylbenzenes	Indenes and naphthalenes
H-ZSM-5 (28)	100	-	-	-	5.2	3.5	2.1	1.1	26.0	0.5	20.2	9.2	32.3
Ni/H-ZSM-5 (28)	100	10.4	12.2	4.0	-	-	0.8	0.6	27.3	0.3	13.0	7.0	24.4
Cu/H-ZSM-5 (28)	100	-	-	-	19.1	5.3	1.7	2.8	21.9	0.7	15.8	8.6	24.1
Zn/H-ZSM-5 (28)	100	-	-	-	24.2	5.0	3.1	1.7	21.8	0.3	15.7	9.2	19.0

(Reaction temperature; 400°C, Feed rate; 0.012 mol/h of absolute ethanol, contact time of Cu-Zn/SiO_2; 15 g.h/mol and contact time of H-ZSM-5 and metal/H-ZSM-5; 15 g.h/mol).

Among heavy hydrocarbons product, the BTX selectivity is increased when the metal is incorporated on H-ZSM-5 (28) as seen from the BTX/C9 aromatics and BTX/indenes and naphthalenes ratio (**Table 4.9**).

Table 4.9 Aromatics ratio from ethanol conversion over various Metal/H-ZSM-5.

Catalysts	Ratio	
	BTX/C9 aromatics	BTX/indenes and naphthalenes
H-ZSM-5 (28)	1.3	0.8
Ni/H-ZSM-5 (28)	2.1	1.1
Cu/H-ZSM-5 (28)	1.4	0.9
Zn/H-ZSM-5 (28)	1.4	1.2

It is suggested that the incorporated metal can hydrogenate coke precursors formed over the acid site resulting in the low amount of C9 aromatics and polynuclear aromatics such as indenes and naphthalenes and hence gives more fraction of single ring aromatics such as BTX.

For Ni/H-ZSM-5 (28), the hydrogen can readily dissociate on the Ni surface, the coke precursor can be hydrogenated by hydrogen spillover from Ni particle resulting in the continuous production of BTX and light hydrocarbons (C_2-C_3 paraffins). However, the methane is observed due to the decarbonylation of acetaldehyde/ethanol over Ni surface as discussed earlier (**Figure 4.10c**). While the light paraffins are produced from decarbonylation/hydrogenolysis of higher aldehyde over Ni site as shown below.

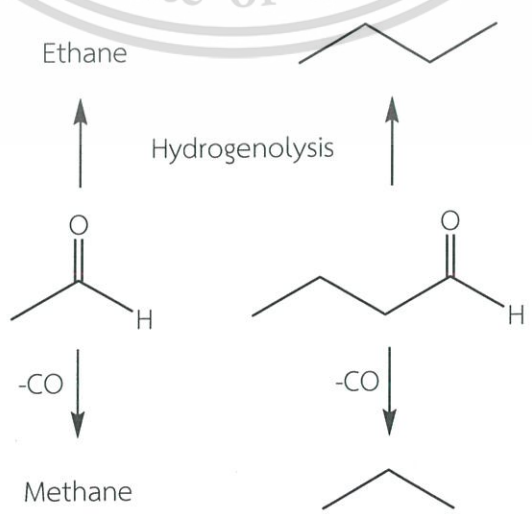

In the case of Cu/H-ZSM-5 (28), the hydrogenation of coke precursor also promotes by hydrogen spillover, but in a lesser extent as compared to that over Ni catalyst. The Cu catalyst hence gives low amount of BTX, indenes, and naphthalenes while the higher ethylene is observed as compared with Ni/H-ZSM-5 (28) (**Table 4.8**). This is suggested that some of the acetaldehyde is hydrogenated to ethanol over the incorporated Cu catalyst. The ethanol can undergo dehydration over the acid site to form ethylene as shown below.

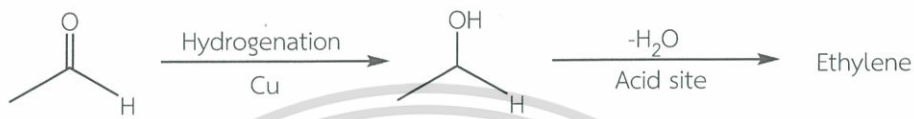

Nonetheless, some of the deactivation can be observed. This is because the Cu can be oxidized to exchangeable Cu ion by the feed over acid sites resulting in the detrimination of the hydrogenating function of Cu/H-ZSM-5 (28).

For the Zn/H-ZSM-5 (28), the active Zn species in H-ZSM-5 is not a metallic Zn but rather as cationic species [73]. This is because Zn^{2+} cannot be reduced to metallic Zn as mentioned in TPR (**Figure 4.3**). However, under H_2 atmosphere, the heterolytic dissociation of H_2 over exchangeable Zn^{2+} cation can result in zinc-hydride (ZnH^+) cation and recoverable Brønsted acid sites as shown below.

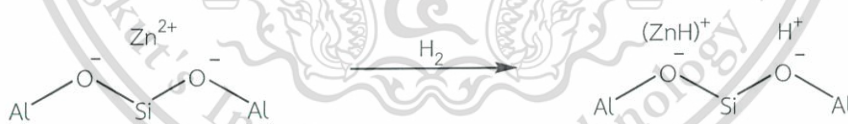

The zinc-hydride (ZnH^+) species can also promote hydrogenation of coke precursors by hydrogen transfer resulting in the low amount of indenes and naphthalenes (**Table 4.8**). The hydrogenation via hydrogen transfer was reported in the literatures that the reaction involves hydrogen donor (ZnH^+) and hydrogen acceptor such as aldehyde/alkene. The aldehyde/alkene are protonated over the acid sites in a close proximity to zinc-hydride (ZnH^+) site. The hydrogen interacts with active Zn species then transfered to aldehyde/alkene located on acid sites to generate alcohol/alkane and exchangeable Zn^{2+} cation. Zinc-hydride (ZnH^+) and Brønsted acid

site can be recovered again from the reaction of active Zn^{2+} species and gas phase H_2 as shown below.

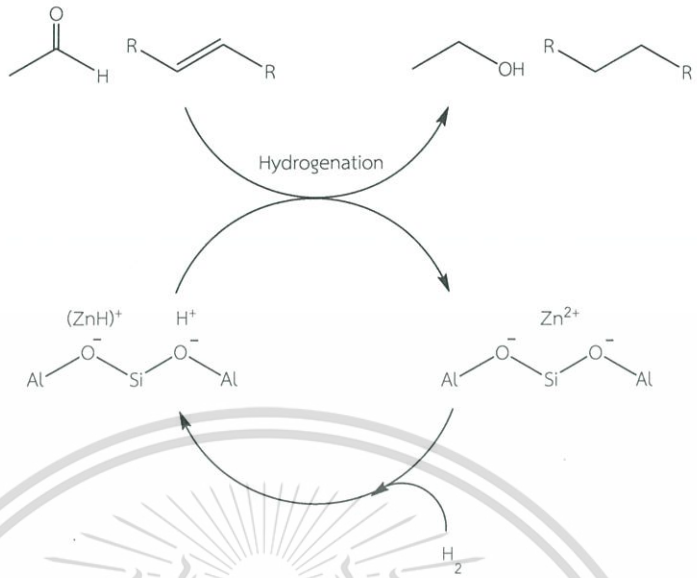

At the same time, the higher yield of ethylene is observed. This is suggested that the zinc-hydride (ZnH^+) can also promote hydrogenation to acetaldehyde over acid sites to formed ethanol that subsequently dehydration to ethylene as show below.

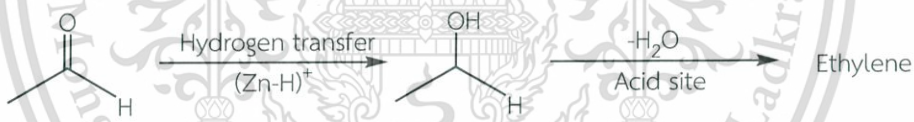

The observed hydrocarbons over the double bed system does not derive from aromatization of light olefins, as generally found over Zn/H-ZSM-5 (28). This is verified by feeding ethanol over single bed of Zn/H-ZSM-5 (28). The products distribution of ethanol conversion over the single bed (Zn/H-ZSM-5 (28) is compared with the double bed system (Cu-Zn/SiO_2 and Zn/H-ZSM-5 (28)).

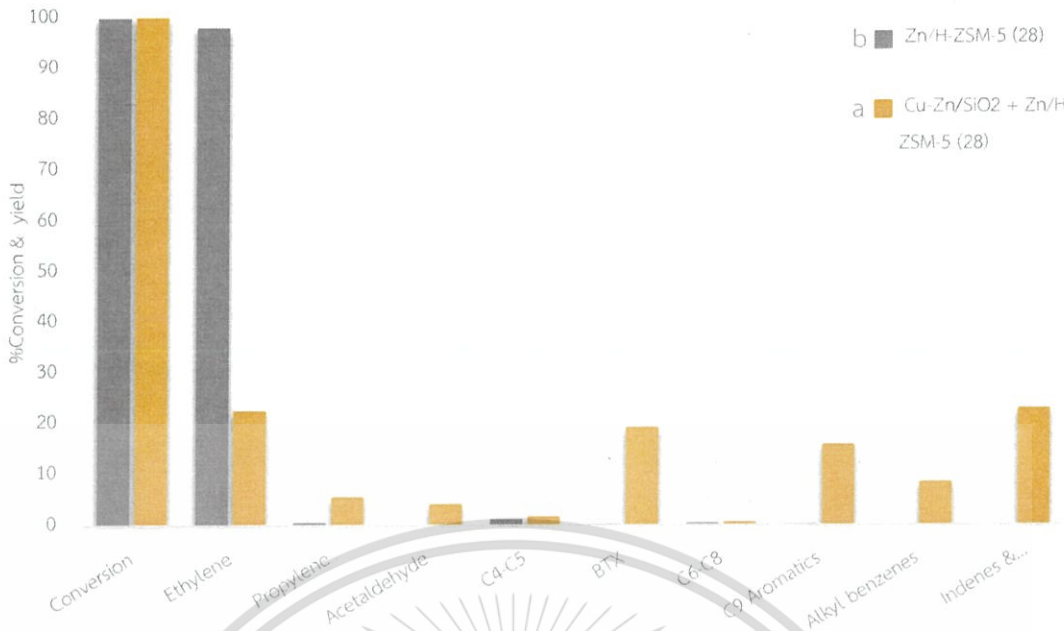

Figure 4.13 Products distribution from ethanol conversion over a) Cu-Zn/SiO_2 + Zn/H-ZSM-5 (28), b) Zn/H-ZSM-5 (28).

(Reaction temperature; 400°C, Feed rate; 0.012 mol/h of absolute ethanol, Contac time of Cu-Zn/SiO_2; 15 g.h/mol, and contact time of Zn/H-ZSM-5 10 g.h/mol.)

It can be seen that the reaction of ethanol in a single bed system, only ethylene is produced from dehydration of ethanol over the acid sites. Ethylene cannot be converted to higher hydrocarbons over Zn/H-ZSM-5 (28). While the reaction in a double bed system, the higher aromatics hydrocarbons are observed. This suggests that the incorporated Zn species does not affect for aromatization of ethylene, but only promoted hydrogenation of coke precursors over the secondary bed of double bed system. This indicated that over the double bed system, the higher hydrocarbons product is only produced by aldol condensation/deoxygenation of acetaldehyde.

4.4.3 Reaction pathway over double bed system of Cu-Zn/SiO_2 and Zn/H-ZSM-5 (28)

In order to verify the reaction pathway for the formation of hydrocarbons over double bed system. The secondary bed of Zn/H-ZSM-5 is tested at various contact time (2.5-15 g.h/mol) as shown in **Figure 4.14**.

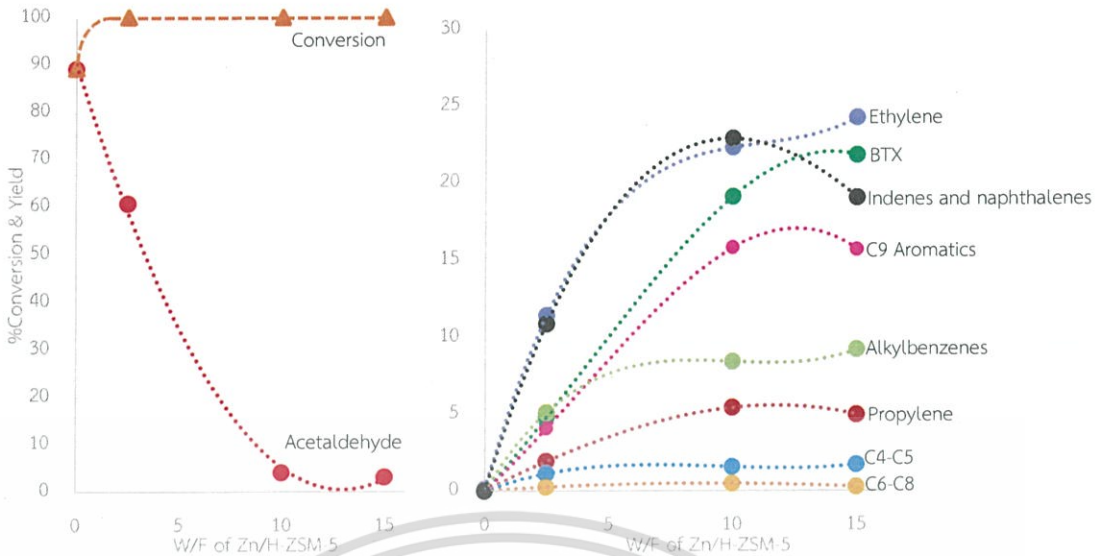

Figure 4.14 Product distribution from ethanol conversion over Cu-Zn/SiO_2 and Zn/H-ZSM-5 (28).

(Reaction temperature; 400°C, Feed rate; 0.012 mol/h of absolute ethanol, Contac time of Cu-Zn/SiO_2; 15 g.h/mol, and contact time of Zn/H-ZSM-5 2.5-15 g.h/mol.)

It is observed that the acetaldehyde is notably decreased, while ethylene and higher molecular weight hydrocarbons including alkyl benzene, indenes, and naphthalene are increased with contact time. At contact time 2.5 g.h/mol, about 10% of ethylene is presumably produced from dehydration of ethanol (remained from the top bed of Cu-Zn catalyst) over acid site.

When contact time is increased (10-15 g.h/mol), the higher ethylene is also observed. It is suggested again ethylene is produced from hydrogenation of acetaldehyde via hydrogen transfer over zinc-hydride (ZnH^+). The ethanol formed can be dehydrated to ethylene over acid sites as shown below.

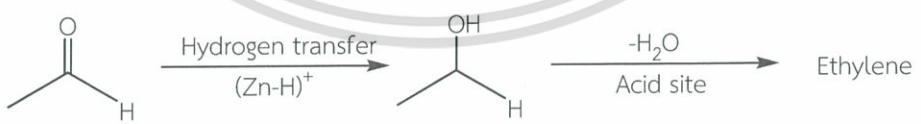

In parallel, the Indenes and alkyl benzene are initially increased with contact time (2.5-10 g.h/mol). This indicated that the ethylene and indene are the primary hydrocarbon products. It is suggested that the Indenes and alkyl benzene are directly produced from aldol condensation of acetaldehyde to heavy unsaturated aldehyde intermediates that undergo dehydracyclization via oxygenated pool over the acid sites

(**Scheme 20**) then declined at contact time 15 g.h/mol. with the increase in BTX and C9 aromatics [74].

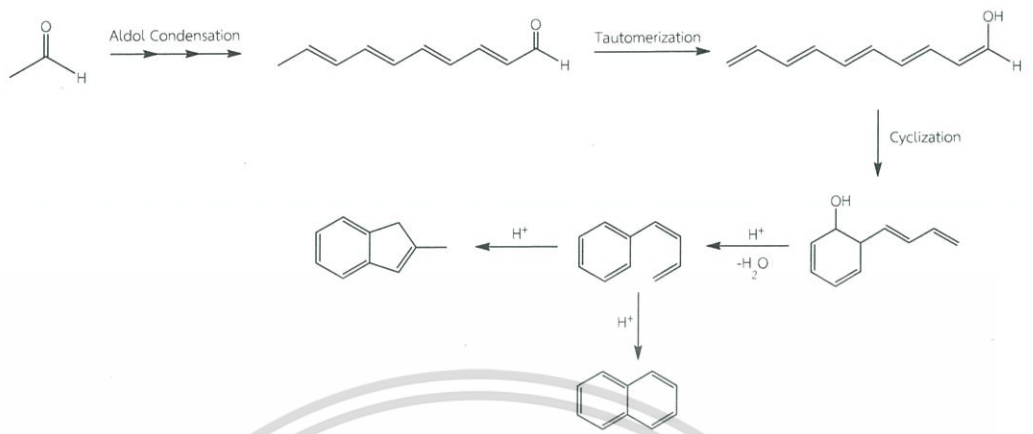

Scheme 20 Aldol condensation/ dehydracyclization of aldehyde.

The Indenes and alkyl benzene are then cracked to BTX, C9 aromatics, and C4-C8 hydrocarbons at higher contact time (15 g.h/mol). In line with this view, propylene, and light hydrocarbons are seen as secondary products from cracking and hydrogen transfer from hydrocarbons pool. The overall reaction pathway can be proposed in **Scheme 21**

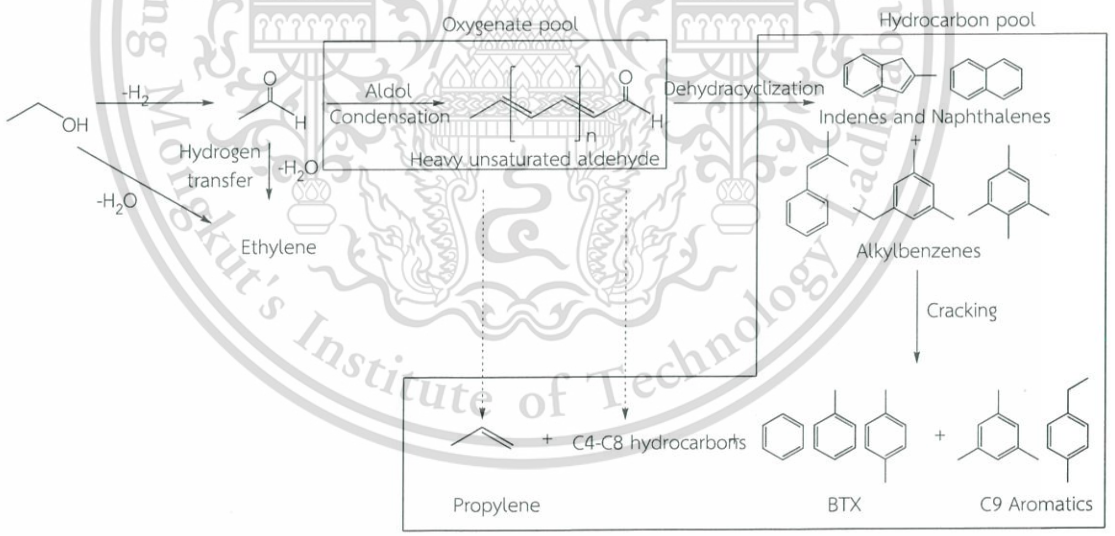

Scheme 21 The reaction pathway of ethanol over double bed system of Cu-Zn/SiO_2 and Zn/H-ZSM-5 (28).

Chapter 5
Conclusions and suggestions

5.1 Conclusions

In this thesis, the conversion of ethanol to liquid fuels over double bed system of metal supported silica and H-ZSM-5 was evaluated. All catalysts are categorized as high surface (206-479 m^2/g) with expected metal loading about 10wt%. for monometallic (Cu and Ag) and 12wt%. for bimetallic (Cu-Zn, Cu-Ag, Cu-Fe, and Cu-Ni) catalysts, as evidenced by X-ray fluorescence (XRF). The XRD pattern and TPR results confirm that the bimetallic phase of Cu and secondary metal (Zn, Ag, Fe, Ni) can be formed. For the metal incorporated H-ZSM-5 (Ni, Cu, and Zn), the ICP-MS evidences that the Ni, Cu, Zn loading are 0.8, 0.5, and 1.4wt%., respectively. TEM image shows high dispersion of Ni nanoparticle (~5 nm) in the Ni incorporated H-ZSM-5. A high reduction temperature observed by TPR corresponds to interaction of the Ni precursor with the BrØnsted acid sites.

Ethanol conversion over the single bed of H-ZSM-5 (28) gives small amounts of hydrocarbons because the ethylene oligomerization initially proceeds via the formation of unstable primary carbocation. In the double bed system (Ag/SiO_2 and H-ZSM-5 (28)), the Ag catalyst on the first bed primarily promotes dehydrogenation of ethanol to acetaldehyde while the second bed of H-ZSM-5 (28) promotes aldol condensation /deoxygenation of the acetaldehyde to hydrocarbons. The double bed system (metal/SiO_2 and H-ZSM-5 (28)) shows activity for production of hydrocarbons higher than that over the single bed of H-ZSM-5 (28). This is because the protonation of acetaldehyde over the acid sites can form enol/enolate intermediate that is thermodynamically more stable than the primary carbocation intermediate formed by protonation of ethylene. However, the methane is also obtained via decarbonylation of ethanol over Ag/SiO_2.

Considering the top bed, the Cu/SiO_2 exhibits higher activity and selectivity to acetaldehyde, as compared to the Ag/SiO_2. However, the Cu/SiO_2 shows a rapid deactivation due to strongly adsorption of η^2(C, O)-carbonyl species on Cu metal surface. After the regeneration and testing under H_2 gas, the hydrogen can be co-adsorbed with ethanol and may well be dissociated, leading to an increase of electron

density of the Cu metal surface. These results in a reduced coverage of η^2(C, O)-carbonyl species. When the reaction temperature is increased (400 to 500 °C), the catalyst shows an improved activity and also stability. However, a higher selectivity of methane is observed because the decarbonylation of ethanol/acetaldehyde to methane and carbon monoxide requires relatively higher activation energy, as compared to that of dehydrogenation. For bimetallic catalysts, Cu-Fe/SiO_2 exhibits higher initial activity but deactivation is still observed. Although the Cu-Ni/SiO_2 gives high stability, only methane is obtained because the Ni virtually promotes decarbonylation of ethanol/acetaldehyde. For Cu-Ag/SiO_2, the catalyst partially promotes decarbonylation of acetaldehyde and improves stability. While Cu-Zn/SiO_2 demonstrates high activity because the Cu dispersion can be enhanced by the addition of Zn. Moreover, the catalyst shows higher stability due to the electropositive nature of Zn which destabilizes the η^2(C, O)-carbonyl species bearing vacant active surface.

Over the double bed system (of Cu-Zn/SiO_2 and H-ZSM-5), when the acidity of the second bed is increased, the oligomerization of acetaldehyde to higher aldehyde intermediate is enhanced due to the close proximity of the acid sites. Such higher aldehyde intermediate can be deoxygenated to produce high molecular weight hydrocarbons. However, a severe deactivation, due to the formation of coke precursors, is observed at higher acidity (0.48 mmol/g). In order to improve catalytic stability by hydrogenation of the coke precursors over the acid sites, the metal is incorporated H-ZSM-5 (28) (Ni, Cu, and Zn). The Ni and Cu/H-ZSM-5 (28) can promote hydrogenation of coke precursors by hydrogen spillover. However, the light hydrocarbons such as methane can be observed over Ni/H-ZSM-5 (28). While some of the deactivation can be observed over Cu/H-ZSM-5 (28) because the Cu can be oxidized to exchangeable Cu ion by feed. For Zn/H-ZSM-5 (28), the catalyst can promote hydrogenation of coke precursors by hydrogen transfer because Zn cannot be reduced and act as Lewis acid sites. The overall results suggested that the double bed system of Cu-Zn/SiO_2 and Zn/H-ZSM-5 is effective for the conversion of ethanol to hydrocarbons via aldol condensation /deoxygenation. The reaction pathway of ethanol to hydrocarbons occurs via ethanol dehydrogenation to acetaldehyde, followed by aldol condensation of acetaldehyde to produce a higher aldehyde intermediate, and finally dehydration and cyclization to higher hydrocarbons over the acid sites.

5.2 Suggestions

1. In order to decreased deactivation over the double bed system, the different loading in a secondary bed of H-ZSM-5 (28) should be investigated.

2. The incorporated metal on high Si/Al ratio should be studied to validate the catalytic activity and stability.

References.

1 **Alcoholic Fuels.** (2006). 6000 Broken Sound Parkway, NW Suite 300, Boca Raton, FL 33487: CRC Press Taylor & Francis Group 2006.

2 **Fuel-Cycle Fossil Energy Use and Greenhouse Gas Emission of Fuel ethanol.** (1997). Illinois Department of Commerce and Community Affairs, Center for transportation Research: Argonne Natiional Laboratory.

3 Abel, J. and Virtanen, S. (2015). **Corrosion of martensitic stainless steel in ethanol-containing gasoline: Influence of contamination by chloride, H_2O and acetic acid.** Corrosion Science, 98, pp.318-326.

4 Costa, E., Ugulna, A., Aguado, J., & J. Herndndez, P. (1985). **Ethanol to Gasoline Process: Effect of Variables, Mechanism, and Kinetics.** Ind. Eng. Chem. Process Des, 24, 239-244.

5 Talukdar, A., Bhattacharyya, K., & Sivasanker, S. (1997). **HZSM-5 catalysed conversion of aqueous ethanol to hydrocarbons.** Applied Catalysis A: General, 148(2), 357-371.

6 de Lima, A., de Assis, A., Hori, C., Reis, M., & Machado, A. (2012). **Thermodynamic Analysis of Ethanol Dehydration to Ethylene through Equilibrium Constant Method Using Classic Thermodynamics and Quantum Chemistry.** I. RE.CH. E., 4(5), 2035-1755.

7 Frame, R., & Barger, P. (1989). **Process for the oligomerization of olefins and a catalyst thereof.** US4795852 A.

8 Sushkevich, V., Ivanova, I., Ordomsky, V., & Taarning, E. (2014). **Design of a Metal-Promoted Oxide Catalyst for the Selective Synthesis of Butadiene from Ethanol.** Chemsuschem, 7(9), 2527-2536.

9 Viswanadham, N., Saxena, S., Kumar, J., Sreenivasulu, P., & Nandan, D. (2012). **Catalytic performance of nano crystalline H-ZSM-5 in ethanol to gasoline (ETG) reaction.** Fuel, 95, 298-304.

10 Sun, J., & Wang, Y. (2014). **Recent Advances in Catalytic Conversion of Ethanol to Chemicals. ACS Catalysis.** 4(4), 1078-1090.

11 Science is Fun in the Lab of Shakhashiri. Scifun.org. Retrieved from http://www.scifun.org, "Chemical of the week, Ethanol" [Online].

12 Sun, J., & Wang, Y. (2014). **Recent Advances in Catalytic Conversion of Ethanol to Chemicals.** ACS Catalysis. 4(4), 1078-1090.

13 Wang, M., Saricks, C., Wu, M., (1997). **Fuel-Cycle Fossil Energy Use and Greenhouse Gas Emission of Fuel ethanol.** Illinois Department of Commerce and Community Affairs, Center for transportation Research, Argonne Natiional Laboratory.

14 Angelici, C., Weckhuysen, B., & Bruijnincx, P. (2013). **Chemocatalytic Conversion of Ethanol into Butadiene and Other Bulk Chemicals.** Chemsuschem, 6(9), 1595-1614.

15 Ausavasukhi, A. (2001). **The Production of Gasoline and Aromatics From Ethanol.** KMITL.

16 Jacqueline, l., & Kroschwitz. (1991). **Executive Editor. Encyclopedia of Chemical Technology vol. 1.** 4th Ed. New York : John Wiley & Son.

17 Bi, J., Guo, X., Liu, M., & Wang, X. (2010). **High effective dehydration of bio-ethanol into ethylene over nanoscale HZSM-5 zeolite catalysts.** Catalysis Today, 149(1-2), 143-147.

18 Jirátová, K., Mikulová, J., Klempa, J., Grygar, T., Bastl, Z., & Kovanda, F. (2009). **Modification of Co–Mn–Al mixed oxide with potassium and its effect on deep oxidation of VOC.** Applied Catalysis A: General, 361(1-2), 106-116.

19 Wittcoff, H. (1983). **Acetaldehyde: a chemical whose fortunes have changed.** Journal of Chemical Education, 60(12), 1044.

20 Chang, F., Yang, H., Roselin, L., & Kuo, W. (2006). **Ethanol dehydrogenation over copper catalysts on rice husk ash prepared by ion exchange.** Applied Catalysis A: General, 304, 30-39.

21 Crabbe, E., Nolasco-Hipolito, C., Kobayashi, G., Sonomoto, K., & Ishizaki, A. (2001). **Biodiesel production from crude palm oil and evaluation of butanol extraction and fuel properties.** Process Biochemistry, 37(1), 65-71.

22 L. I. Volkova, A. Y. Zaitova, A. A. Yoakimis, T. P. Mochalnikova, L. Y. Nazarova, V. I. Nazarov, M. S. Pyrakhina, V. N. Petrov, E. E. Rachkovskii, A. P. Savelev, et al., USSR pat. 175,929, n.d.

23 V. Nagarajan, Chem. Eng. World 1970, 5, 31–35.

24 Jones, M. D.; Keir, C. G.; Di Iulio, C.; Robertson, R. A. M.; Williams, C. V.; Apperley, D. C. Catal. Sci. Technol. 2011, 1, 267–272.

25 J. Grub, E. Loser, Butadiene in Ullmann's Encyclopedia of Industrial Chemistry, Wiley-VCH, Weinheim 2012.

26 Quattlebaum, W., Toussaint, W., & Dunn, J. (1947). **Deoxygenation of Certain Aldehydes and Ketones: Preparation of Butadiene and Styrene1.** Journal of The American Chemical Society, 69(3), 593-599.

27 "MFI." [Online]. Available: http://izasc-mirror.la.asu.edu/fmi/xsl/IZA-SC/ftc_fw.xsl?-db=Atlas_main&-lay=fw&-max=25&STC=MFI&-find. 2007.

28 Chen, N., Garwood, W., & Dwyer, F. (1996). **Shape selective catalysis in industrial applications.** New York: Dekker.

29 Bhatia, S. (1990). **Zeolite catalysis.** Boca Raton, Fla.: CRC Press.

30 Gates, B. (1992). **Catalytic chemistry.** New York et al.: Wiley.

31 L, H. (1987). **Catalyst Design Progress and Perspective.** New York: John Wiley & Son.

32 Bekkum H. Van., Editors. (1991) **Introduction to Zeolite Science and practice.** Amsterdam: Elsevier Science.

33 KOKOTAILO, G., LAWTON, S., OLSON, D., & MEIER, W. (1978). **Structure of synthetic zeolite ZSM-5.** Nature, 272(5652), 437-438.

34 Arganer, R., M, K., Landolt, G., & J, A. (1972). **Crystalline Zeolite ZSM-5 and Method of Preparing the Same.** U.S patent no. 3702886.

35 Sitthisa, S., Pham, T., Prasomsri, T., Sooknoi, T., Mallinson, R., & Resasco, D. (2011). **Conversion of furfural and 2-methylpentanal on Pd/SiO_2 and $Pd–Cu/SiO_2$ catalysts.** Journal Of Catalysis, 280(1), 17-27.

36 Sitthisa, S., Sooknoi, T., Ma, Y., Balbuena, P., & Resasco, D. (2011). **Kinetics and mechanism of hydrogenation of furfural on Cu/SiO_2 catalysts.** Journal of Catalysis, 277(1), 1-13.

37 "**Aldol Condensation.**" [Online]. Available http://en.wikipedia.org/wiki/Aldol_condensation. 2015.

38 T.W. GRAHAM SOLOMONS. "**Organic Chemistry.**" 4th Ed. U.S.: John Wiley & Son, INC. 2011.

39 "**Hydrogenation.**" [Online]. Available: http://en.wikipedia.org/wiki/Hydrogenation. 2015.

40 " **MPV reaction**" https: / / en. wikipedia. org/ wiki/ Meerwein- Ponndorf-Verley_reduction.

41 Zhu, Y., Liu, S., Jaenicke, S., & Chuah, G. (2004). **Zirconia catalysts in Meerwein-Ponndorf-Verley reduction of citral.** Catalysis Today, 97(4), 249-255.

42 **"Oligomerization."** [Online]. Available: https://www.ihs.com/products/chemical-technology-pep-reviews-oligomerization-for-gasoline-2009.html. 2009.

43 Olah, G., Molnár, A., & Prakash, G. (1995). **Hydrocarbon chemistry.** New York: John Wiley & Son.

44 Zhang, X., Liu, Z., Xu, X., Yue, H., Tian, G., & Feng, S. (2013). **Hydrothermal Synthesis of 1- Butanol from Ethanol Catalyzed with Commercial Cobalt Powder.** ACS Sustainable Chemistry & Engineering, 1(12), 1493-1497.

45 TSUCHIDA, T., KUBO, J., YOSHIOKA, T., SAKUMA, S., TAKEGUCHI, T., & UEDA, W. (2008). **Reaction of ethanol over hydroxyapatite affected by Ca/P ratio of catalyst.** Journal of Catalysis, 259(2), 183-189.

46 S. Totong, K. Faungnawakij, N. Laosiripojana. **"Hydrogen Production from Dehydrogenation of Ethanol over Ag-Based Catalysts."** World Academy of Science, Engineering and TechnologyInternational Journal of Chemical, Nuclear, Metallurgical and Materials Engineering Vol:8 No:2, 2014.

47 Shiau, C., Chen, S., Tsai, J., & Lin, S. (2000). **Effect of zinc addition on copper catalyst in isoamyl alcohol dehydrogenation.** Applied Catalysis A: General, 198(1-2), 95-102.

48 Makshina, E., Janssens, W., Sels, B., & Jacobs, P. (2012). **Catalytic study of the conversion of ethanol into 1,3-butadiene.** Catalysis Today, 198(1), 338-344.

49 Sushkevich, V., Ivanova, I., Ordomsky, V., & Taarning, E. (2014). **Design of a Metal-Promoted Oxide Catalyst for the Selective Synthesis of Butadiene from Ethanol.** Chemsuschem, 7(9), 2527-2536.

50 Rad, A., Khoshgouei, M., Rezvani, S., & Rezvani, A. (2012). **Study of Cu–Ni/SiO_2 catalyst prepared from a novel precursor, $[Cu(H_2O)_6][Ni(dipic)_2].2H_2O/SiO_2$, for water gas shift reaction.** Fuel Processing Technology, 96, 9-15.

51 Yoshida, R., Sun, D., Yamada, Y., Sato, S., & Hutchings, G. (2017). **Vapor-phase hydrogenation of levulinic acid to γ-valerolactone over Cu-Ni bimetallic catalysts.** Catalysis Communications, 97, 79-82.

52 Bhaskar, S., & Jagirdar, B. (2017). **A journey from bulk brass to nanobrass: A comprehensive study showing structural evolution of various Cu/Zn bimetallic nanophases from the vaporization of brass.** Journal of Alloys And Compounds, 694, 581-595.

53 Singh, M., Sinha, I., & Mandal, R. (2009). **Synthesis of nanostructured Ag–Cu alloy ultra-fine particles.** Materials Letters, 63(26), 2243-2245.

54 Kim, J., Chung, M., Ka, B., Ku, J., Park, S., Ryu, J., & Oh, S. (2010). **The Role of Metallic Fe and Carbon Matrix in Fe_2O_3/ Fe/ Carbon Nanocomposite for Lithium- Ion Batteries.** Journal of The Electrochemical Society, 157(4), A412-A417.

55 Ausavasukhi, A., Suwannaran, S., Limtrakul, J., & Sooknoi, T. (2008). **Reversible interconversion behavior of Ag species in AgHZSM-5: XRD, 1H MAS NMR, TPR, TPHE, and catalytic studies.** Applied Catalysis A: General, 345(1), 89-96.

56 Ji, D., Zhu, W., Wang, Z., Wang, G. (2007) **Dehydrogenation of cyclohexanol on Cu–ZnO/SiO2 catalysts: The role of copper species.** Catalysis Communications, 8(12), 1891-1895.

57 Sun, C., Mao, D., Han, L., & Yu, J. (2016). **Effect of preparation method on performance of Cu–Fe/SiO_2 catalysts for higher alcohols synthesis from syngas.** RSC Advances, 6(60), 55233-55239.

58 Jeon, G., & Chung, J. (1997). **Effect of iron on Cu/SiO_2 catalysts for the dehydrogenation of cyclohexanol to cyclohexanone.** Korean Journal of Chemical Engineering, 14(1), 49-58.

59 Kubo, K., Iida, H., Namba, S., & Igarashi, A. (2015). **Comparison of steaming stability of Cu-ZSM-5 with those of Ag-ZSM-5, P/H-ZSM-5, and H-ZSM-5 zeolites as naphtha cracking catalysts to produce light olefin at high temperatures.** Applied Catalysis A: General, 489, 272-279. 1

60 Witsuthammakul, A., & Sooknoi, T. (2016). **Selective hydrodeoxygenation of bio-oil derived products: acetic acid to propylene over hybrid CeO_2– Cu/ zeolite catalysts.** Catalysis Science & Technology, 6(6), 1737-1745.

61 Vitale, G., Molero, H., Hernandez, E., Aquino, S., Birss, V., & Pereira-Almao, P. (2013). **One-pot preparation and characterization of bifunctional Ni-containing ZSM-5 catalysts.** Applied Catalysis A: General, 452, 75-87.

62 Johansson, R., Hruby, S., Rass-Hansen, J., & Christensen, C. (2008). **The Hydrocarbon Pool in Ethanol-to-Gasoline over HZSM-5 Catalysts.** Catalysis Letters, 127(1-2), 1-6.

63 Sun, X., Mueller, S., Liu, Y., Shi, H., Haller, G., & Sanchez-Sanchez, M. et al. (2014). **On reaction pathways in the conversion of methanol to hydrocarbons on HZSM-5.** Journal of Catalysis, 317, 185-197.

64 Phung, T., Radikapratama, R., Garbarino, G., Lagazzo, A., Riani, P., & Busca, G. (2015). **Tuning of product selectivity in the conversion of ethanol to hydrocarbons over H-ZSM-5 based zeolite catalysts.** Fuel Processing Technology, 137, 290-297.

65 Ploynisa Phichitsurathaworn, Supanut Ketaniruj, Settawat Sitthithai **"Conversion of ethanol to gasoline over metal transition loaded H-ZSM-5 zeolite catalysts"** A SPECIAL PROJECT FACULTY OF SCIENCE KING MONGKUT'S INSTITUTE OF TECHNOLOGY LADKRABANG.

66 Lisiane V. Mattos, Gary Jacobs, Burtron H. Davis, and Fabio B. Noronha **Production of Hydrogen from Ethanol: Review of Reaction Mechanism and Catalyst Deactivation** Chemical reviews 2012, 112, 4094-4123.

67 Inui, K., Kurabayashi, T., & Sato, S. (2002). **Direct synthesis of ethyl acetate from ethanol over Cu-Zn-Zr-Al-O catalyst.** Applied Catalysis A: General, 237(1-2), 53-61.

68 MEKHEMER, G., HALAWY, S., MOHAMED, M., & ZAKI, M. (2005). **Ketonization of acetic acid vapour over polycrystalline magnesia: in situ Fourier transform infrared spectroscopy and kinetic studies.** Journal of Catalysis, 230(1), 109-122.

69 Rao, R., Walters, A., & Vannice, M. (2005). **Influence of Crystallite Size on Acetone Hydrogenation over Copper Catalysts†.** The Journal of Physical Chemistry B, 109(6), 2086-2092.

70 Zheng, Z., Sun, C., Dai, R., Wang, S., Wu, X., & An, X. et al. (2017). **Ethanol Steam Reforming on Ni-Based Catalysts: Effect of Cu and Fe Addition on the Catalytic Activity and Resistance to Deactivation.** Energy & Fuels, 31(3), 3091-3100.

71 Mavrikakis, M., & Barteau, M. (1998). **Oxygenate reaction pathways on transition metal surfaces.** Journal of Molecular Catalysis A: Chemical, 131(1-3), 135-147.

72 Zhu, X., Lobban, L., Mallinson, R., & Resasco, D. (2010). **Tailoring the mesopore structure of HZSM-5 to control product distribution in the conversion of propanal.** Journal of Catalysis, 271(1), 88-98.

73 Tamiyakul, S., Sooknoi, T., Lobban, L., & Jongpatiwut, S. (2016). **Generation of reductive Zn species over Zn/HZSM–5 catalysts for n–pentane aromatization.** Applied Catalysis A: General, 525, 190-196.

74 Hoang, T., Zhu, X., Sooknoi, T., Resasco, D., & Mallinson, R. (2010). **A comparison of the reactivities of propanal and propylene on HZSM-5.** Journal of Catalysis, 271(2), 201-208.

APPENDIXES

Appendix A

CHARACTERIZATION OF CATALYSTS

1. X-ray diffraction

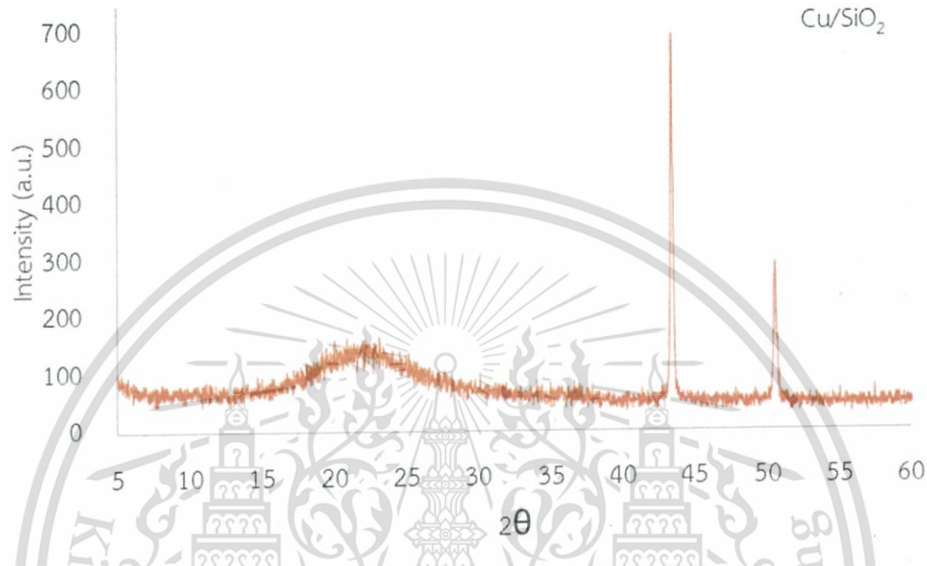

Fig.A1 X-ray pattern of 10wt%. Cu/SiO_2.

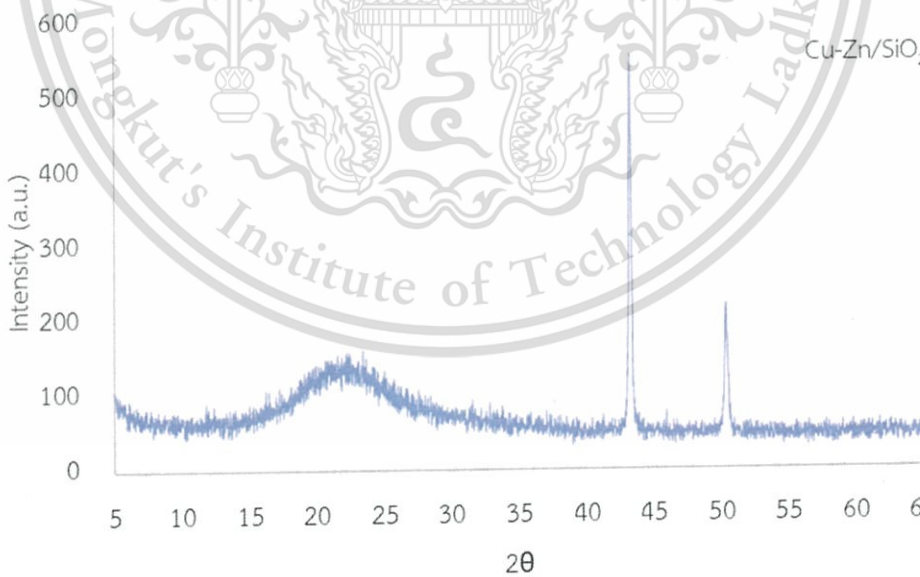

Fig.A2 X-ray pattern of 10wt%. Cu-2wt% Zn/SiO_2.

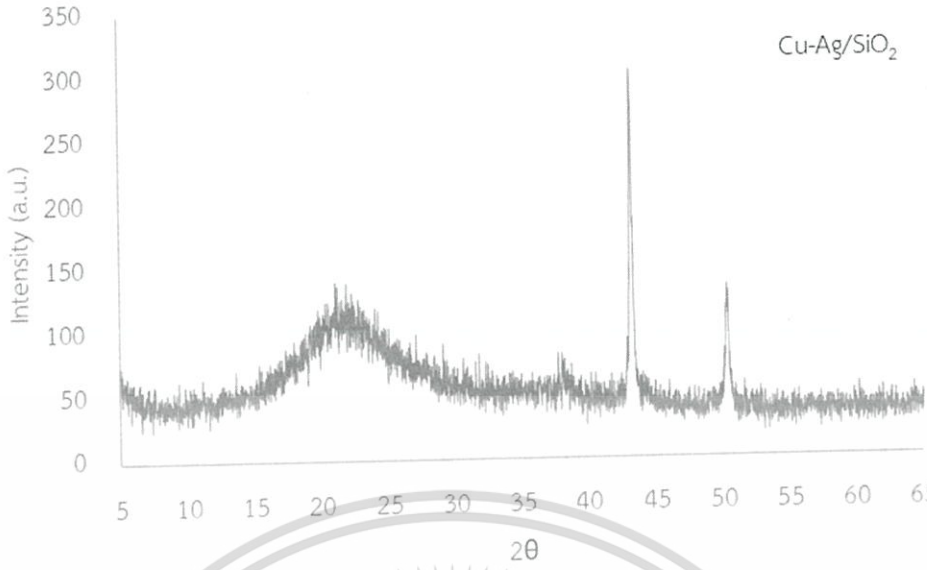

Fig.A3 X-ray pattern of 10wt%. Cu-2wt% Ag/SiO_2.

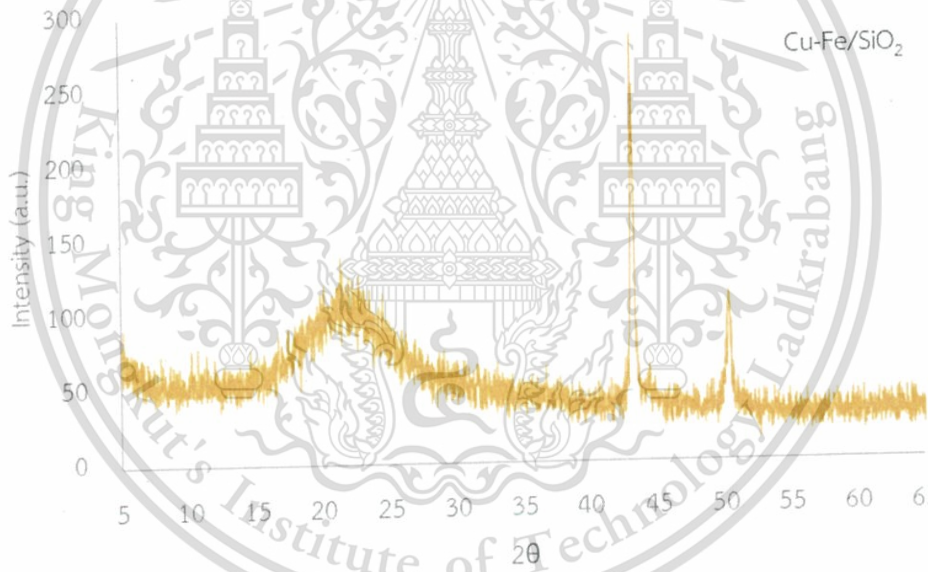

Fig.A4 X-ray pattern of 10wt%. Cu-2wt% Fe/SiO_2.

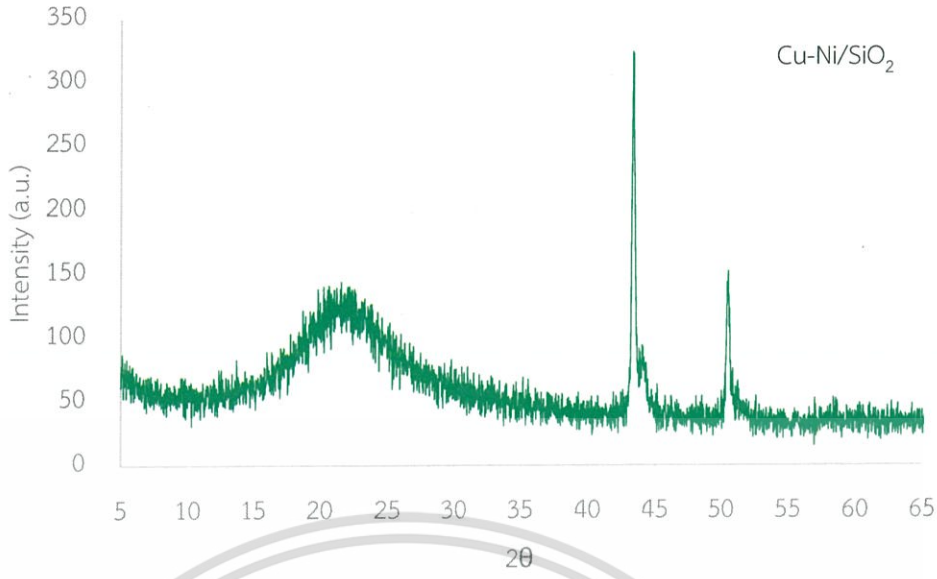

Fig.A5 X-ray pattern of 10wt%. Cu-2wt% Ni/SiO_2.

2. X-ray fluorescence.

Table A1 Elemental composition of 10%wt. Cu/SiO_2 catalyst.

SiO_2	CuO	Intensity Scal
70.9 KCps	211.4 KCps	
89.70%	9.76%	0.9165

Table A2 Elemental composition of 10%wt. Ag/SiO_2 catalyst.

SiO_2	AgO	Intensity Scal
1044.5 KCps	277.2 KCps	
85.50%	13.80%	0.9272

Table A3 Elemental composition of 10wt%. Cu-2wt% Ni/SiO_2catalyst.

SiO_2	CuO	NiO	Intensity Scal
88.5%	9.14%	2.29%	

Table A4 Elemental composition of 10wt%. Cu-2wt% Zn/SiO_2 catalyst.

SiO_2	Cu	Zn	Intensity Scal
48.7 KCps	146.1 KCps	44.3 KCps	
90.4%	7.75%	1.87%	0.9420

Table A5 Elemental composition of 10wt%. Cu-2wt% Ag/SiO_2 catalyst.

SiO_2	Cu	Ag	Intensity Scal
50.8 KCps	139.1 KCps	5 KCps	
91.7%	7.44%	0.88%	0.9477

Table A6 Elemental composition of 10wt%. Cu-2wt% Fe/SiO_2 catalyst.

SiO_2	Cu	Fe	Intensity Scal
43.7 KCps	153.2 KCps	18.7 KCps	
87.80%	9.80%	1.99%	

Example of elemental composition calculation from **Table A1**

Mole of each compositions :

SiO_2 = 89.70 g / (60.08 g/mol) = 1.4930 mol

CuO = 9.760 g / (79.55 g/mol) = 0.1227 mol

Weight of each elementals :

Si = 1.4930 mol × (28.09 g/mol) = 41.93840 g

Cu = 0.1227 mol × (63.55 g/mol) = 7.7976 g

Example of elemental composition calculation from **Table A3**

Mole of each compositions :

SiO_2 = 88.5 g / (60.08 g/mol) = 1.4730 mol

NiO = 2.29 g / (74.71 g/mol) = 0.0307 mol

CuO = 9.14 g / (79.55 g/mol) = 0.1149 mol

Weight of each elementals :

Si = 1.4730 mol × (28.09 g/mol) = 41.3766 g

Ni = 0.0307 mol × (58.71 g/mol) = 1.8024 g

Cu = 0.1149 mol × (63.55 g/mol) = 7.3019 g

3. Gas adsorption analysis

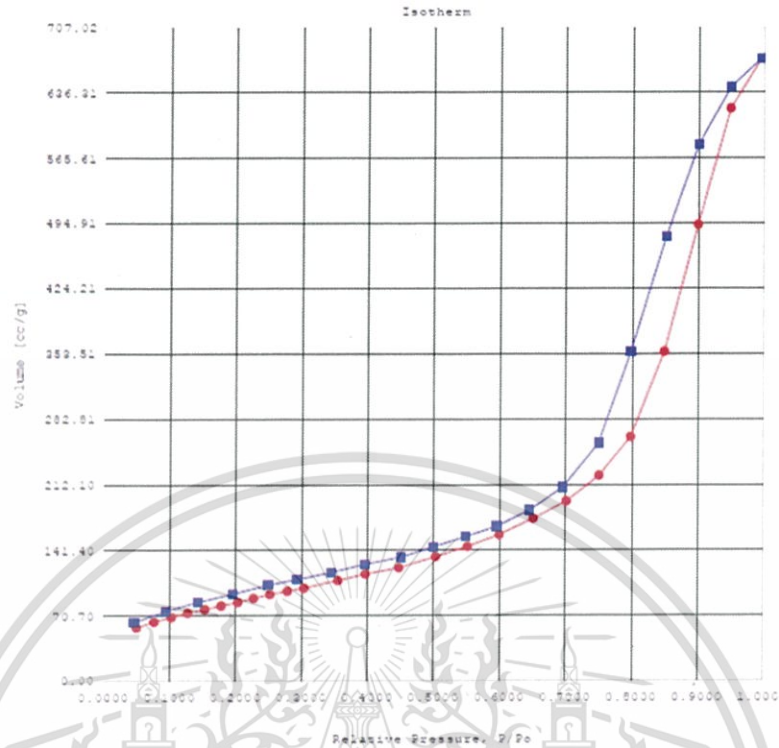

Area 319.05 m²/g

Fig.A6 Isotherm of SiO_2.

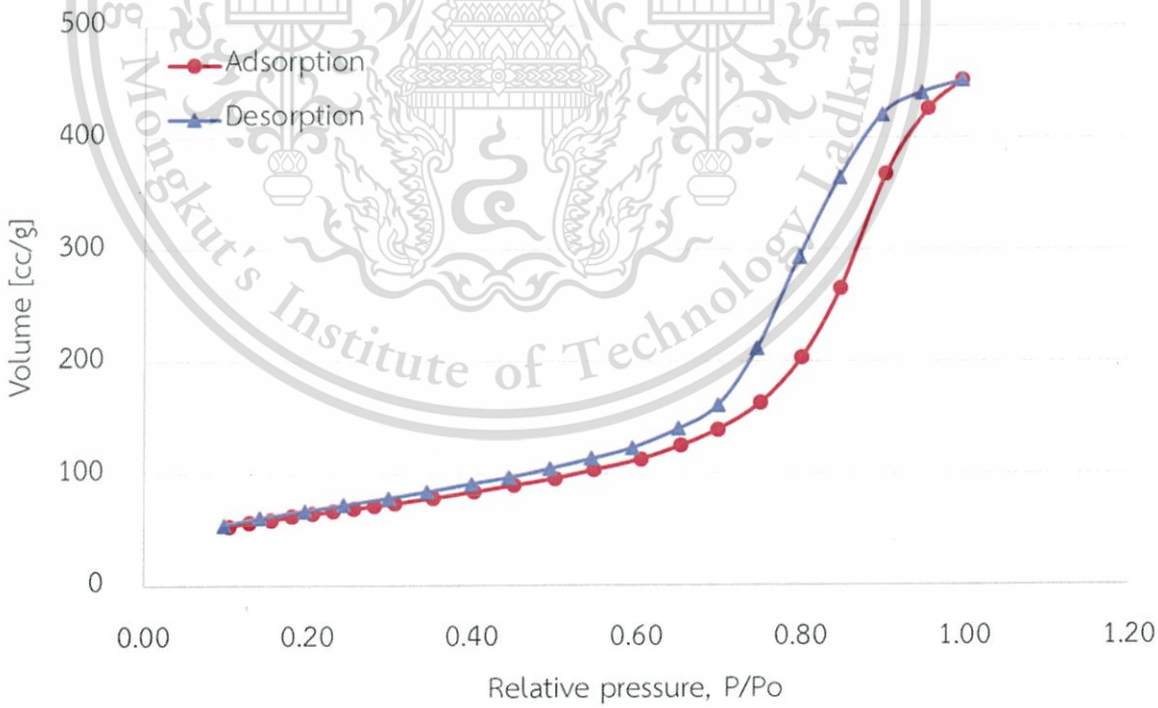

Area 228.61 m²/g

Fig.A7 Isotherm of 10wt%. Cu/SiO_2.

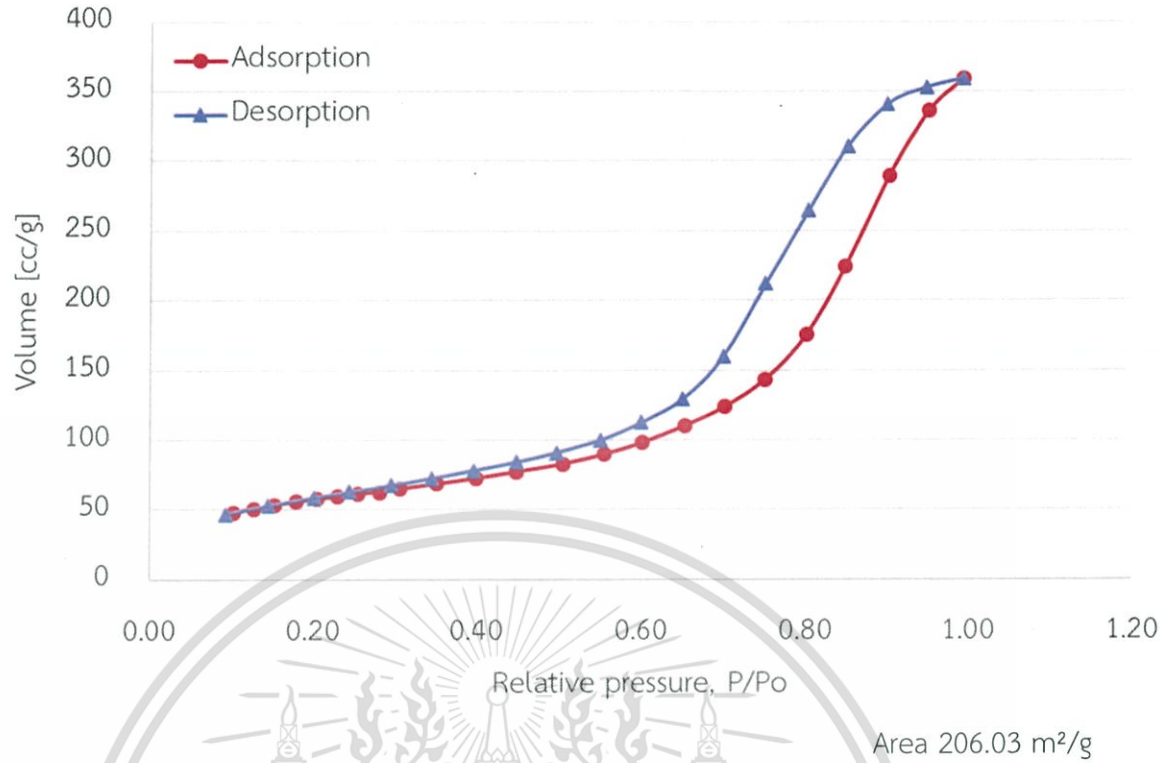

Area 206.03 m²/g

Fig.A8 Isotherm of 10wt%. Ag/SiO_2.

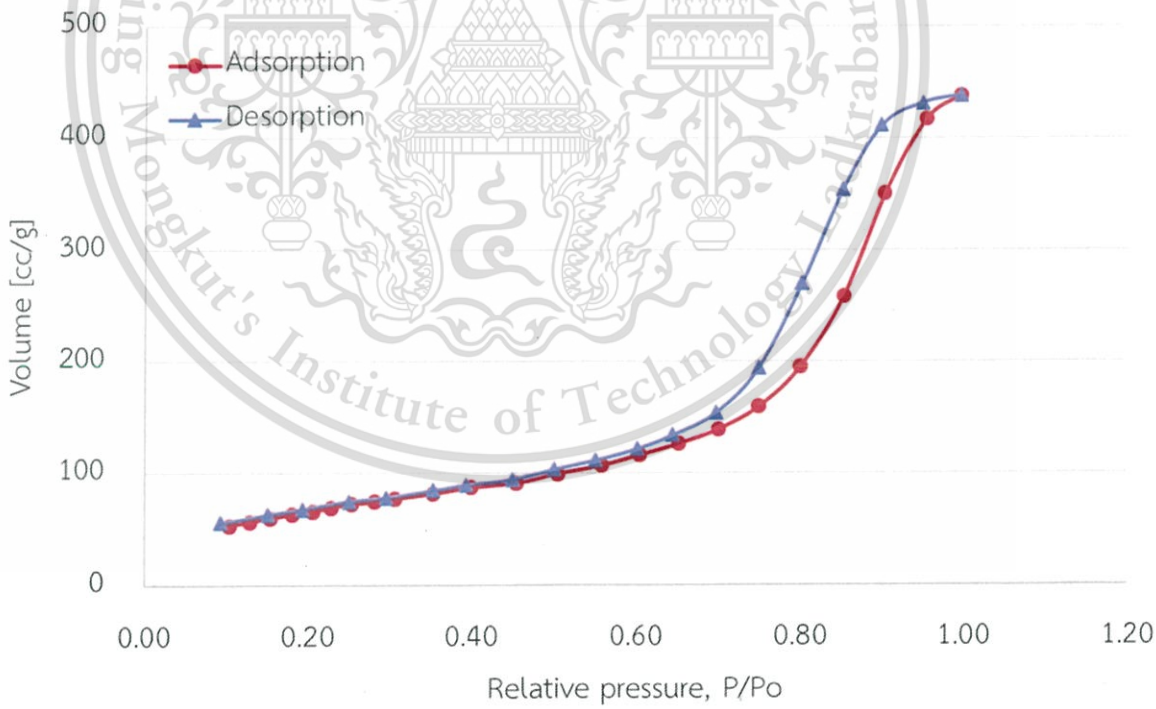

Area 243.97 m²/g

Fig.A9 Isotherm of 10%wt. Cu-2wt%. Zn/SiO_2.

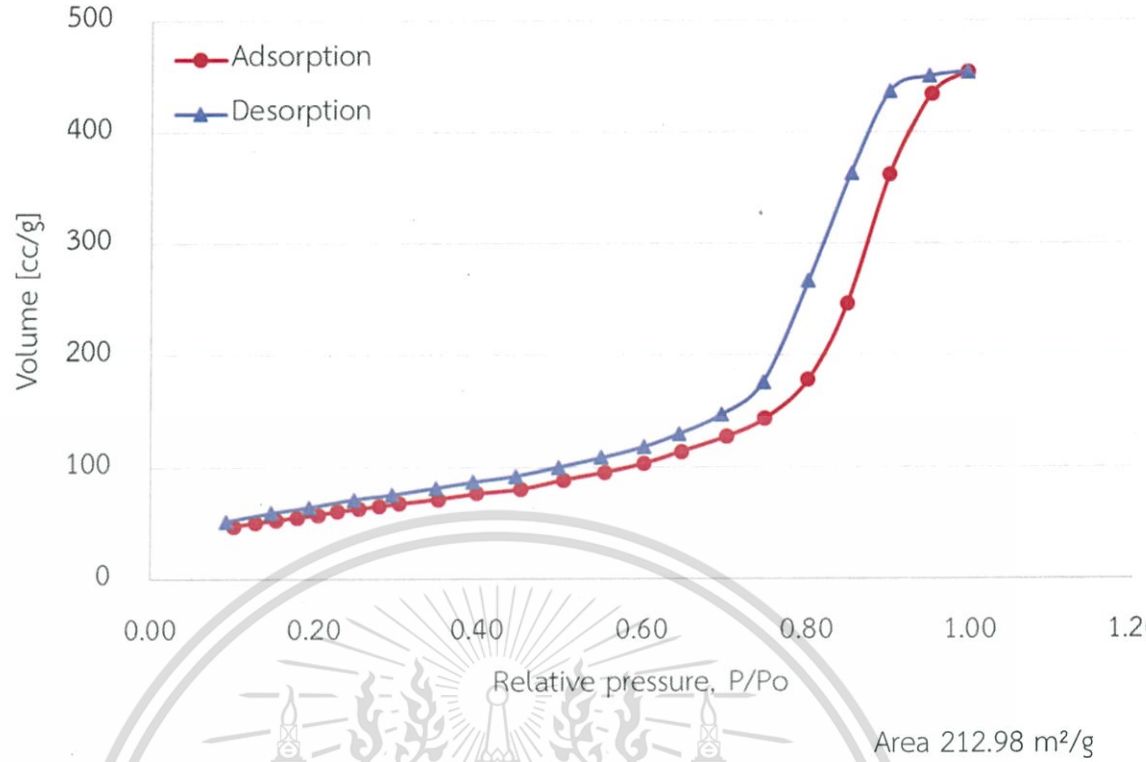

Fig.A10 Isotherm of 10%wt. Cu-2wt%. Ag/SiO_2.

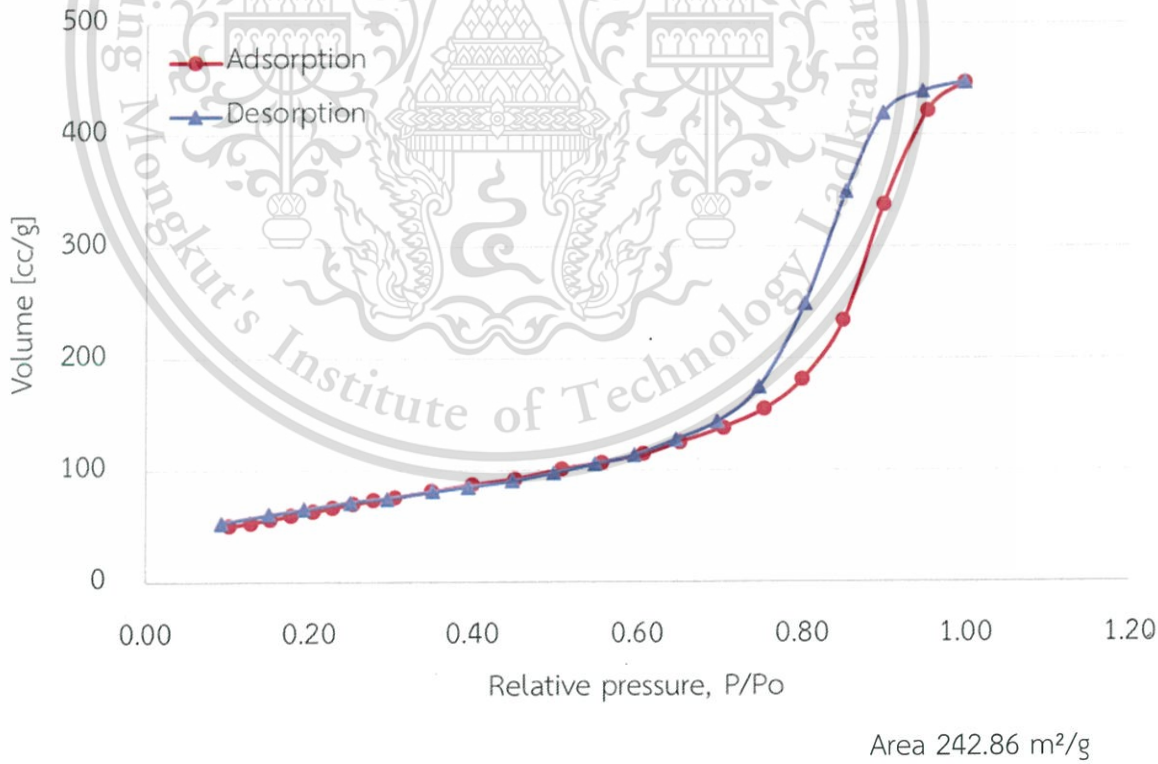

Fig.A11 Isotherm of 10%wt. Cu-2wt%. Fe/SiO_2.

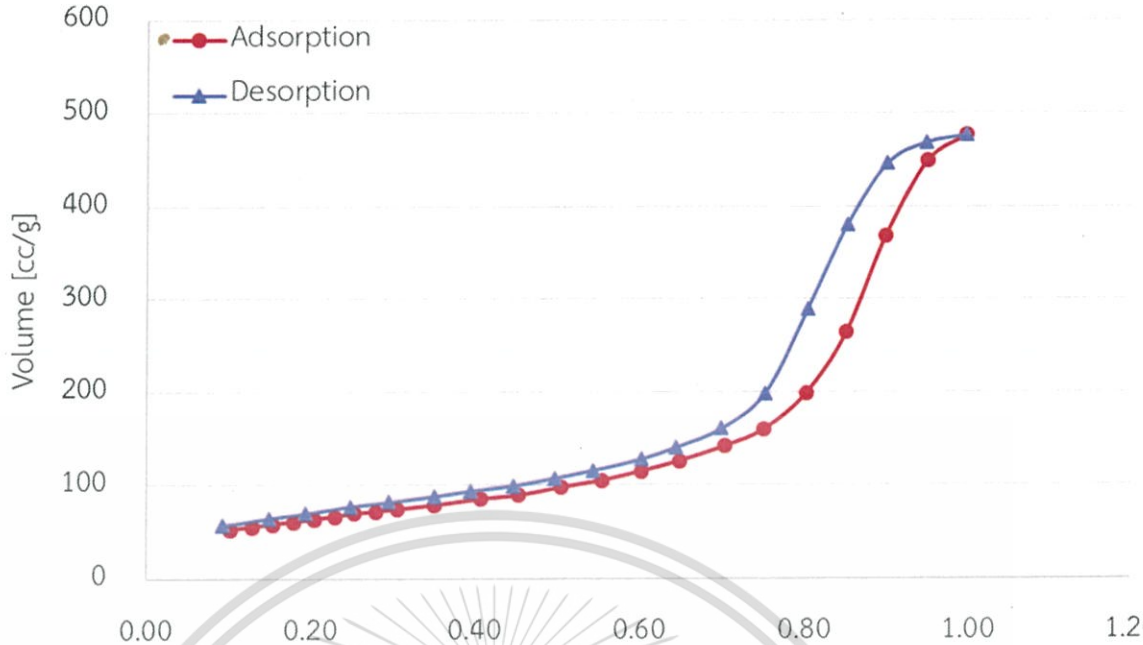

Area 233.11 m²/g

Fig.A12 Isotherm of 10%wt. Cu-2wt%. Ni/SiO_2.

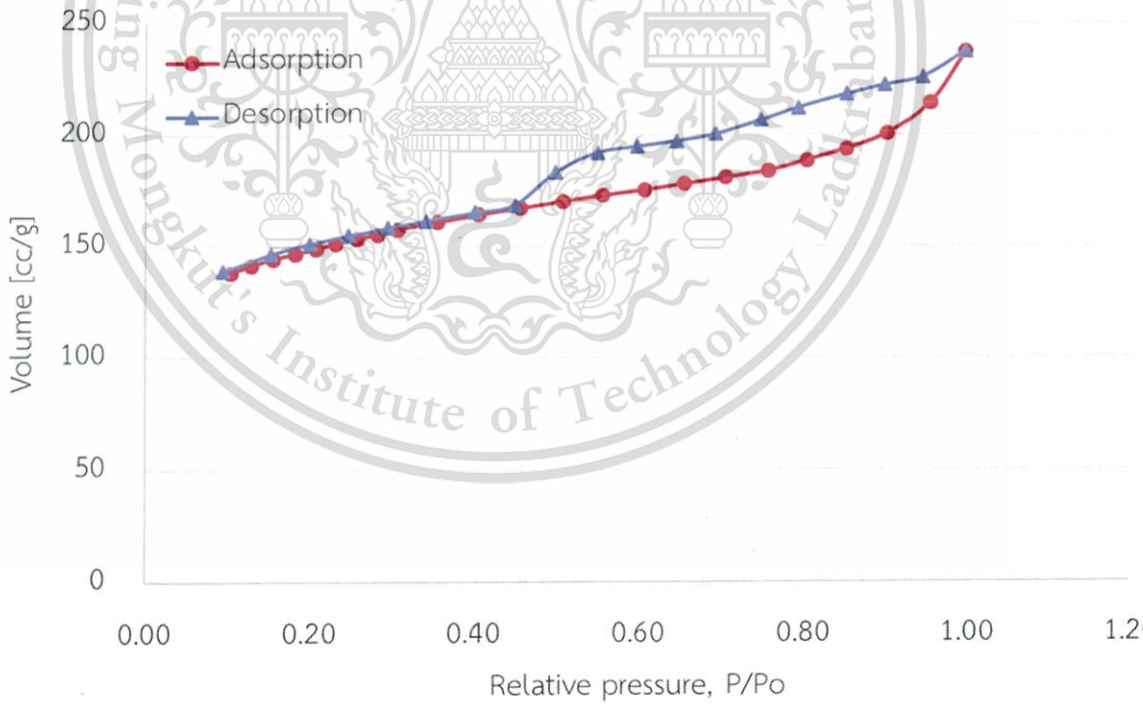

Area 479.18 m²/g

Fig.A13 Isotherm of H-ZSM-5 (28).

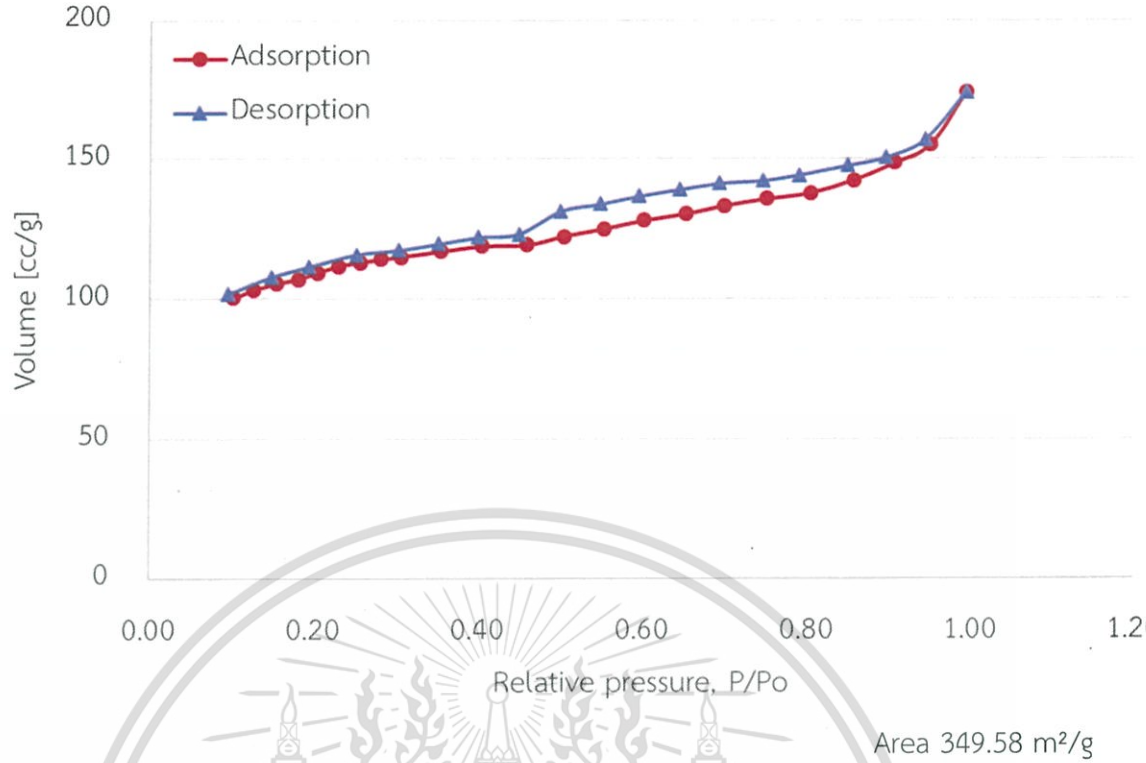

Fig.A14 Isotherm of Cu/H-ZSM-5 ratio 28.

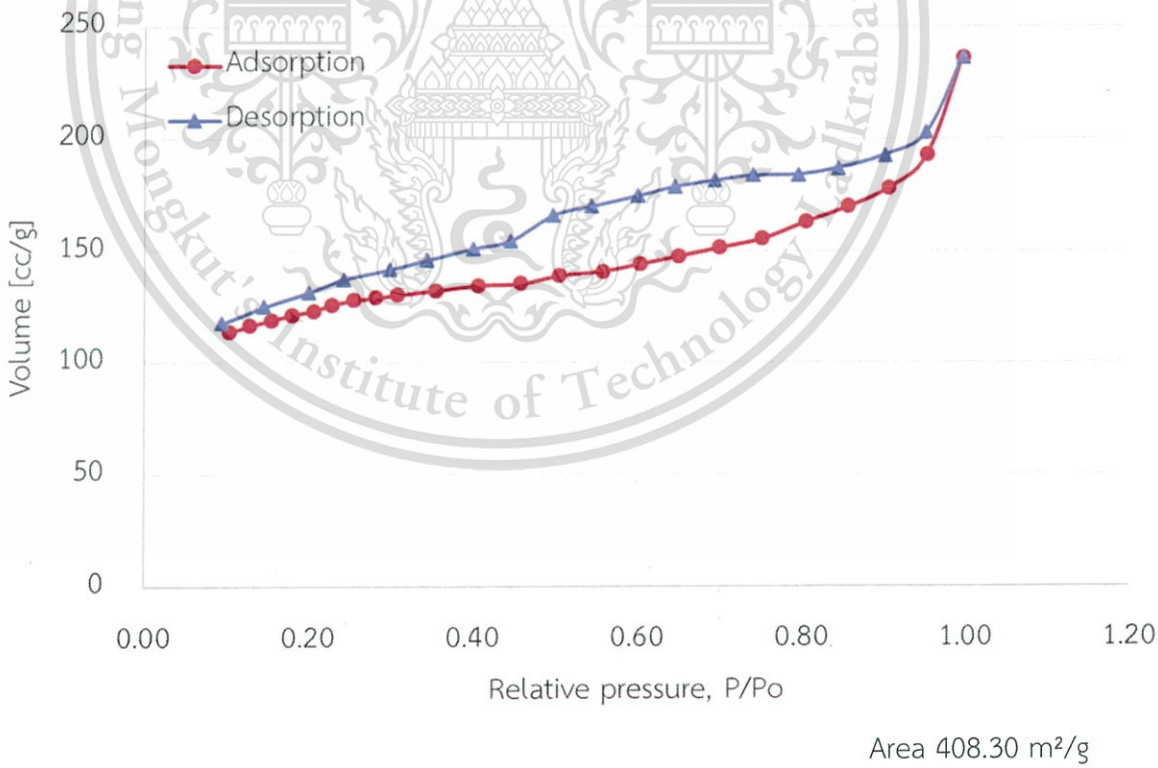

Fig.A15 Isotherm of Ni/H-ZSM-5 ratio 28.

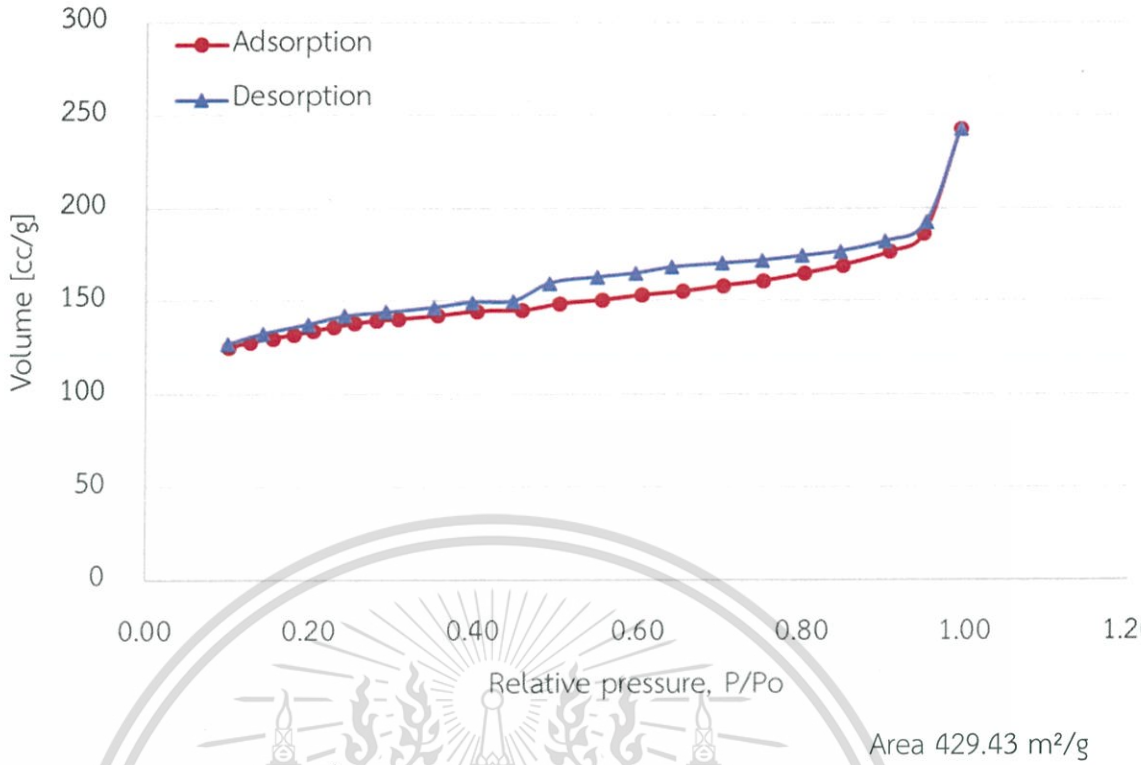

Fig.A16 Isotherm of Zn/H-ZSM-5 ratio 28.

4. Temperature programmed reduction.

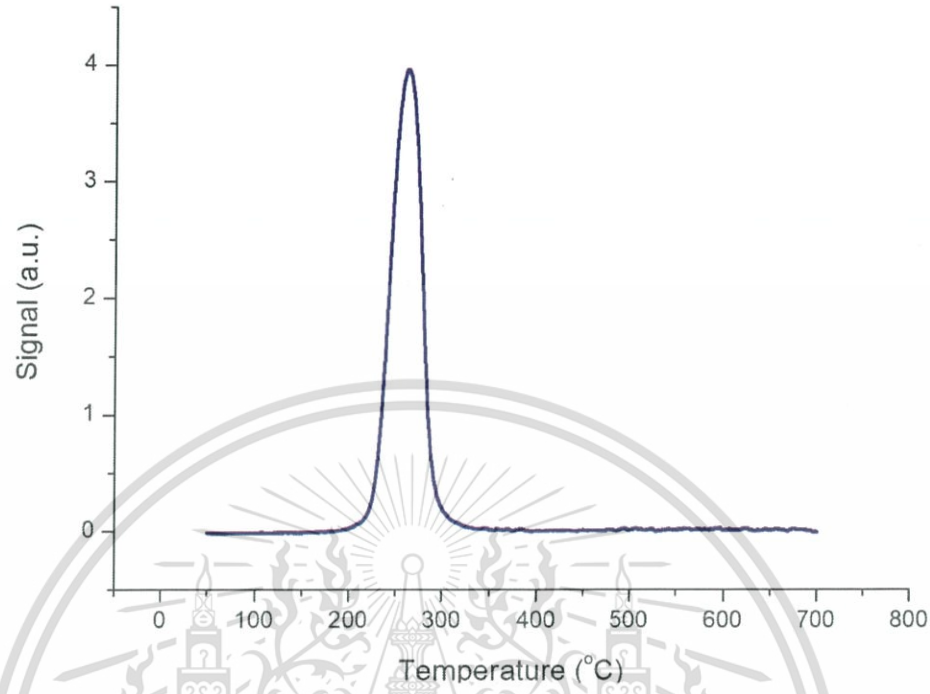

Fig.A17 Temperature programmed reduction of 10%wt. Cu/SiO_2.

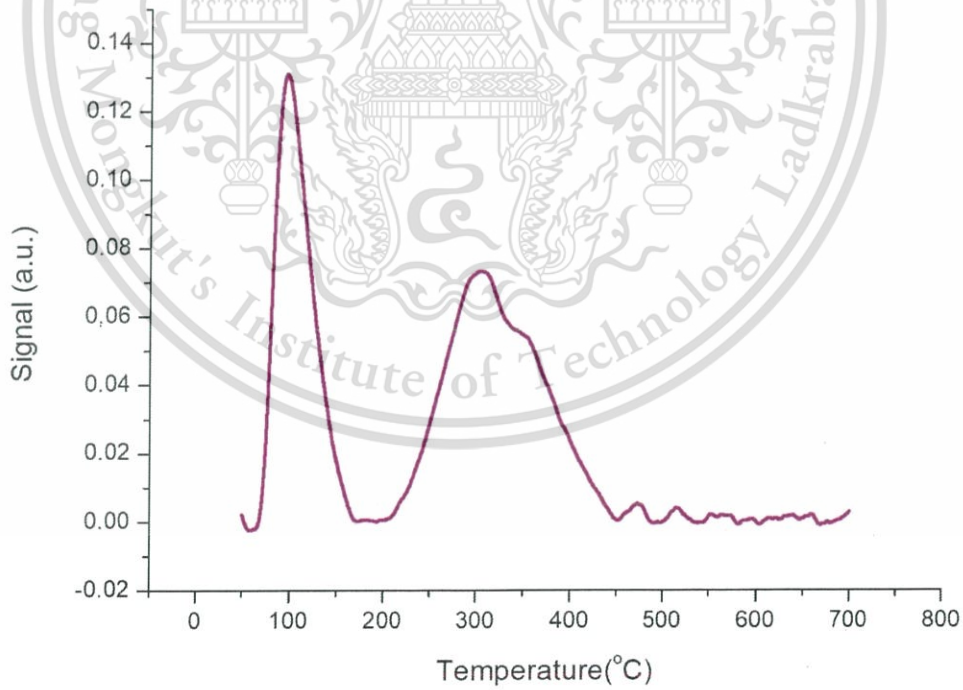

Fig.A18 Temperature programmed reduction of 10%wt. Ag/SiO_2.

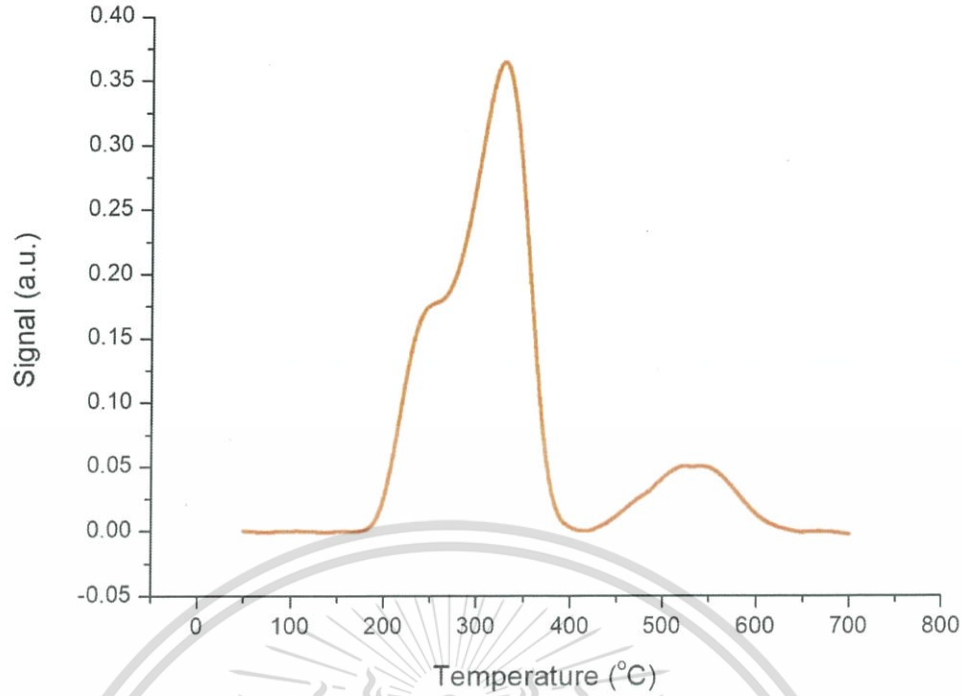

Fig.A19 Temperature programmed reduction of 10%wt. Cu-2wt%. Zn/SiO_2.

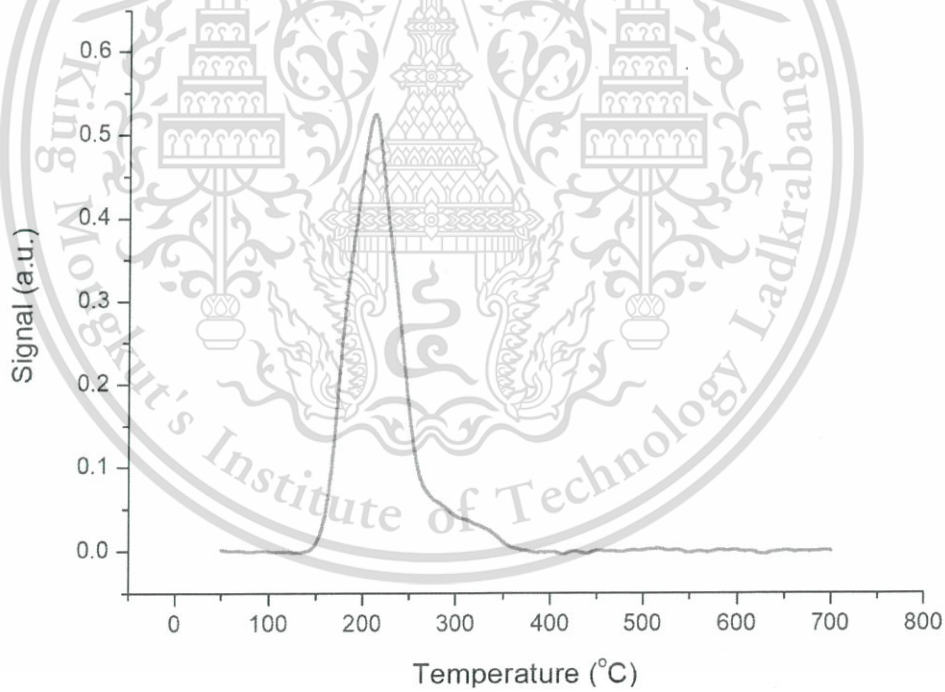

Fig.A20 Temperature programmed reduction of 10%wt. Cu-2wt%. Ag/SiO_2.

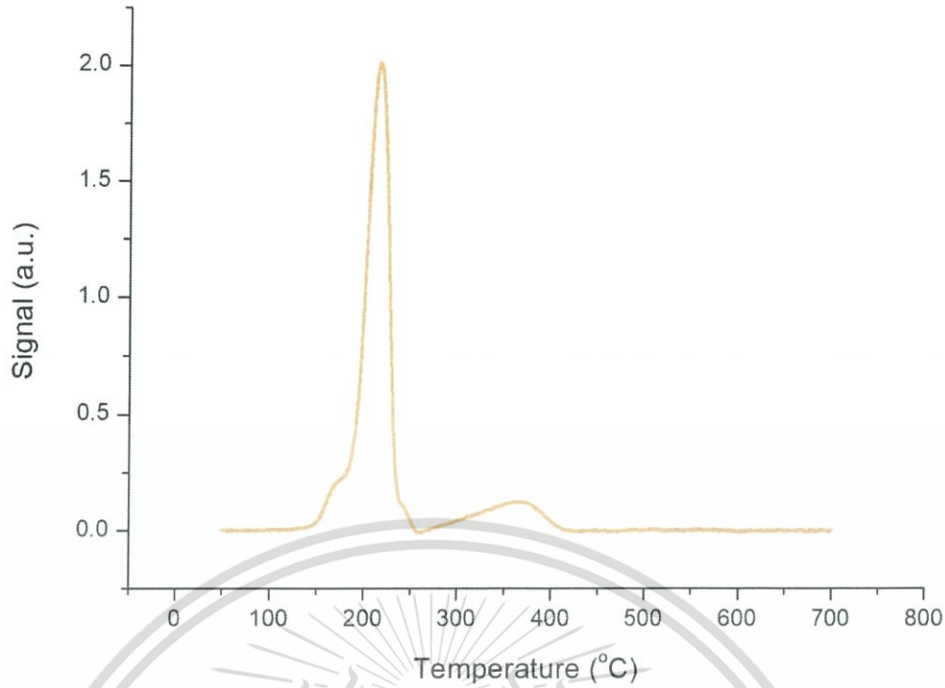

Fig.A21 Temperature programmed reduction of 10%wt. Cu-2wt%. Fe/SiO_2.

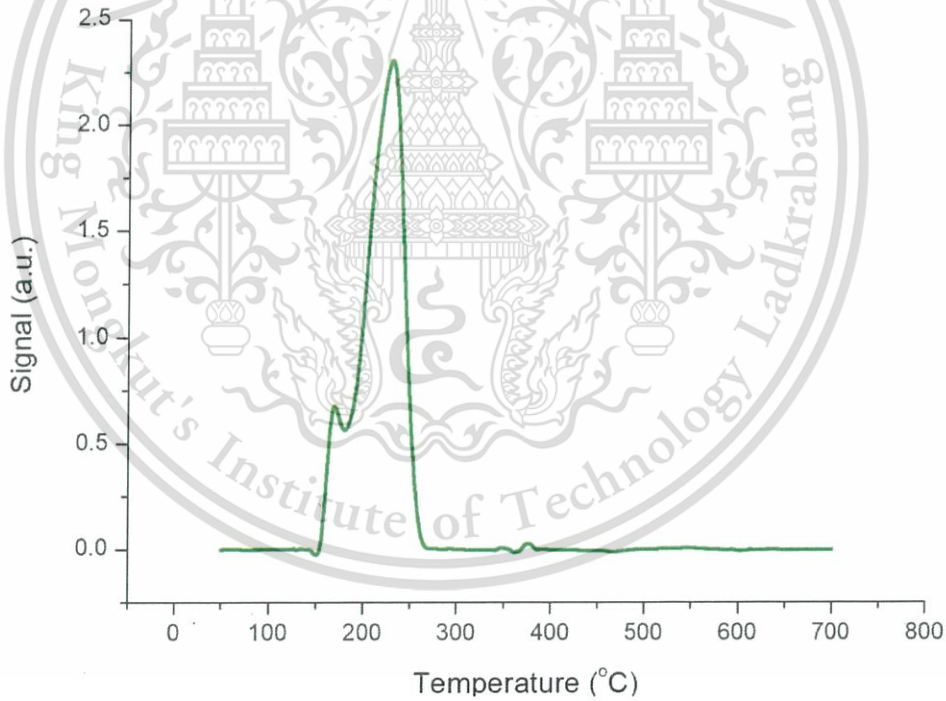

Fig.A22 Temperature programmed reduction of 10%wt. Cu-2wt%. Ni/SiO_2.

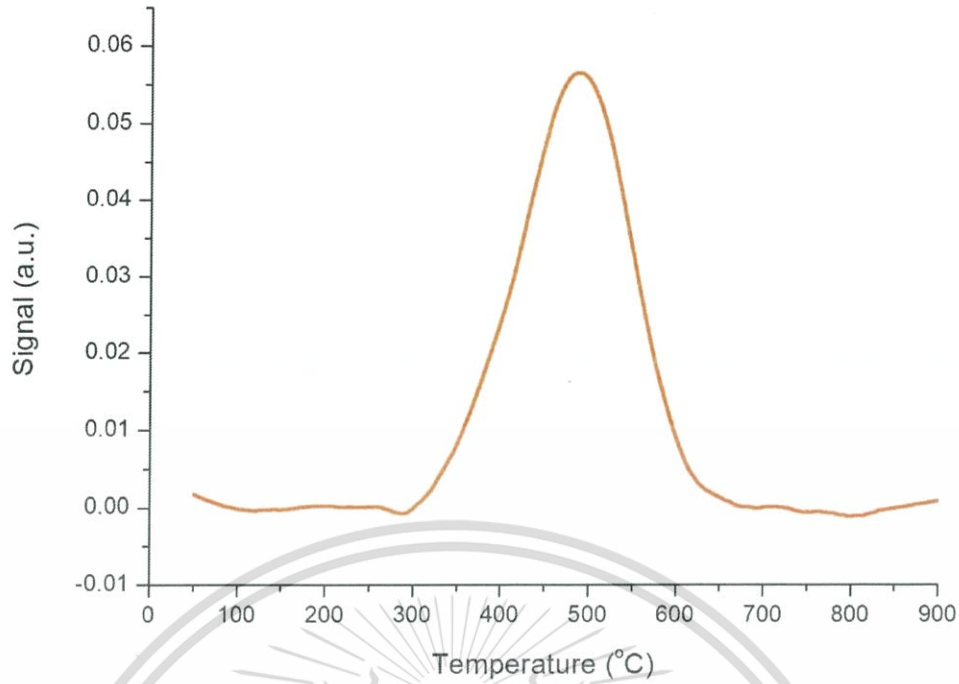

Fig.A23 Temperature programmed reduction of Ni/H-ZSM-5 ratio 28.

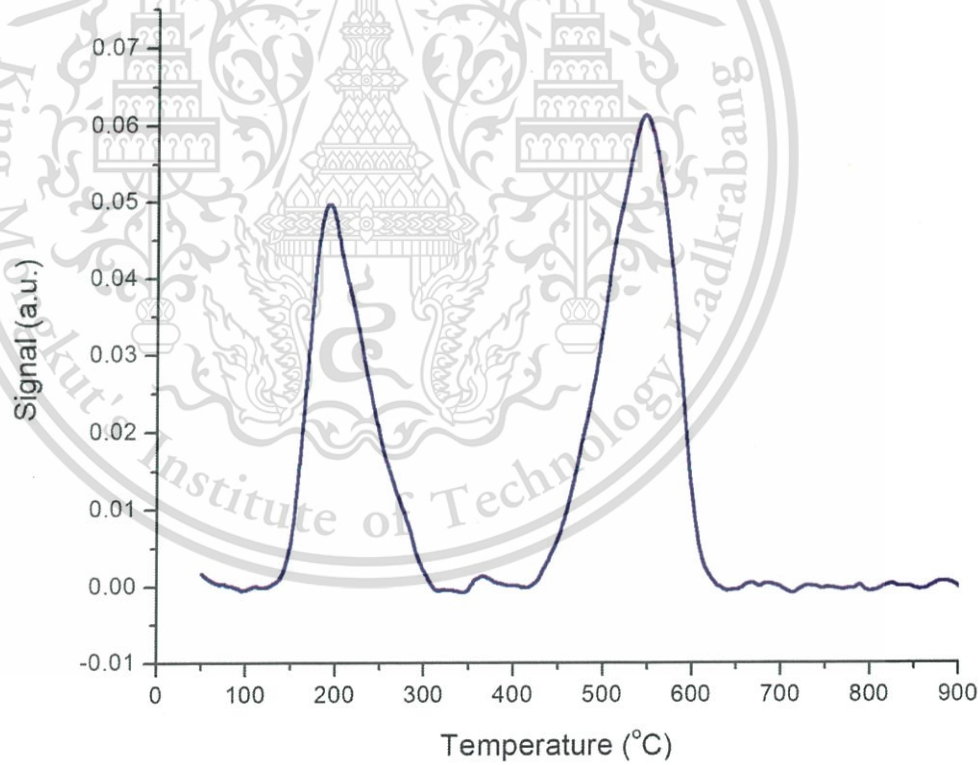

Fig.A24 Temperature programmed reduction of Cu/H-ZSM-5 ratio 28.

5. Temperature programmed desorption.

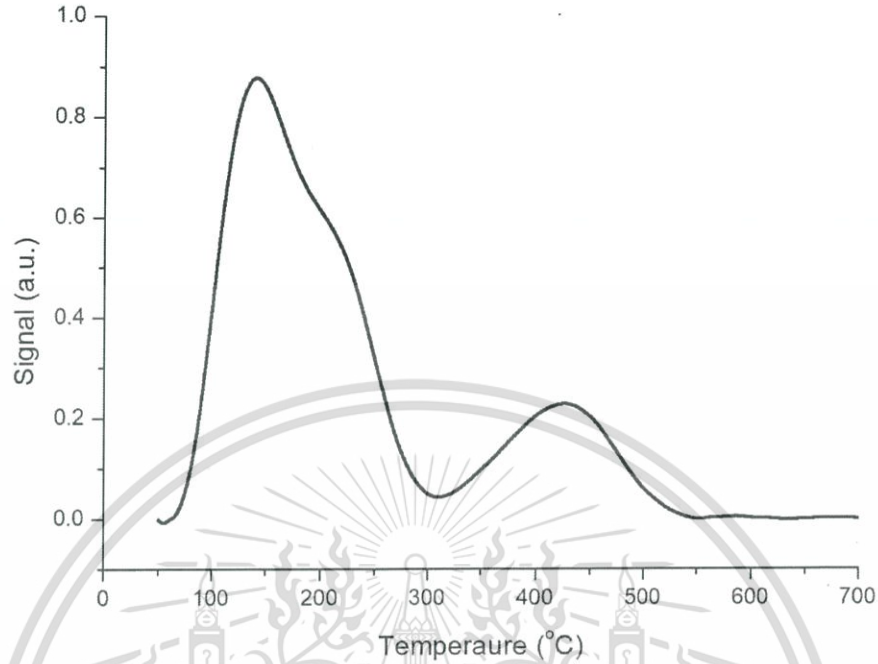

Fig.A25 Temperature programmed desorption of H-ZSM-5 ratio 28.

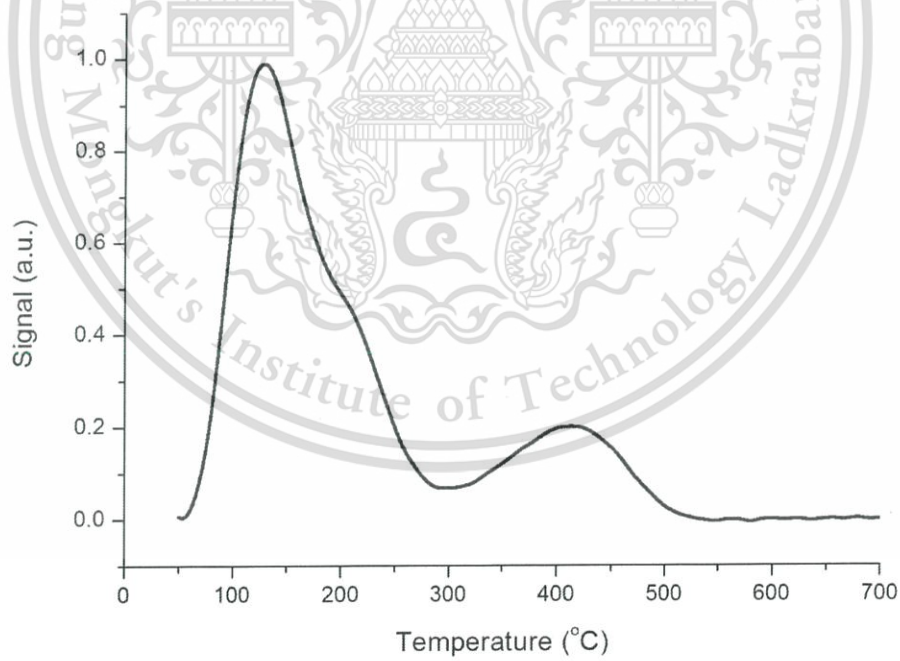

Fig.A26 Temperature programmed desorption of H-ZSM-5 ratio 40.

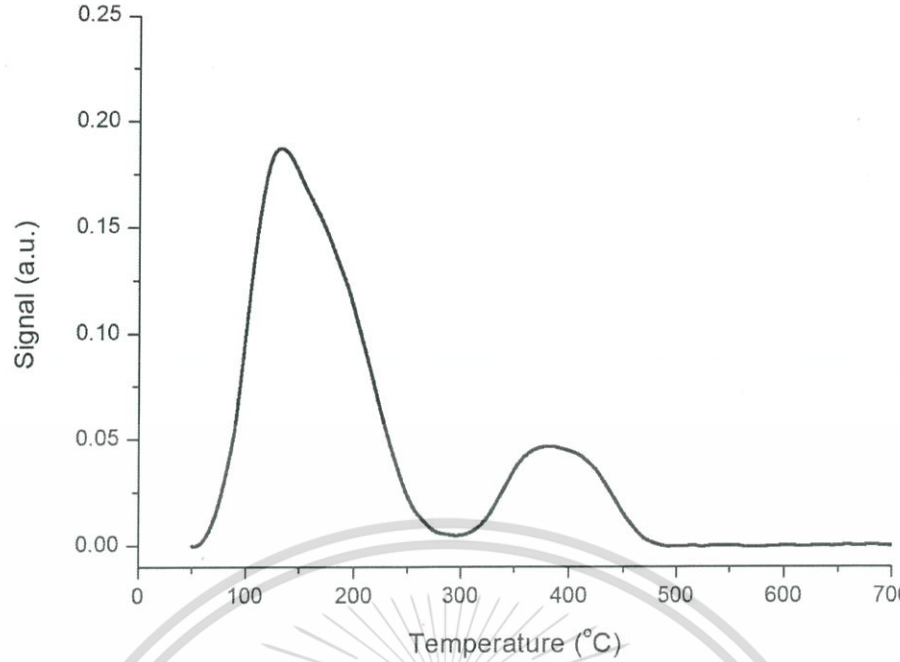

Fig.A27 Temperature programmed desorption of H-ZSM-5 ratio 140.

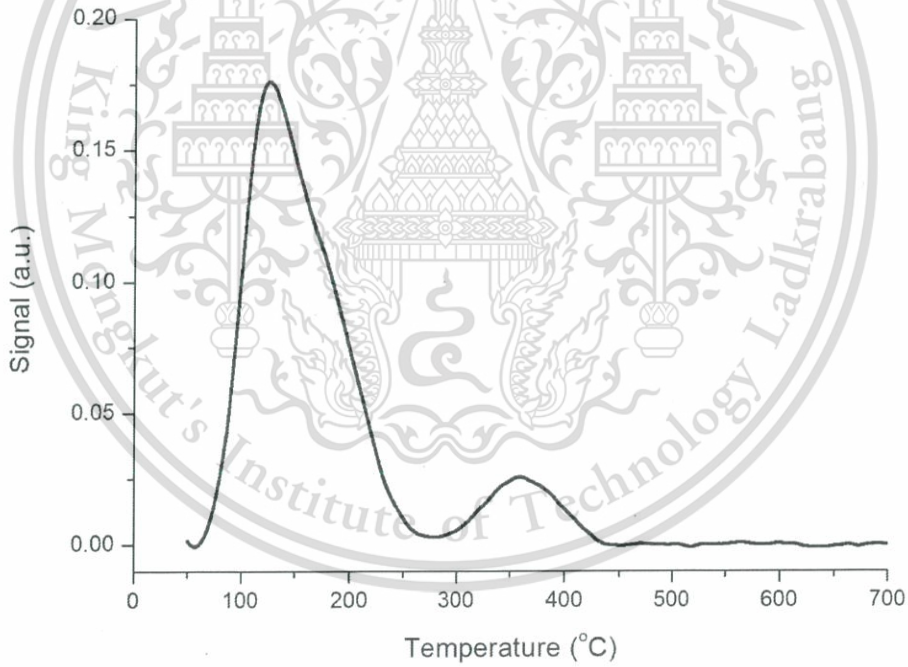

Fig.A28 Temperature programmed desorption of H-ZSM-5 ratio 250.

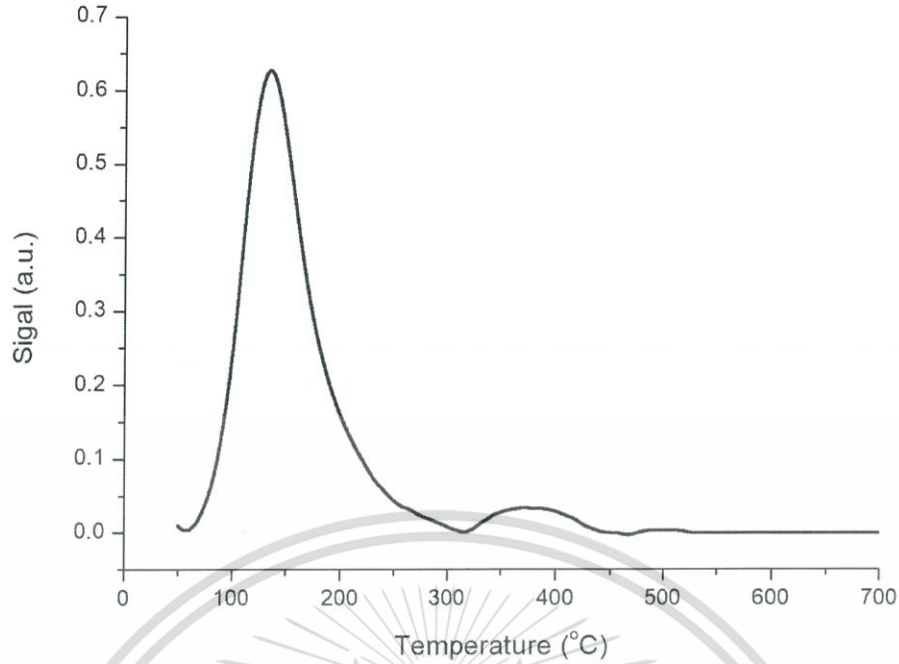

Fig.A29 Temperature programmed desorption of H-ZSM-5 ratio 500.

6. Transmission electron microscopy.

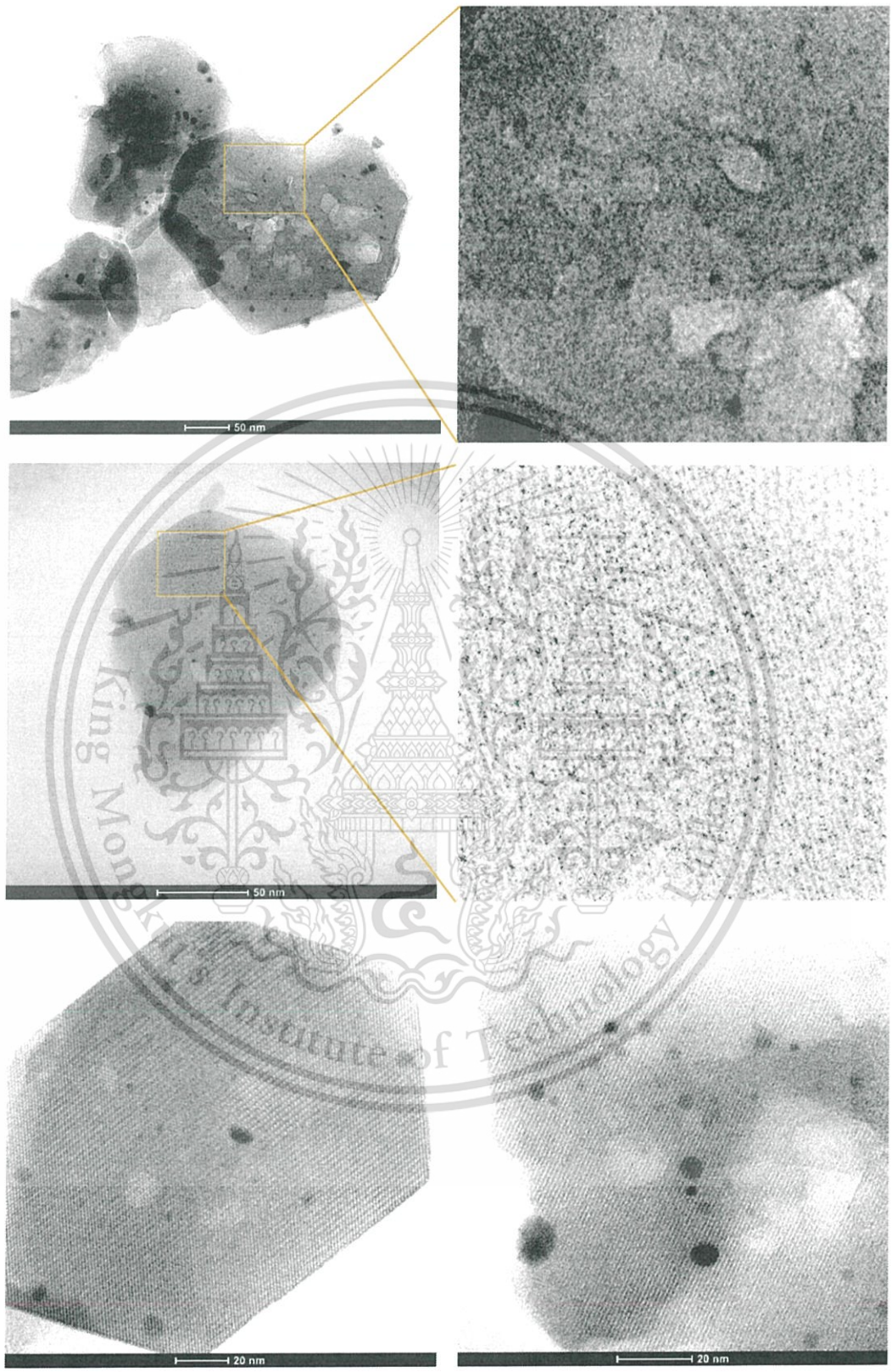

Fig.A31 Transmission electron microscope of Ni/H-ZSM-5 ratio 28.

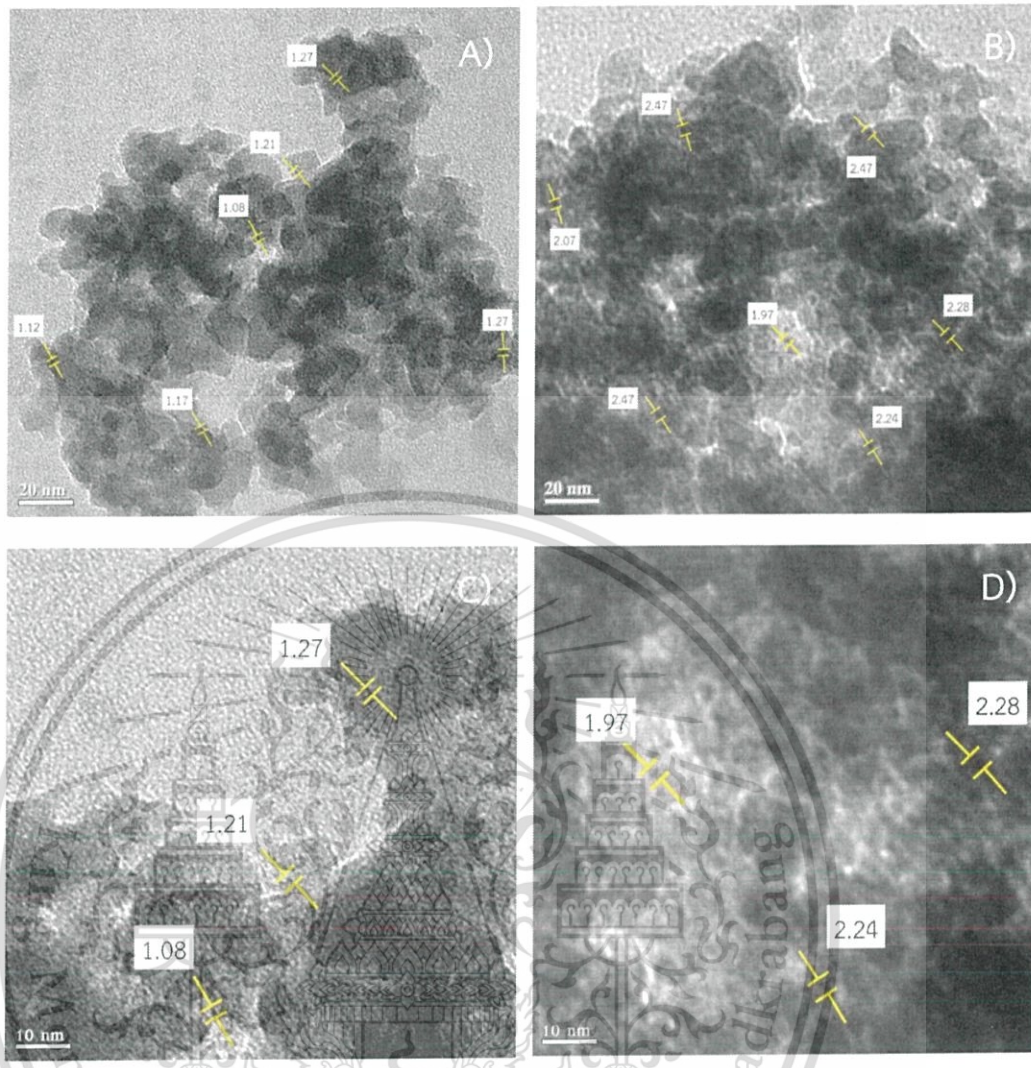

Fig.A31 Transmission electron microscope of fresh 10%wt. Cu/SiO_2 catalyst (A, C) and spent 10%wt. Cu/SiO_2 catalyst (B, D)

7. Thermogravimetric Analysis.

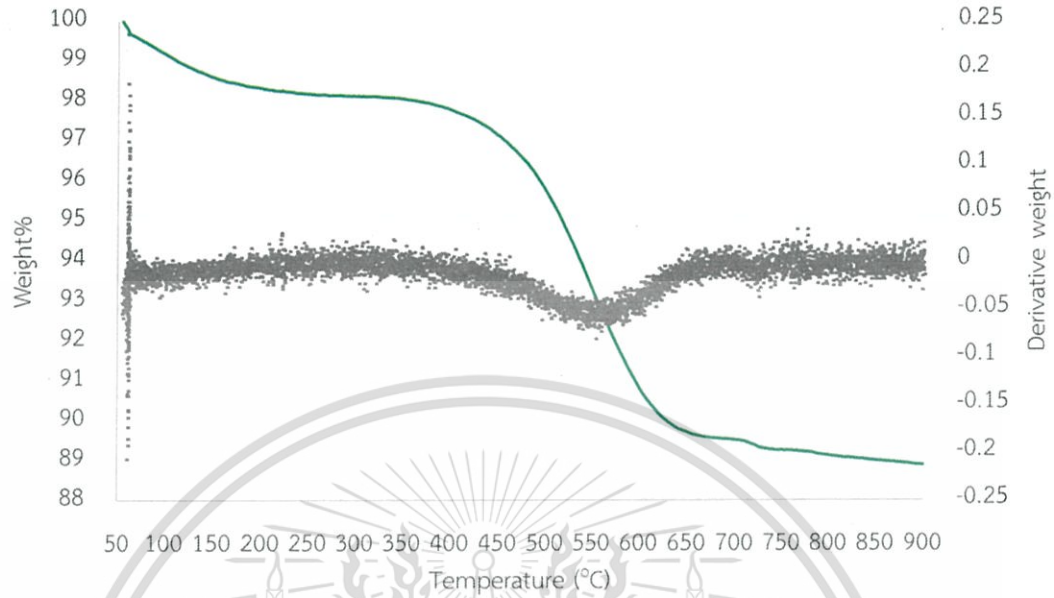

Fig.A32 Thermogravimetric Analysis of double bed system of 10wt%. Cu-2wt%. Zn/SiO_2 and H-ZSM-5 ratio 28.

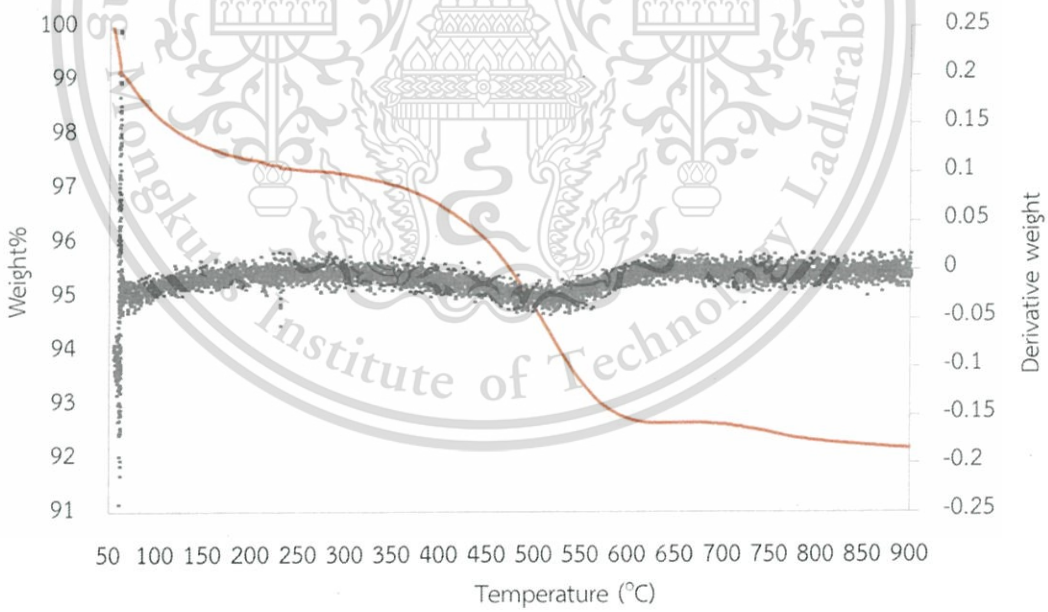

Fig.A33 Thermogravimetric Analysis of double bed system of 10wt%. Cu-2wt%. Zn/SiO_2 and Zn/H-ZSM-5 ratio 28.

8. Phase diagram.

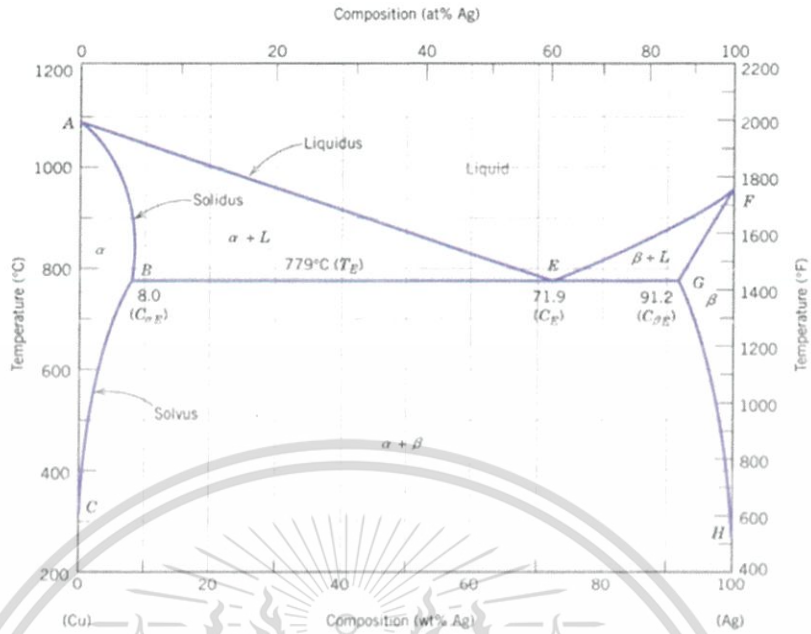

Fig.A34 Phase diagram of Cu-Ag

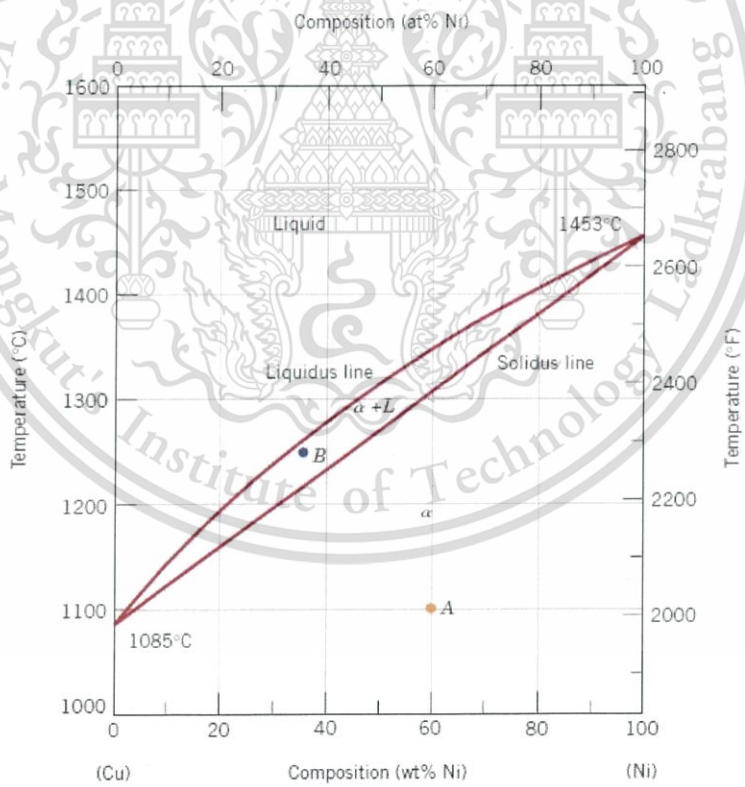

Fig.A35 Phase diagram of Cu-Ni

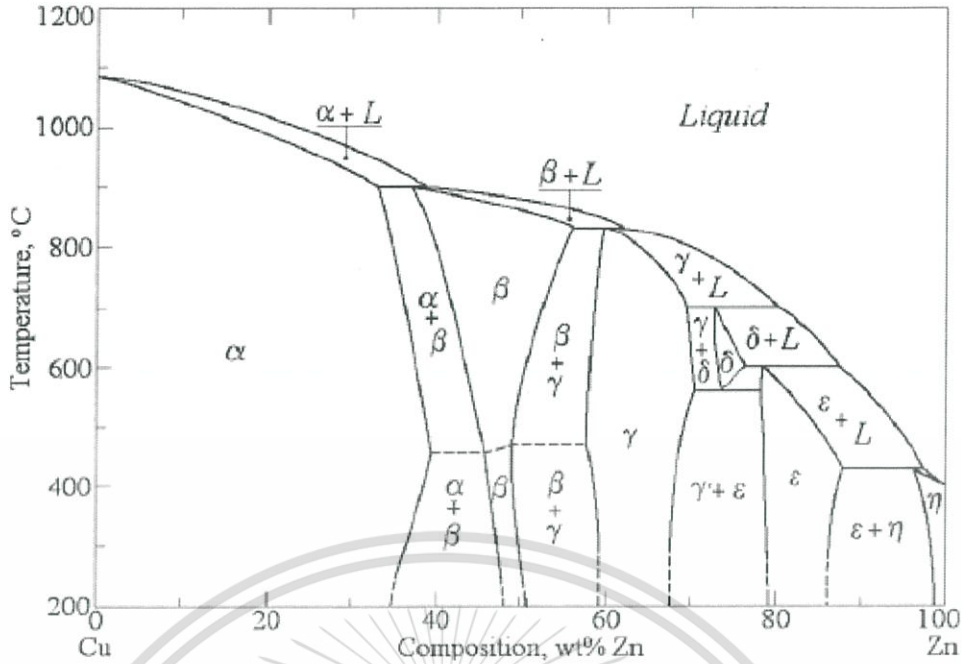

Fig.A36 Phase diagram of Cu-Zn

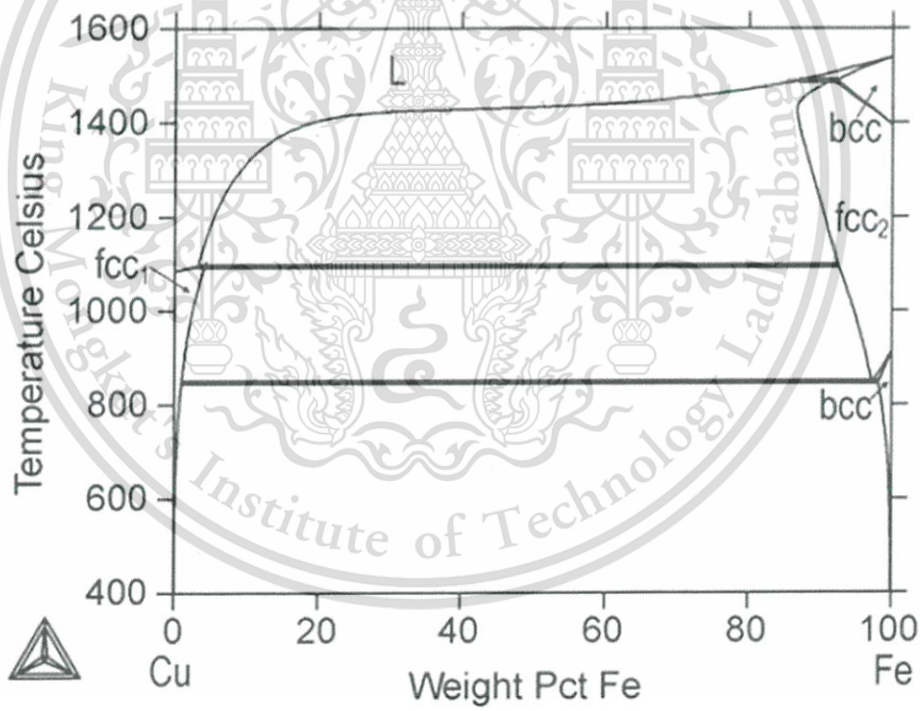

Fig.A37 Phase diagram of Cu-Fe

APPENDIX B

GAS CHROMATOGRAM

Analysis gas product from gas chromatography

Prior analysis, GC-MS (gas chromatography with mass spectrometer detector) was used to identify the structure of products in the sample and the GC-FID (gas chromatography with flam ionization detector) was used to determine the quantitative of the product with the condition expressed in **Table B1.**

Table B1 The GC condition for quantitative analysis

Column	Equity-1, 30 m x 0.53 mm x 3 μm
Temperature program	33°C (5 min hold) ramp to 85°C (2 min hold) at 15°/min and ramp to 220°C (3 min hold) at 10°/min
Carrier gas	Nitrogen gas, flow rate 5.2mL/min (40 cm/sec)
Injector temperature	230 °C
Detector temperature	FID at 280 °C

The products from ethanol were identified by comparing the retention time as listed in Table B2.

Table B2 Chromatogram data of standard product and feed.

Component	Retention time	Structure of Product
Ethylene	1.700	
Propylene	1.883	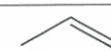
Acetaldehyde	2.183	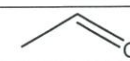
Ethanol	2.933	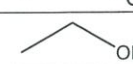

C4	2.300-2.583	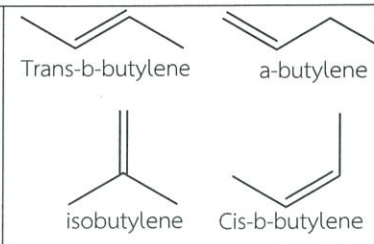
C5	4.050	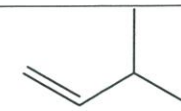 3-methyl-1-butene
	4.416	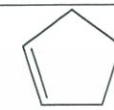 cyclopentene
C6	6.800	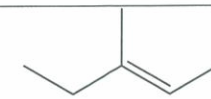 3-methyl-2-pentene
	7.100	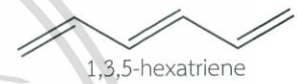 1,3,5-hexatriene
	8.050	 Benzene
C7	9.750	 4,4dimethyl-cyclopentene
	10.083	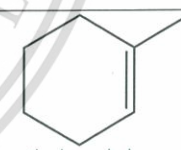 1-methyl-cyclohexene
	10.566	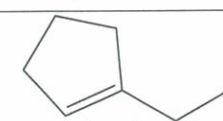 1-ethyl-cyclopentene
	11.216	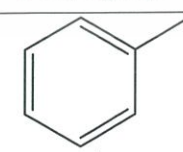 Toluene
C8	12.350	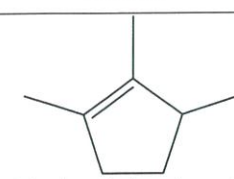 1,2,3-trimethyl-cyclopentene

C8	12.733	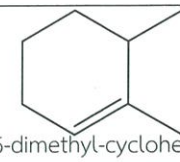 1,6-dimethyl-cyclohexene
	13.233	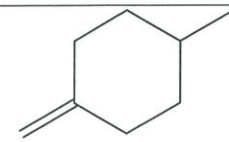 1-methyl-4-methylene-Cyclohexane
	13.533	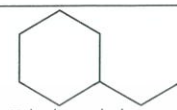 Ethyl-cyclohexane
	14.033	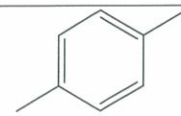 P-xylene
	14.266	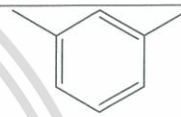 M-xylene
	14.900	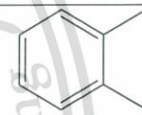 O-xylene
C9	16.450	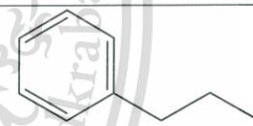 propyl-benzene
	16.633	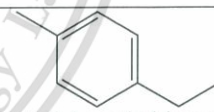 1-ethyl-4-methyl-benzene
	17.416	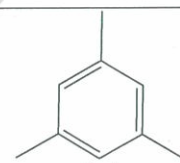 mesitylene
	18.066	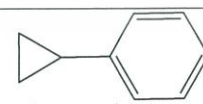 cyclopropyl-benzene
	18.400	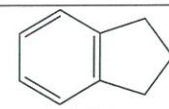 Indane
	18.583	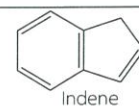 Indene

C10	18.733	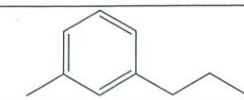 1-methyl-3-propyl-benzene
	19.383	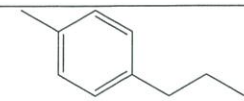 1-methyl-4-propyl-benzene
	20.066	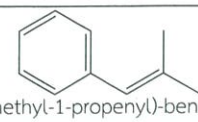 (2-methyl-1-propenyl)-benzene
	20.566	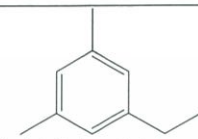 1-ethyl-3,5-dimethyl-benzene
	20.750	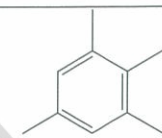 1,2,3,5-tetramethyl-benzene
	21.400	 5-methyl-2,3-dihydro-1H-Indene
	22.766	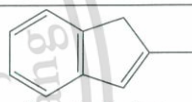 2-methylindene
	22.983	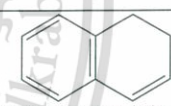 1,2-dihydro-Naphthalene
C11	22.300	 1-methyl-4-(1-methylpropyl)-Benzene
	23.500	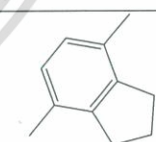 2,3-dihydro-4,7-dimethyl-1H-Indene
	25.250	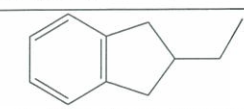 2-ethyl-2,3-dihydro-1H-indene
	25.466	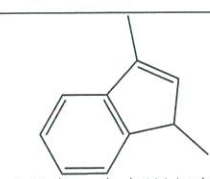 1,3-dimethyl-1H-Indene

C11	25.766	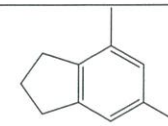 2,3-dihydro-4,6-dimethyl-1H-indene
	26.183	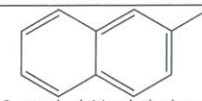 2-methyl-Naphthalene

APPENDIX C

CALCULATION

Calculation of catalytic parameters

Contact time **(W/F)**

$$W/F = \frac{\text{Weight of catalysts } (g)}{\text{Mole of reactant feed } (mol/h)}$$

Example

In the reaction using 0.0120 mol/h of ethanol in feed and using 0.1830 grams of catalyst, the W/F is calculated as follow:

$$W/F = [0.1830\ (g)\ /0.0120\ (mol/h)]$$

$$= 15.2500\ g.h/mol$$

In similar manner; W/F of catalyst with different catalyst weight and different feed rate are calculated.

Calculation of % yield of products from gas chromatography

From the chromatogram, the peaks of hydrocarbon samples were identified using of reference standard for comparison. The peak area of hydrocarbon (or oxygenated compounds) which possesses the equal number of carbon was summarized. The example of the peak area obtained from chromatogram of a mixture reactor outlet is shown in Table C1.

Table C1 the summation of the peak area for reactor outlet.

Product	Peak area	Corrected peak area	RF
Methane	34.67	34.67	1
Acetaldehyde	2265.88	16184.86	0.14
Ethanol (Feed)	1049.53	1639.88	0.64
Total	3350.08	17859.41	-

*In formation of 10%Cu-2%Zn/SiO_2, Temperature 400 °C, Contact time 15 g.h/mol, time on steam = 15 minutes

$$\text{Corrected peak area in each product} = \frac{\textbf{Peak area}}{\textbf{RF}}$$

Where RF is the response factor of the analyzed sample showing in Table C1.

For example;

$$\text{Corrected peak area of acetaldehyde} = \frac{2265.88}{0.14}$$

$$= 16184.86$$

In the normalization method, the areas of all eluted peak were compute after correcting these areas for differences in the detector response (RF) to different compound types. After correcting areas, the concentration of the analyzed was found from the ratio of its area to the total area of all peaks.

Calculate the percent yield of each component in sample as follows:

$$\%\text{Yield in each product} = \frac{\text{Corrected peak area of sample x 100}}{\text{Total corrected area}}$$

For example;

$$\%\text{Yield of Acetaldehyde} = \frac{16184.86 \text{ x } 100}{17859.41}$$

$$= 90.62$$

The percent yield of each product obtained from above calculation is shown in **Table C2**.

Table C2 %Yield of product derived by normalization method.

Product	% Yield
Methane	0.19
Acetaldehyde	90.62
Ethanol (Feed)	9.19
Total	100

Conversion

%Conversion can be calculated from the following equation:

$$\%\text{Conversion} = \frac{(\text{Area total} - \text{Area feed x } 100)}{\text{Area total}}$$

For example;

$$\%\text{Conversion} = \frac{(17859.41 \qquad .88) \text{ x } 10}{17859.41}$$

$$= 90.81$$

Selectivity

%Selectivity can be obtained from the following equation:

$$\%\text{Selectivity in each product} = \frac{\%\text{Yield of each product x } 100}{\%\text{Conversion}}$$

For example;

$$\%\text{Selectivity of acetaldehyde} = \frac{90.62 \text{ x } 100}{90.81}$$

$$= 99.79$$

APPENDIX D

REACTION DATA

D1: The production of hydrocarbons from ethanol.

D1.1 Effect of contact time

Table D1 Product distribution from ethanol conversion at contact time 10 g.h/mol.

Time on stream (min)	%Conversion	%Yields							
		Ethylene	Propylene	C4-C5	BTX	C6-C8	C9 Aromatics	Alkylbenzees	Indenes & naphthalenes
30	100	95.8	0.0	1.6	1.3	0.3	1.0	0.0	0.0
70	100	97.6	0.0	1.0	0.8	0.1	0.5	0.0	0.0
110	100	97.4	0.0	1.4	0.6	0.2	0.4	0.0	0.0
150	100	97.3	0.0	1.6	0.6	0.2	0.3	0.0	0.0
190	100	97.5	0.0	1.5	0.5	0.2	0.3	0.0	0.0

Reaction condition; Catalyst: H-ZSM-5 (28), Temperature: 400°C, Feed rate: 0.0085g/h of absolute ethanol, Carrier gas; 166ml/min of nitrogen, Ambient pressure.

Table D2 Product distribution from ethanol conversion at contact time 15 g.h/mol.

Time on stream (min)	%Conversion	%Yields							
		Ethylene	Propylene	C4-C5	BTX	C6-C8	C9 Aromatics	Alkylbenzees	Indenes & naphthalenes
30	100	92.8	1.4	2.6	1.7	0.2	1.3	0.0	0.0
70	100	95.3	0.8	1.5	1.0	0.3	1.1	0.0	0.0
110	100	96.5	0.9	1.7	0.6	0.0	0.3	0.0	0.0
150	100	95.9	1.1	2.1	0.6	0.0	0.3	0.0	0.0
190	100	94.7	1.4	2.8	0.7	0.0	0.4	0.0	0.0

Reaction condition; Catalyst: H-ZSM-5 (28), Temperature: 400°C, Feed rate: 0.0085g/h of absolute ethanol, Carrier gas; 166ml/min of nitrogen, Ambient pressure.

Table D3 Product distribution from ethanol conversion at contact time 25 g.h/mol.

Time on stream (min)	%Conversion	%Yields							
		Ethylene	Propylene	C4-C5	BTX	C6-C8	C9 Aromatics	Alkylbenzees	Indenes & naphthalenes
30	100	77.2	5.7	5.9	3.8	0.5	2.7	1.2	2.9
70	100	83.7	2.8	3.1	3.7	0.7	2.7	1.6	1.7
110	100	79.5	7.8	7.7	2.1	0.6	1.3	0.6	0.5
150	100	81.2	6.5	7.0	2.3	0.5	1.4	0.6	0.5
190	100	78.7	8.4	8.4	2.1	0.7	1.2	0.3	0.1

Reaction condition; Catalyst: H-ZSM-5 (28), Temperature: 400°C, Feed rate: 0.0085g/h of absolute ethanol, Carrier gas; 166ml/min of nitrogen, Ambient pressure.

Table D4 Product distribution from ethanol conversion at contact time 42 g.h/mol.

Time on stream (min)	%Conversion	%Yields							
		Ethylene	Propylene	C4-C5	BTX	C6-C8	C9 Aromatics	Alkylbenzees	Indenes & naphthalenes
30	100	56.2	11.7	9.9	7.1	1.0	4.8	2.0	7.3
70	100	60.4	11.8	10.1	6.4	1.4	5.1	1.5	3.4
110	100	54.6	14.2	13.0	7.9	1.6	5.2	1.5	1.9
150	100	56.9	13.8	11.9	6.9	1.3	4.5	1.5	3.1
190	100	56.9	14.0	12.4	7.0	1.5	4.7	1.4	2.2

Reaction condition; Catalyst: H-ZSM-5 (28), Temperature: 400°C, Feed rate: 0.0085g/h of absolute ethanol, Carrier gas; 166ml/min of nitrogen, Ambient pressure.

D1.2 The reaction over double bed system.

Table D5 Product distribution from ethanol conversion over double bed system of Ag/SiO_2 (top) and H-ZSM-5 (28) (bottom) catalysts.

Time on stream (min)	%Conversion	%Yields								
		Methane	Propylene	Acetaldehyde	C4-C5	BTX	C6-C8	C9 Aromatics	Alkylbenzees	Indenes & naphthalenes
30	100	1.5	1.7	6.2	0.1	7.6	0.2	12.4	5.0	65.3
70	100	2.7	2.9	39.2	0.2	6.3	0.1	8.8	16.8	22.9
110	100	3.0	3.0	72.5	0.3	2.4	0.3	3.6	6.4	8.5
150	100	3.1	2.4	84.7	0.3	1.0	0.1	1.1	3.2	4.1
190	100	3.1	2.3	89.1	0.3	0.4	0.0	0.8	1.5	2.5
240	100	3.2	2.2	91.1	0.2	0.3	0.0	0.6	0.7	1.6
280	100	3.0	2.0	93.0	0.2	0.1	0.0	0.4	0.3	1.0
320										
360	100	2.9	1.6	94.3	0.2	0.1	0.0	0.2	0.1	0.6
400	100	2.9	1.4	94.0	0.2	0.1	0.0	0.2	0.0	1.2

Reaction condition; Contact time of Ag/SiO_2: 60 g.h/mol. and contact time of H-ZSM-5 (28): 15 g.h/mol., Temperature: 400°C, Feed rate: 0.0085g/h of absolute ethanol, Carrier gas; 166ml/min of nitrogen, Ambient pressure.

D2: Dehydrogenation of ethanol to acetaldehyde.

D2.1 Effect of carrier gas.

Table D6 Dehydrogenation of ethanol over Cu/SiO_2 catalyst (section a).

Time on stream (min)	% Conversion	% Yield	
		CH_4	Acetaldehyde
15	79.34	0.14	79.02
55	42.20	0.15	41.95
95	22.75	0.15	22.60
135	13.58	0.15	13.44
175	9.24	0.15	9.08

Reaction condition; Calcined 450 °C in N_2 gas, Contact time: 30 g.h/mol., Temperature: 400°C, Feed rate: 0.012g/h of absolute ethanol, Carrier gas; 166ml/min of nitrogen, Ambient pressure.

Table D7 Dehydrogenation of ethanol over Cu/SiO_2 catalyst (section b).

Time on stream (min)	% Conversion	% Yield	
		CH_4	Acetaldehyde
15	18.85	0.19	18.66
55	9.60	0.17	9.43
95	6.57	0.15	6.42

Reaction condition; Treat 450 °C in N_2 gas, Contact time: 30 g.h/mol., Temperature: 400°C, Feed rate: 0.012g/h of absolute ethanol, Carrier gas; 166ml/min of nitrogen, Ambient pressure.

Table D8 Dehydrogenation of ethanol over Cu/SiO_2 catalyst (section c).

Time on stream (min)	% Conversion	% Yield	
		CH_4	Acetaldehyde
15	9.18	0.25	8.94
55	7.48	0.16	7.32
95	7.02	0.15	6.87

Reaction condition; Treat 450 °C in H_2 gas, Contact time: 30 g.h/mol., Temperature: 400°C, Feed rate: 0.012g/h of absolute ethanol, Carrier gas; 166ml/min of nitrogen, Ambient pressure.

Table D9 Dehydrogenation of ethanol over Cu/SiO_2 catalyst (section d).

Time on stream (min)	% Conversion	% Yield	
		CH_4	Acetaldehyde
15	95.02	0.68	94.34
55	94.93	0.29	94.64
95	93.76	0.20	93.56

Reaction condition; Calcined 450 °C in air and reduced 400 °C, Contact time: 30 g.h/mol., Temperature: 400°C, Feed rate: 0.012g/h of absolute ethanol, Carrier gas; 166ml/min of hydrogen, Ambient pressure.

Table D10 Dehydrogenation of ethanol over Cu/SiO_2 catalyst (section e).

Time on stream (min)	% Conversion	% Yield	
		CH_4	Acetaldehyde
15	49.20	0.13	48.97
55	28.05	0.13	27.92
95	19.73	0.12	19.61
135	15.04	0.11	14.93
175	14.83	0.11	14.71
215	12.65	0.12	12.54
255	11.59	0.12	11.48
295	10.58	0.13	10.46
335	9.71	0.09	9.62
375	9.08	0.09	8.99

Reaction condition; Contact time: 30 g.h/mol., Temperature: 400°C, Feed rate: 0.012g/h of absolute ethanol, Carrier gas; 166ml/min of nitrogen, Ambient pressure.

Table D11 Dehydrogenation of ethanol over Cu/SiO_2 catalyst (section f).

Time on stream (min)	% Conversion	% Yield	
		CH_4	Acetaldehyde
15	91.18	0.31	90.87
55	90.93	0.20	90.73
95	90.35	0.21	90.14
135	85.62	0.16	85.46
175	83.86	0.16	83.71
215	82.19	0.14	82.05

Reaction condition; Calcined 450 °C in air and reduced 400 °C, Contact time: 30 g.h/mol., Temperature: 400 °C, Feed rate: 0.012g/h of absolute ethanol, Carrier gas; 166ml/min of hydrogen, Ambient pressure.

D2.2 Effect of Temperature

Table D12 Dehydrogenation of ethanol over Cu/SiO_2 at temperature 400 °C.

Time on stream (min)	% Conversion	% Yield	
		CH_4	Acetaldehyde
15	-	-	-
55	70.85	0.10	70.75
95	66.45	0.10	66.35
135	60.62	0.09	60.53
175	55.54	0.09	55.45
215	54.32	0.09	54.23
255	48.80	0.09	48.71
295	41.99	0.07	41.92
335	36.94	0.09	36.85
375	35.09	0.08	35.01

Reaction condition; Contact time: 15 g.h/mol., Feed rate: 0.012g/h of absolute ethanol, Carrier gas; 166ml/min of hydrogen, Ambient pressure.

Table D13 Dehydrogenation of ethanol over Cu/SiO_2 at temperature 500 °C.

Time on stream (min)	% Conversion	% Yield	
		CH_4	Acetaldehyde
15	89.72	1.16	88.56
55	84.83	1.11	83.72
95	82.61	1.22	81.39
135	81.03	0.91	80.12
175	78.84	1.27	77.57
215	80.71	1.12	79.59
255	80.25	1.12	79.14
295	79.85	1.09	78.76

Reaction condition; Contact time: 15 g.h/mol., Feed rate: 0.012g/h of absolute ethanol, Carrier gas; 166ml/min of hydrogen, Ambient pressure.

D2.3 Effect of alloyed metal with Cu.

Table D14 Dehydrogenation of ethanol over Cu-Fe/SiO_2.

Time on stream (min)	% Conversion	% Yields		
		CH_4	Propylene	Acetaldehyde
15	88.75	2.47	0.56	85.72
55	75.04	1.26	0.17	73.61
95	71.10	1.20	0.13	69.76
135	67.06	1.04	0.11	65.91
175	65.59	1.09	0.10	64.40
215	65.82	1.11	0.10	64.62
255	60.83	1.01	0.08	59.74
295	62.38	1.01	0.07	61.29
335	59.44	0.95	0.07	58.41
375	60.88	1.04	0.07	59.77

Reaction condition; Contact time: 15 g.h/mol., Temperature: 400 °C, Feed rate: 0.012g/h of absolute ethanol, Carrier gas; 166ml/min of hydrogen, Ambient pressure.

Table D15 Dehydrogenation of ethanol over $Cu\text{-}Ni/SiO_2$.

Time on stream (min)	% Conversion	% Yield	
		CH_4	Acetaldehyde
15	100.00	100.00	-
55	100.00	100.00	-
95	100.00	100.00	-
135	100.00	100.00	-
175	100.00	100.00	-

Reaction condition; Contact time: 15 g.h/mol., Temperature: 400 °C, Feed rate: 0.012g/h of absolute ethanol, Carrier gas; 166ml/min of hydrogen, Ambient pressure.

Table D16 Dehydrogenation of ethanol over $Cu\text{-}Zn/SiO_2$.

Time on stream (min)	% Conversion	% Yield	
		CH_4	Acetaldehyde
15	90.82	0.19	90.62
55	89.77	0.14	89.63
95	89.48	0.14	89.34
135	88.30	0.13	88.17
175	89.86	0.10	89.76

Reaction condition; Contact time: 15 g.h/mol., Temperature: 400 °C, Feed rate: 0.012g/h of absolute ethanol, Carrier gas; 166ml/min of hydrogen, Ambient pressure.

Table D17 Dehydrogenation of ethanol over Cu-Ag/SiO_2.

Time on stream (min)	% Conversion	% Yield	
		CH_4	Acetaldehyde
15	75.76	0.90	74.86
55	73.54	0.86	72.68
95	71.46	0.84	70.62
135	73.53	0.61	72.92
175	74.23	0.71	73.53
215	74.20	0.59	73.61
255	74.16	0.60	73.56
295	73.89	0.80	73.09
335	72.88	0.78	72.10

Reaction condition; Contact time: 15 g.h/mol., Temperature: 400 °C, Feed rate: 0.012g/h of absolute ethanol, Carrier gas; 166ml/min of hydrogen, Ambient pressure.

D2.4 Effect of contact time.

Table D18 Dehydrogenation of ethanol over Cu-Zn/SiO_2 at contact time 4 g.h/mol.

Time on stream (min)	% Conversion	% Yield			
		CH_4	Acetaldehyde	Butanal	Butanol
15	69.06	0.12	68.95	-	-
55	69.61	0.10	69.51	-	-
95	67.99	0.08	67.90	-	-
135	67.04	0.08	66.96	-	-
175	65.77	0.07	65.70	-	-

Reaction condition; Temperature: 400 °C, Feed rate: 0.012g/h of absolute ethanol, Carrier gas; 166ml/min of hydrogen, Ambient pressure.

Table D19 Dehydrogenation of ethanol over Cu-Zn/SiO_2 at contact time 8 g.h/mol.

Time on stream (min)	% Conversion	% Yield			
		CH_4	Acetaldehyde	Butanal	Butanol
15	79.92	0.20	79.71	-	-
55	77.57	0.16	77.41	-	-
95	79.38	0.18	79.20	-	-
135	76.57	0.14	76.42	-	-
175	77.19	0.15	77.04	-	-

Reaction condition; Temperature: 400 °C, Feed rate: 0.012g/h of absolute ethanol, Carrier gas; 166ml/min of hydrogen, Ambient pressure.

Table D20 Dehydrogenation of ethanol over Cu-Zn/SiO_2 at contact time 30 g.h/mol.

Time on stream (min)	% Conversion	% Yield			
		CH_4	Acetaldehyde	Butanal	Butanol
15	93.84	0.31	92.56	0.72	0.24
55	94.01	0.27	93.03	0.62	0.09
95	94.17	0.33	93.14	0.62	0.09
135	93.26	0.29	92.30	0.59	0.07
175	93.01	0.27	92.07	0.59	0.07

Reaction condition; Temperature: 400 °C, Feed rate: 0.012g/h of absolute ethanol, Carrier gas; 166ml/min of hydrogen, Ambient pressure.

D3: Production of hydrocarbons from ethanol over double bed system of Cu-Zn/SiO_2 and H-ZSM-5 catalysts

D3.1 Effect of acidity.

Table D21 Product distribution from ethanol conversion over double bed system of Cu-Zn/SiO_2.and H-ZSM-5 ratio 500.

Time on stream (min)	%Conversion	%Yields								
		Ethylene	Propylene	Acetaldehyde	C4-C5	BTX	C6-C8	C9 Aromatics	Alkylbenzees	Indenes & naphthalenes
15	100	6.00	1.10	68.42	2.33	4.47	0.34	3.15	6.43	7.74
55	100	6.23	0.81	79.15	2.46	3.03	0.28	1.55	3.48	3.03
95	100	10.20	0.09	79.94	2.22	1.97	0.26	0.85	2.07	2.39
135	100	3.99	0.50	88.80	1.97	1.26	0.23	0.46	1.30	1.49
175	100	6.31	0.50	86.29	2.22	1.39	0.27	0.44	1.60	0.99
215	100	6.22	0.52	88.59	1.92	0.80	0.21	0.27	0.80	0.67
255	100	6.15	0.50	88.72	1.84	0.81	0.21	0.25	0.58	0.93
295	100	6.59	0.45	88.65	1.77	0.63	0.19	0.18	0.71	0.84
335	100	7.28	0.66	87.82	1.85	0.52	0.19	0.19	0.48	0.99
375	100	6.39	0.60	89.70	1.47	0.62	0.22	0.14	0.63	0.23

Reaction condition; Contact time of Cu-Zn/SiO_2: 15 g.h/mol. and contact time of H-ZSM-5 (500): 15 g.h/mol., Temperature: 400°C, Feed rate: 0.012g/h of absolute ethanol, Carrier gas; 166ml/min of hydrogen, Ambient pressure.

Table D22 Product distribution from ethanol conversion over double bed system of Cu-Zn/SiO_2.and H-ZSM-5 ratio 250.

Time on stream (min)	%Conversion	%Yields								
		Ethylene	Propylene	Acetaldehyde	C4-C5	BTX	C6-C8	C9 Aromatics	Alkylbenzees	Indenes & naphthalenes
15	100	6.29	1.37	63.26	2.49	5.64	0.35	3.72	8.05	8.82
55	100	7.38	1.12	69.87	2.84	3.94	0.29	2.29	5.61	6.66
95	100	6.59	0.86	75.76	2.78	3.18	0.24	1.64	4.80	4.15
135	100	8.19	0.88	77.84	2.77	2.22	0.21	1.19	3.41	3.29
175	100	6.55	0.66	83.73	2.49	1.61	0.17	0.73	2.26	1.79
215	100	5.20	0.58	85.07	2.66	1.52	0.19	0.75	2.13	1.90
255	100	5.41	0.64	84.11	2.86	1.69	0.22	0.81	2.29	1.97
295	100	12.18	0.00	81.32	2.24	1.06	0.17	0.48	1.59	0.96
335	100	5.13	0.52	86.86	2.48	1.12	0.22	0.50	1.45	1.71
375	100	5.26	0.54	85.84	2.62	1.14	0.30	0.54	2.11	1.65

Reaction condition; Contact time of Cu-Zn/SiO_2: 15 g.h/mol. and contact time of H-ZSM-5 (250): 15 g.h/mol., Temperature: 400°C, Feed rate: 0.012g/h of absolute ethanol, Carrier gas; 166ml/min of hydrogen, Ambient pressure.

Table D23 Product distribution from ethanol conversion over double bed system of Cu-Zn/SiO_2.and H-ZSM-5 ratio 140.

Time on stream (min)	%Conversion	%Yields								
		Ethylene	Propylene	Acetaldehyde	C4-C5	BTX	C6-C8	C9 Aromatics	Alkylbenzees	Indenes & naphthalenes
15	100	2.07	1.30	18.82	0.65	13.81	0.60	16.36	19.57	26.83
55	100	3.35	1.13	21.83	1.07	12.24	0.83	13.79	18.89	26.87
95	100	3.38	1.21	34.41	1.70	12.71	1.09	10.42	25.23	9.85
135	100	4.42	1.24	51.69	1.94	8.03	0.69	7.48	15.99	8.51
175	100	6.10	1.30	51.91	2.68	7.71	0.81	6.71	14.11	8.68
215	100	5.45	1.29	59.76	3.05	6.28	0.71	5.15	10.65	7.64
255	100	7.40	1.35	53.52	3.20	7.09	0.65	5.96	12.26	8.57
295	100	8.94	1.50	55.03	2.71	6.81	0.68	5.22	10.87	8.23
335	100	6.47	1.18	65.82	2.44	4.31	0.49	3.35	8.85	7.10
375	100	8.02	1.30	62.54	3.32	5.40	0.81	3.66	11.08	3.87

Reaction condition; Contact time of Cu-Zn/SiO_2: 15 g.h/mol. and contact time of H-ZSM-5 (140): 15 g.h/mol., Temperature: 400°C, Feed rate: 0.012g/h of absolute ethanol, Carrier gas; 166ml/min of hydrogen, Ambient pressure.

Table D24 Product distribution from ethanol conversion over double bed system of Cu-Zn/SiO_2.and H-ZSM-5 ratio 40.

Time on stream (min)	%Conversion	%Yields								
		Ethylene	Propylene	Acetaldehyde	C4-C5	BTX	C6-C8	C9 Aromatics	Alkylbenzees	Indenes & naphthalenes
15	100	5.87	3.23	1.50	0.26	20.67	0.55	25.91	14.96	27.06
55	100	4.70	3.30	10.05	0.21	16.43	0.65	20.87	13.96	29.83
95	100	3.33	2.61	13.78	0.22	13.75	0.72	18.00	20.30	27.28
135	100	4.85	3.09	20.76	0.32	12.59	0.65	14.44	19.82	23.48
175	100	4.07	2.66	23.90	0.39	13.16	0.61	13.10	21.98	20.15
215	100	7.15	3.10	36.28	0.54	10.43	0.49	8.96	21.70	11.35
255	100	7.55	2.74	42.11	0.68	7.90	0.49	7.94	19.17	11.42
295	100	4.21	2.60	50.50	1.02	6.62	0.62	5.96	20.19	8.28
335	100	5.79	2.58	52.83	0.99	7.01	0.44	5.30	15.41	9.62
375	100	6.17	2.28	68.41	1.01	3.82	0.30	3.68	10.02	4.31

Reaction condition; Contact time of Cu-Zn/SiO_2: 15 g.h/mol. and contact time of H-ZSM-5 (40): 15 g.h/mol., Temperature: 400°C, Feed rate: 0.012g/h of absolute ethanol, Carrier gas; 166ml/min of hydrogen, Ambient pressure.

Table D25 Product distribution from ethanol conversion over double bed system of Cu-Zn/SiO_2.and H-ZSM-5 ratio 28.

Time on stream (min)	%Conversion	%Yields								
		Ethylene	Propylene	Acetaldehyde	C4-C5	BTX	C6-C8	C9 Aromatics	Alkylbenzees	Indenes & naphthalenes
15	100	5.17	3.51	2.14	1.06	26.01	0.53	20.15	9.19	32.25
55	100	4.85	3.71	20.78	0.52	13.32	0.46	14.09	7.91	34.36
95	100	4.85	2.69	36.74	0.93	9.89	0.50	8.28	11.75	24.38
135	100	5.40	2.24	63.12	1.36	7.58	0.45	3.61	9.21	7.03
175	100	4.56	1.82	72.88	1.64	5.03	0.29	2.49	7.06	4.25
215	100	5.13	1.51	78.42	1.84	2.54	0.22	1.47	6.32	2.55
255	100	6.61	1.48	81.51	1.88	1.96	0.12	1.32	2.95	2.17
295	100	5.72	1.25	85.46	1.97	1.34	0.09	0.88	1.95	1.35
335	100	6.30	1.37	83.77	2.33	1.54	0.12	1.04	2.08	1.45
375	100	7.40	1.25	84.47	2.25	1.38	0.09	0.68	1.49	0.99

Reaction condition; Contact time of Cu-Zn/SiO_2: 15 g.h/mol. and contact time of H-ZSM-5 (28): 15 g.h/mol., Temperature: 400°C, Feed rate: 0.012g/h of absolute ethanol, Carrier gas; 166ml/min of hydrogen, Ambient pressure.

D3.2 Effect of metal incorporated on H-ZSM-5.

Table D25 Product distribution from ethanol conversion over double bed system of Cu-Zn/SiO_2.and Ni/H-ZSM-5 ratio 28.

Time on stream (min)	%Conversion	%Yields									
		Methane	Ethane	propane	Acetaldehyde	C4-C5	BTX	C6-C8	C9 Aromatics	Alkylbenzees	Indenes & naphthalenes
15	100	10.46	12.18	4.03	0.76	0.58	27.27	0.34	13.00	7.01	24.36
55	100	13.25	10.00	4.15	0.65	0.38	21.82	0.71	12.58	7.34	29.11
95	100	11.36	9.73	3.87	0.59	0.51	19.80	0.69	13.47	11.67	28.32
135	100	12.48	10.75	4.33	0.87	0.54	19.54	0.93	13.23	16.88	20.44
175	100	10.36	13.69	4.94	2.26	0.64	19.80	0.61	15.41	9.63	22.66
215	100	9.43	13.60	4.73	2.78	0.67	16.71	1.68	14.34	14.50	21.55
255	100	10.99	14.78	5.31	3.50	0.77	17.01	1.05	13.83	13.84	18.92
295	100	11.51	14.39	5.50	7.40	0.77	16.81	0.73	13.64	10.98	18.28
335	100	11.68	13.18	5.19	7.70	0.77	16.52	0.53	13.64	15.39	15.39
375	100	11.56	16.31	5.91	11.43	1.00	16.37	0.47	12.67	12.12	12.16

Reaction condition; Contact time of Cu-Zn/SiO_2: 15 g.h/mol. and contact time of Ni/H-ZSM-5 (28): 15 g.h/mol., Temperature: 400°C, Feed rate: 0.012g/h of absolute ethanol, Carrier gas; 166ml/min of hydrogen, Ambient pressure.

Table D26 Product distribution from ethanol conversion over double bed system of Cu-Zn/SiO_2.and Cu/H-ZSM-5 ratio 28.

Time on stream (min)	%Conversion	%Yields								
		Ethylene	Propylene	Acetaldehyde	C4-C5	BTX	C6-C8	C9 Aromatics	Alkylbenzees	Indenes & naphthalenes
15	100	19.12	5.33	1.67	2.79	21.92	0.65	15.78	8.61	24.14
55	100	20.90	5.21	0.91	1.92	20.16	0.42	17.28	8.15	25.06
95	100	17.02	4.61	4.36	1.32	20.91	0.42	19.84	12.08	19.44
135	100	14.90	4.60	5.41	1.54	20.51	0.57	17.43	15.94	19.10
175	100	18.54	4.48	8.14	1.67	17.31	0.49	16.23	11.36	21.78
215	100	19.77	4.57	11.64	2.02	17.92	0.62	13.39	17.18	12.91
255	100	17.78	5.04	22.30	1.98	16.48	0.57	12.58	11.20	12.06
295	100	21.89	4.20	22.46	2.34	12.88	0.53	11.34	13.43	10.94
335	100	23.61	4.11	26.16	2.68	11.19	0.55	9.82	12.44	9.45
375	100	25.55	4.06	26.70	3.08	9.12	0.56	8.78	11.14	11.01

Reaction condition; Contact time of Cu-Zn/SiO_2: 15 g.h/mol. and contact time of Cu/H-ZSM-5 (28): 15 g.h/mol., Temperature: 400°C, Feed rate: 0.012g/h of absolute ethanol, Carrier gas; 166ml/min of hydrogen, Ambient pressure.

Table D27 Product distribution from ethanol conversion over double bed system of Cu-Zn/SiO_2.and Zn/H-ZSM-5 ratio 28.

Time on stream (min)	%Conversion	%Yields								
		Ethylene	Propylene	Acetaldehyde	C4-C5	BTX	C6-C8	C9 Aromatics	Alkylbenzees	Indenes & naphthalenes
15	100	24.25	4.97	3.06	1.72	21.82	0.26	15.68	9.20	19.04
55	100	26.01	5.03	1.78	1.75	20.45	0.29	15.45	8.99	20.25
95	100	28.39	5.04	2.09	2.07	19.18	0.63	14.22	9.87	18.52
135	100	28.39	4.74	2.16	2.17	16.97	0.56	13.61	10.76	20.64
175	100	31.81	5.14	3.75	2.12	18.14	0.70	13.04	11.88	13.41
215	100	31.32	4.94	4.17	2.29	17.78	0.68	14.18	11.18	13.44
255	100	36.18	5.16	4.49	2.74	16.00	0.82	12.08	12.14	10.39
295	100	38.94	5.23	5.01	3.16	15.09	0.83	11.42	9.35	10.96
335	100	40.89	5.21	5.36	3.48	14.63	0.94	10.79	9.17	9.53
375	100	39.48	4.96	9.13	3.01	14.34	0.82	11.04	9.04	8.20

Reaction condition; Contact time of Cu-Zn/SiO_2: 15 g.h/mol. and contact time of Zn/H-ZSM-5 (28): 15 g.h/mol., Temperature: 400°C, Feed rate: 0.012g/h of absolute ethanol, Carrier gas; 166ml/min of hydrogen, Ambient pressure.

Table D28 Product distribution from ethanol conversion over single bed system of Zn/H-ZSM-5 ratio 28.

Time on stream (min)	%Conversion	%Yields							
		Ethylene	Propylene	C4-C5	BTX	C6-C8	C9 Aromatics	Alkylbenzees	Indenes & naphthalenes
15	100	97.93	0.45	1.08	0.14	0.30	0.10	-	-
55	100	98.69	0.45	0.86	-	-	-	-	-
95	100	98.68	0.46	0.86	-	-	-	-	-
135	100	98.63	0.49	0.88	-	-	-	-	-
175	100	98.69	0.46	0.85	-	-	-	-	-

Reaction condition; Contact time of Zn/H-ZSM-5 (28): 10 g.h/mol., Temperature: 400°C, Feed rate: 0.012g/h of absolute ethanol, Carrier gas; 166ml/min of hydrogen, Ambient pressure.

D3.3 Effect of contact time of secondary bed (Zn/H-ZSM-5 ratio 28).

Table D29 Product distribution from ethanol conversion over double bed system of Cu-Zn/SiO_2.and Zn/H-ZSM-5 ratio 28 at contact time 2.5 g.h/mol.

Time on stream (min)	%Conversion	%Yields								
		Ethylene	Propylene	Acetaldehyde	C4-C5	BTX	C6-C8	C9 Aromatics	Alkylbenzees	Indenes & naphthalenes
15	100	11.42	1.91	60.39	1.16	4.83	0.24	4.06	5.11	10.88
55	100	12.57	1.01	75.44	1.51	2.83	0.15	1.23	2.06	3.19
95	100	12.86	0.75	77.57	1.74	1.91	0.14	0.75	2.40	1.88
135	100	13.40	0.66	79.35	1.88	1.27	0.13	0.46	1.77	1.08
175	100	13.97	0.58	80.90	1.75	0.81	0.11	0.29	1.16	0.42
215	100	14.72	0.50	80.97	1.85	0.58	0.10	0.26	0.72	0.30
255	100	15.00	0.50	81.14	1.85	0.45	0.08	0.20	0.56	0.23
295	100	15.49	0.46	80.97	1.74	0.40	0.05	0.19	0.54	0.16
335	100	15.72	0.44	80.85	1.75	0.37	0.07	0.16	0.41	0.25
375	100	16.49	0.39	80.32	1.66	0.31	0.06	0.14	0.40	0.23

Reaction condition; Contact time of Cu-Zn/SiO_2: 15 g.h/mol. and contact time of Zn/H-ZSM-5 (28): 2.5 g.h/mol., Temperature: 400°C, Feed rate: 0.012g/h of absolute ethanol, Carrier gas; 166ml/min of hydrogen, Ambient pressure.

Table D30 Product distribution from ethanol conversion over double bed system of Cu-Zn/SiO_2.and Zn/H-ZSM-5 ratio 28 at contact time 10 g.h/mol.

Time on stream (min)	%Conversion	%Yields								
		Ethylene	Propylene	Acetaldehyde	C4-C5	BTX	C6-C8	C9 Aromatics	Alkylbenzees	Indenes & naphthalenes
15	100	22.32	5.42	4.01	1.58	19.12	0.47	15.79	8.42	22.87
55	100	23.16	5.37	12.80	1.70	16.04	1.04	13.36	7.38	19.15
95	100	19.83	4.17	29.73	1.21	12.64	0.52	10.35	7.56	13.99
135	100	22.81	3.82	23.60	2.51	10.45	0.89	9.71	10.50	15.71
175	100	25.44	4.56	29.11	3.87	10.73	1.13	5.61	10.29	9.26
215	100	27.72	3.52	29.58	3.70	8.22	0.66	6.37	10.00	10.25
255	100	26.22	3.00	35.65	3.49	6.67	0.51	5.35	12.19	6.92
295	100	27.76	2.86	35.44	3.86	6.58	0.54	4.68	12.09	6.19
335	100	29.96	2.65	40.42	3.93	5.04	0.51	3.76	8.54	5.19
375	100	32.64	2.56	42.18	4.30	4.18	0.52	3.21	5.84	4.58

Reaction condition; Contact time of Cu-Zn/SiO_2: 15 g.h/mol. and contact time of Zn/H-ZSM-5 (28): 10 g.h/mol., Temperature: 400°C, Feed rate: 0.012g/h of absolute ethanol, Carrier gas; 166ml/min of hydrogen, Ambient pressure.